

Article

Ore and Geochemical Specialization and Substance Sources of the Ural and Timan Carbonatite Complexes (Russia): Insights from Trace Element, Rb–Sr, and Sm–Nd Isotope Data

Irina Nedosekova ^{1,*} , Nikolay Vladykin ², Oksana Udoratina ³  and Boris Belyatsky ⁴ 

¹ A.N. Zavaritsky Institute of Geology and Geochemistry, Ural Branch of Russian Academy of Sciences, Vonsovskogo Str. 15, 620016 Ekaterinburg, Russia

² A.P. Vinogradov Institute of Geochemistry, Siberian Branch of Russian Academy of Sciences, Favorskogo Str. 1A, 664033 Irkutsk, Russia; vlad@igc.irk.ru

³ Institute of Geology, Komi Scientific Center Ural Branch of Russian Academy of Sciences, Pervomayskaya Str. 54, 167982 Syktyvkar, Russia; udoratina@geo.komisc.ru

⁴ Karpinsky Russian Geological Research Institute (VSEGEI), Avenue Sredny V.O. 74, 199106 St. Petersburg, Russia; bbelyatsky@mail.ru

* Correspondence: nedosekova@igg.uran.ru

Abstract: The Ilmeno–Vishnevogorsk (IVC), Buldym, and Chetlassky carbonatite complexes are localized in the folded regions of the Urals and Timan. These complexes differ in geochemical signatures and ore specialization: Nb-deposits of pyrochlore carbonatites are associated with the IVC, while Nb–REE-deposits with the Buldym complex and REE-deposits of bastnäsite carbonatites with the Chetlassky complex. A comparative study of these carbonatite complexes has been conducted in order to establish the reasons for their ore specialization and their sources. The IVC is characterized by low $^{87}\text{Sr}/^{86}\text{Sr}_i$ (0.70336–0.70399) and ϵNd (+2 to +6), suggesting a single moderately depleted mantle source for rocks and pyrochlore mineralization. The Buldym complex has a higher $^{87}\text{Sr}/^{86}\text{Sr}_i$ (0.70440–0.70513) with negative ϵNd (–0.2 to –3), which corresponds to enriched mantle source EMI-type. The REE carbonatites of the Chetlassky complex show low $^{87}\text{Sr}/^{86}\text{Sr}_i$ (0.70336–0.70369) and a high ϵNd (+5–+6), which is close to the DM mantle source with ~5% marine sedimentary component. Based on Sr–Nd isotope signatures, major, and trace element data, we assume that the different ore specialization of Urals and Timan carbonatites may be caused not only by crustal evolution of alkaline-carbonatite magmas, but also by the heterogeneity of their mantle sources associated with different degrees of enrichment in recycled components.

Keywords: carbonatites; Sr–Nd isotopes; Nb–REE deposits; pyrochlore; bastnäsite; Urals; Timan



Citation: Nedosekova, I.; Vladykin, N.; Udoratina, O.; Belyatsky, B. Ore and Geochemical Specialization and Substance Sources of the Ural and Timan Carbonatite Complexes (Russia): Insights from Trace Element, Rb–Sr, and Sm–Nd Isotope Data. *Minerals* **2021**, *11*, 711. <https://doi.org/10.3390/min11070711>

Academic Editor: Antonio Simonetti

Received: 28 May 2021

Accepted: 28 June 2021

Published: 30 June 2021

Publisher's Note: MDPI stays neutral with regard to jurisdictional claims in published maps and institutional affiliations.



Copyright: © 2021 by the authors. Licensee MDPI, Basel, Switzerland. This article is an open access article distributed under the terms and conditions of the Creative Commons Attribution (CC BY) license (<https://creativecommons.org/licenses/by/4.0/>).

1. Introduction

Complexes of carbonatites and alkaline rocks are known to host economically significant deposits of critical metals, for example, Nb and rare earth elements (REE) [1]. Carbonatite deposits comprise about 90% of the world's Nb reserves. Three operating carbonatite deposits—Araxá and Catalão-II (Brazil) and St. Honoré (Canada)—account for about 99% of the total worldwide production of ferroniobium and other sources make up 1% [2]. The largest REE-deposits are associated with carbonatites: Mountain Pass (USA) and Bayun-Obo (China) provide more than half of the world production of rare earth elements of the cerium group.

Carbonatites are usually cogenetic with alkaline rocks and occur in almost all known tectonic settings. Most often, carbonatite complexes are associated with intraplate settings for example, continental rifts, localized on cratons, and in the margins of platforms, composing ring zonal plutons of ultramafic, alkaline-ultramafic, and alkaline rocks with carbonatites [3–6]. However, alkaline-carbonatite complexes have also been found in accretion-collisional orogenic belts [7–15].

Most of the intraplate carbonatites are associated with alkaline-ultramafic magmatism. Their geochemical feature is the simultaneous enrichment of high field strength elements (HFSE) (i.e., Ti, Nb, Ta, Zr, Hf as well as Sr, Ba, LREE, and P, F). In Russia, they are represented by the largest provinces of carbonatite magmatism: Karelian-Kola (Baltic Craton), Maymecha-Kotuiszkaya, Udzhinskaya, East Sayan, Sette-Daban, and East Aldan (at the edges of the Siberian platform) [4,6,16]. The largest rare-metal multicomponent deposits are confined to this type of carbonatite: the giant Nb-REE Tomtor deposit (Yakutia); large Nb-P deposits in Eastern Siberia—White Winter, Middle Winter (East Sayan province); the Nb-REE Chuktukonskoe deposit (Chadobetsky Uplift); the Nb-Ta-P Neske-Vaara (Kola region) deposits; and some others.

Carbonatites of folded regions are often associated with alkaline-gabbroid and alkaline-syenite magmatism [7–12,17–24]. Carbonatites of these complexes are enriched only in LILE (namely, Sr, Ba, REE), while contents of HFSE (Nb, Ta, Zr, Hf) are low. As a consequence, they have a REE-ore specialization and the largest REE deposits are associated with these carbonatites such as Mountain Pass (USA); Karasug (Central Tuva, Russia); and Dashigou, Miaoya, Daluxiang, Maoniuping (Qinling and Mianning-Dechang orogenic belts, China [11,17–19]). In the Russian territory, such complexes are found in the Altai-Sayan fold region [8,20–22], Central Tuva [23], Western Transbaikalia [12,24], and Middle Timan [25,26]. In addition, carbonatite complexes of the “linear type” associated with nepheline-syenite magmatism and/or with linear zones of alkaline metasomatites are found in the folded regions of the Urals and Siberia [27–29]. They have Nb-specialization: the Nb-deposits associated with these complexes (Vish-nevogorskoe, Urals; Tatarskoe, Yenisei Ridge, E. Siberia) were the first of the carbonatite deposits in Russia where mining was carried out.

The carbonatite origin and associated rare metal deposit sources are still relevant. In this aspect, alkaline-ultramafic complexes and carbonatites formed under the conditions of continental rifting are well studied. Petrological [30] and isotope-geochemical models [31–40] of their origin have been developed in sufficient detail and make it possible to successfully interpret the origin and their sources. The isotope data suggest that the origin of alkaline-ultramafic complexes and rare-metal (Nb-Ta-REE) carbonatite deposits is associated with a deep depleted mantle source, possibly with mantle plumes (HIMU, FOZO), and mixing of plume material with an enriched mantle component of the EM1-type [31,33,36–38]. Their Sr-Nd systematics correspond to the mantle compositions according to [41].

The issue of origin and sources of carbonatite complexes and associated rare metal deposits located in folded areas is being actively discussed. In contrast to the carbonatite complexes of within craton settings, off-craton carbonatites often have a high initial $^{87}\text{Sr}/^{86}\text{Sr}$ and/or low ϵNd , which is outside the Sr-Nd mantle array [7–9,12,20–22,42]. Various models of sources for these carbonatite complexes have been proposed: (1) sublithospheric mantle sources (SCLM), which are obscured by the interaction of magmas with crustal material and fluids [8,20,42,43]; and (2) metasomatic-enriched SCLM with involvement of subducted marine sediments [17,44,45]. Mantle sources DM and EM1 types are established for the “linear type” carbonatite complexes [28,29,46] of fold array, which is common to within-plate carbonatite magmatism [47].

The Ilmeno-Vishnevogorsk (IVC), Buldym, and Chetlassky carbonatite complexes to which this article is devoted, are localized in the folded regions of the Urals and Timan, framing (from the east and northeast) the East European platform. They are represented by an ultramafic-mafic-carbonatite dyke series (Chetlassky complex) in the Middle Timan and carbonatite complexes of the “linear type” (IVC miaskite-carbonatite and Buldym ultramafic-carbonatite) in the Southern Urals. These carbonatite complexes also differ in geochemical signatures and ore specialization (a set of ore-forming and associated components and mineral type of the ores, which determines the mining type of the deposits): Nb-deposits of carbonatites are associated with the IVC complex; Nb-REE carbonatite deposits with the Buldym complex; and REE-deposits of bastnäsite carbonatites with the

Chetlassky complex. Despite an economic significance, the reasons for different rare metal enrichments of these complexes remain unclear.

The enrichment of carbonatite complexes by various ore components (Nb, Ta, REE, Sr, Ba) can be associated with intra-crustal processes (e.g., crystallization fractionation, liquid immiscibility [48,49], subsolidus remobilization, and subsequent evolution of the late hydrothermal system [50–52]). An alternative hypothesis is the enrichment of the mantle source (“metasomatic refertilization of the SCLM” according to [17]) formed by metasomatic fluids from recycled marine sediments. Testing these hypotheses on the example of carbonatite complexes of the Urals and Timan was one of the main goals of our study.

In this article, new geochemical, mineralogical, and Sr–Nd isotope data are presented on the carbonatite complexes of the Ural and Timan fold regions, and issues of their sources including sources of ore substance, genesis of ore mineralization, and ore specialization of these complexes are proposed.

2. Geological Background

The Ilmeno–Vishnevogorsk (IVC), Buldym, and Chetlassky carbonatite complexes are positioned within the Urals and Timan Fold Belts, framing (from the east and northeast) the East European platform. The major structure of the Timan orogen formed during the Neoproterozoic (Rf–V) and received the name Timanids [53–55]. Geodynamic development of the Ural collisional orogen consisted of two complete cycles: (1) Neoproterozoic, culminating in the formation of Timanids (Rf–V); and (2) Paleozoic (PZ), the main stage of folding, ending with the formation of the Uralids (C₃–P₁) [55]. Alkaline-carbonatite magmatism within the Urals and Timan Fold Belt are located in the Precambrian blocks of basement, which underwent a complicated tectonic evolution from Late Vendian orogeny (Rf–V), through the continental margin to Hercynian collisional orogeny (in the Urals).

Chetlassky alkaline–ultramafic–mafic dyke complex with carbonatite of Middle Timan was formed in the Neoproterozoic (~590 Ma, according to K–Ar and Ar–Ar dating [26,56]) and was about coeval with rifting and was maintained by plume, which was responsible for the breakup of Rodinia [55,57,58]. In addition, Neoproterozoic (700–515 Ma) gabbro-syenite, syenite, and granite magmatism as well as Paleozoic (~390 Ma) alkaline-ultramafic kimberlite and basaltic magmatism are manifested in the Timan basement rocks [26,59–61]. Early Permian (~290 Ma) ultrapotassic syenites are the latest occurrences of alkaline magmatism in Middle Timan [62].

IVC and Buldym carbonatite complexes of Southern Urals were formed in the Paleozoic (443–417 Ma (O–S), according to the U–Pb and Rb–Sr dating [63–71], which correlates to the rifting within the East European Platform [72]. Paleozoic mafic–ultramafic (O–D) and island arc volcano-sedimentary (O–D complexes) of the Urals were about coeval, forming during the opening of the Urals Ocean (see Figure 1). The collision of the East European, Siberian, and Kazakhstan continents at ~380 and ~320 Ma (D₃–C₁) formed the Main Ural Fault (MUF) and a series of submeridian strike-slip faults (Figure 1), which adjusted to the collisional deformation [55]. Accompanying the collisional strike-slip faults (Figure 1), Ilmeno–Vishnevogorsk and Buldym carbonatite complexes were brought into the upper crustal horizons, plastically deformed and recrystallized [73,74]. Collisional and postcollisional (~250 Ma) granite magmatism also occurs here [55].

2.1. Ilmeno–Vishnevogorsk and Buldym Carbonatite Complexes (Southern Urals)

The IVC miaskite–syenite–carbonatite complex is located within the East Ural collisional megazone of the South Urals, near the Main Urals Fault (MUF) and subconforms to the submeridional collisional strike-slip tectonic structures (Figure 1). IVC intrudes Archean-Proterozoic crystalline basement rocks of the Selyankino domain, composed of gneiss-granulites, migmatites (AR) and amphibolites as well as plagiogneisses with interlayers of marbles and calciphyres (PR₁). Framing of the Selyankino domain is represented by the Middle Riphean quartzite-schist strata, metaultramafics, and metagabbroids (Rf₂).

The Selyankino basement block is separated from the zone of MUF by a fault along which gabbro-ultramafic massifs (O) are associated with arc volcanogenic-sedimentary rocks (D₂) (Figure 1), suggesting the subduction of the oceanic plate beneath the Siberian craton in the Paleozoic [75].

IVC consists of two phacolith-like intrusive massifs—Vishnevogorsk and Ilmenogorsk (20–25 × 6 km), composed of K–Na plumasite nepheline syenites (miaskites) and syenites. The massifs are connected by the Central Alkaline Belt (CAB), stretching submeridionally for a distance of more than 100 km and composed by a chain of sheet-like bodies of miaskites, syenites, glimmerite-like rocks, fenite halos, alkaline metasomatites, and carbonatites (see Figure 1). Miaskite-pegmatites (nepheline-feldspar, nepheline-cancrinite-feldspar) and syenite-pegmatite (biotite-feldspar, pyroxene-feldspar) are widespread in both endo- and exocontacts of miaskite massifs.

Carbonatites with pyrochlore mineralization form sheet-like and vein bodies in the apical part of the Vishnevogorsk massif and in the CAB. Carbonatite veins and stockworks also occur in fenite halos of miaskite intrusions. Siliciocarbonatites (sövites I) are represented by massive, fluidal, and taxite calcite varieties, with nepheline, potassium feldspar, albite, biotite, and sometimes pyroxene, with accessory black uranpyrochlore, rarely brown pyrochlore (with black pyrochlore core), zircon, ilmenite, apatite, magnetite, pyrrhotite, and pyrite. Calcite carbonatites (sövites II) are leucocratic, coarse-grained, with a banded distribution of silicate and accessory minerals, with large (up to 10–20 cm) crystals of biotite, albite, apatite and red pyrochlore, ilmenite, zircon, magnetite, pyrrhotite, and pyrite. In fenites, vein and stockwork-like calcite carbonatites contain aegirine-augite, orthoclase, biotite, apatite, titanite, red pyrochlore, ilmenite, magnetite, pyrrhotite, pyrite, zircon, monazite, ortite, and chevkinite.

The Buldym ultramafic–carbonatite complex includes the Buldym, Spirikhinsky, and Khaldikhinsky massifs with carbonatites (see Figure 1). The massifs are composed of metadunites, olivine-enstatite rocks, olivinite, with linear zones of alkaline metasomatites and carbonatites. Carbonatites of dolomite–calcite composition (sövites III) contain amphiboles of the richterite–magnesianferrosilite series, micas of the phlogopite–tetraferriphlogopite series, and accessory red-brown pyrochlore, magnetite, ilmenite, pyrrhotite, pyrite, zircon, and are accompanied by thick zones of phlogopite–richterite metasomatites. In addition, dolomite carbonatites (beforsites) are found containing monazite, aeshinite, rare earth pyrochlore, columbite, fersmite, apatite, ilmenite, zircon, strontianite, and other accessory minerals.

The largest Vishnevogorsk Nb-deposit in the IVC is confined to the northern ending of the miaskite massif. It represents three ore zones of pyrochlore-bearing carbonatites and miaskite-pegmatites. The first ore zone (147 zone) is 4 km long and 30 m wide (see Figure 1b). It is composed of sheet-like and vein bodies of carbonatites up to 10 m thick and hundreds of meters long at the endocontact of the miaskite massif. The second ore zone (140 zone) is confined to the northern satellite miaskite-syenite body (“saddle deposit”), lying 50 m north of the Vishnevogorsk massif, and is composed of subparallel veins of carbonatites, albitites, and miaskite pegmatoids. The third ore zone (125 zone) is located in the fenite halo of the Vishnevogorsk intrusion among the fenitized rocks of the Vishnevogorsk gneiss-amphibolite suite, forming stockworks and vein bodies.

The Potaninskoe Nb-deposit, second in importance, is located in the Central Alkaline Belt of the IVC (see Figure 1). It is a linear, sometimes stockwork-like, zone of carbonatites in miaskites and fenites about 15 km long and up to 40 m thick. In addition, Ishkul, Baidashevskoe, Uvildinskoe, and Svetloozerskoe Nb occurrences are known here.

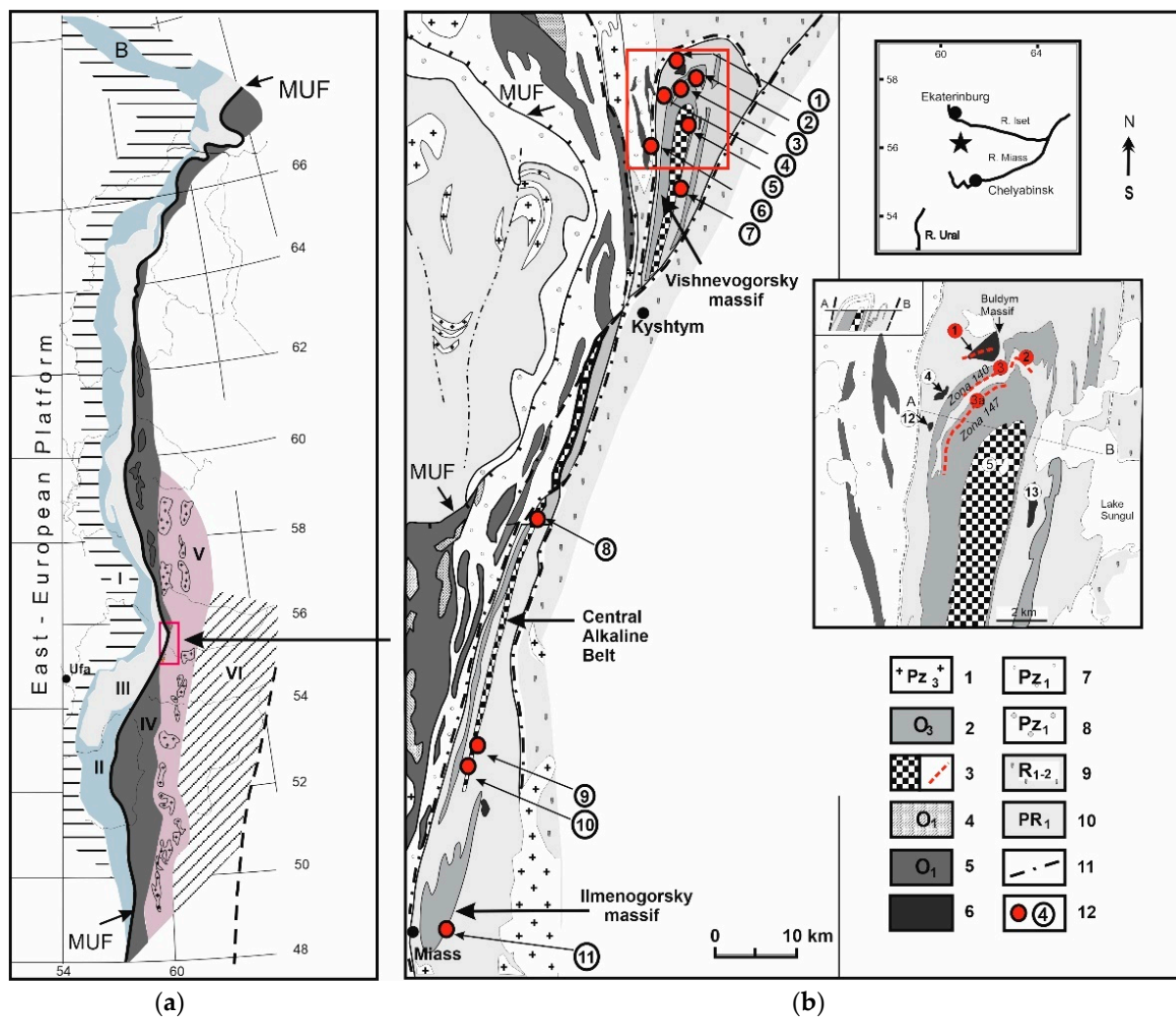


Figure 1. (a) Tectonic scheme of the Urals, after [55]. Tectonic zones: I—Preuralian foredeep (evaporites, molasse, flysch, Pz); II—West Ural megazone (sediments of the passive continental margin, O-P); III—Central Ural megazone (metasediments and volcanic rocks, Rf, with crystalline basement ledges, AR-PR₁); MUF—suture zone of the Main Ural Fault (serpentinites, megabreccias, high pressure rocks (eclogites, etc.), mafic-ultramafic complexes, O-D); IV—Tagilo-Magnitogorsk megazone (island arc sedimentary-volcanic complexes, O₂–D₃); V—East Ural megazone (tectonic collage of gneisses, granite intrusions, Pz, island-arc, O-D, collisional complexes, D-P, and “microcontinents”, AR-PR); VI—Transuralian megazone; (b) Geological map of the Ilmeno–Vishnevogorsk and Buldym carbonatite complexes (Southern Urals) with the main deposits and ore occurrences of Nb, Zr, and REE (based on [27,76]). 1—granites (Pz₃); 2, 3—Ilmeno–Vishnevogorsk complex (O₃): 2—miaskites of the Vishnevogorsk and Ilmenogorsk massifs, 3—zones of metasomatites, carbonatites, silicate-carbonate rocks of the Central Alkaline Belt (CAB); 4—gabbro of the ophiolite formation (O₁); 5—ultrabasites of the ophiolite formation (O₁); 6—metaultramafics of the Buldym complex; 7—volcanogenic-sedimentary strata of the Tagilo-Magnitogorsk megasyclineorium (Pz₁); 8—garnet-mica schists and eclogites (Pz₁); 9—plagioschists and quartzites (R₁₋₂); 10—plagiogneisses, granite migmatites, crystalline schists, amphibolites, quartzites (Selyankino domain, AR-PR₁₋₂); 11—tectonic faults and unconformities; 12—main deposits and ore occurrences of Nb and REE associated with carbonatites (numbers in circles): 1—Buldym (Nb and REE), 2, 3—Vishnevogorskoe—Nb (2—zone 125; 3—zone 140, 3a—147), 4—Spirikhinskoe (REE), 5—Svetlinskoe (Nb), 6—Kaganskoe (REE), 7—Potaninskoe (Nb), 8—Uvildinskoe (Nb), 9—Baidashevskoe (Nb), 10—Ishkulscoe (Nb), 11—Ilmenskoe, 97 mine (Nb and REE), 12—Khaldikhinskoe, 13—Sungulskoe.

The largest Nb–TR-deposit of the Buldym complex is associated with carbonatites and alkaline metasomatites in the Buldym ultramafic massif. Pyrochlore carbonatites form vein zones of hundreds of meters long and are accompanied by thick carbonate-phlogopite-richterite, phlogopite-richterite, and phlogopite metasomatites bearing Nb and REE mineralization. The total thickness of the carbonatite zones and their accompanying

metasomatites reach 50 m. The Spirikhinskoe REE-deposit as well as the Khaldikhinskoe and Ilmensky Nb-REE ore occurrences are associated with the ultramafic-carbonatite complex (see Figure 1).

2.2. Chetlassky Carbonatite Complex (Middle Timan)

The Chetlassky complex of dyke K-alkaline ultrabasites and carbonatites is located in the Middle Timan, occupying an area of about 1000 km², in the southeastern part of the Chetlassky Kamen, which is a ledge of Riphean rocks in the pericratonic trough of the East European platform (Figure 2). The host rocks for the Chetlassky complex are terrigenous and terrigenous-carbonate strata of the Chetlassky (Rf₂) suite and the Bystrinsky (Rf₃) series. Ultramafic dyke bodies trace northeast-trending faults, forming dyke fields (Kosyu, Mezenskoe, Bobrovskoe, and Oktyabrskoe, etc.) in which there are several thousand dykes. Alkaline metasomatites (fenites, phlogopite, and feldspar metasomatites) and carbonatites as well as goethite-feldspar and quartz-goethite-hematite hydrothermal rocks are found in close spatial, structural, and temporal connection with ultrabasic dykes.

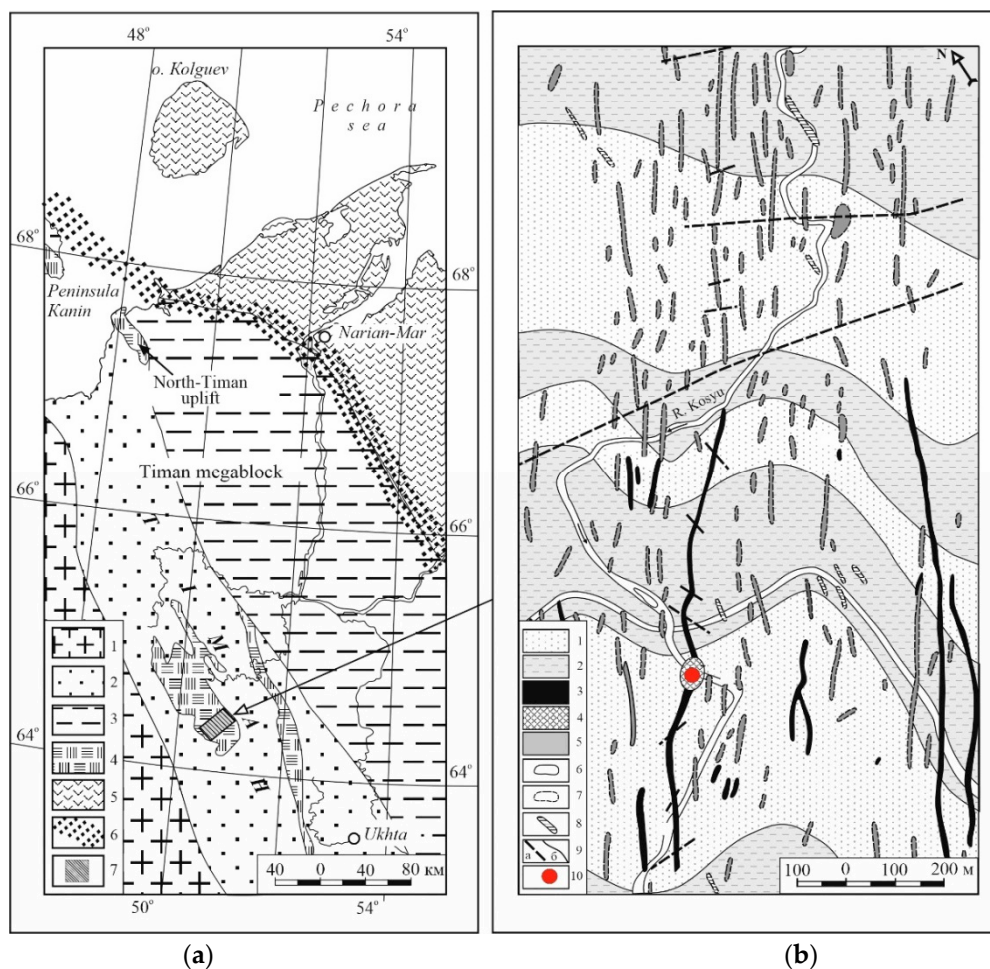


Figure 2. (a) Tectonic scheme of the Middle Timan (after [25]): 1—East European Craton; 2–5—basement of the Pechora plate: 2—Timan; 3—Izhemsky zone; 4—outcrops of the basement complexes; 5—Pechora zone; 6—Pripechorsko-Ilych-Chikshinskaya fault zone; 7—Chetlassky dike complex with carbonatites; (b) Geological scheme of Chetlassky complex (in the central part of the Kosyu field), after [54]: 1, 2—terrigenous sediments of Chetlassky suite (PR₂ ct₂): 1—quartz and feldspar-quartz sandstones and fenitized quartzites; 2—argillite and siltstone; 3–5—magmatites of Chetlassky complex: 3—picrites, lamprophyres and breccias, 4—Kosyu massif carbonatites; 5—alkaline and subalkaline gabbros. Intrusive bodies: 6—bodies fixed by outcrops, 7—submerged bodies, 8—bodies alleged by geophysical survey; 9—faults, 10—REE-Kosyu occurrence.

The Chetlassky dyke complex is composed of picrite-lamprophyric rock series. The most magnesian varieties are represented by subalkaline picrites and are comparable to veined “kimberlite-picrites” [26,77,78]. The lamprophyres of the alneite–polzenite [25] and spessartite–kersantite series [60,79] have been identified. It should be noted that a significant part of the dyke ultramafics is composed of carbonate-bearing lamprophyres, containing, along with phlogopite and pyroxene, carbonate (5–50%), apatite, amphibole, and garnet.

Dyke ultramafic rocks of the Chetlassky complex are holocrystalline rocks of porphyry and “amygdaloid” structure, containing phenocrysts of olivine (7–30% to 60%), clinopyroxene (augite-Ti-augite) (5–40%), phlogopite (5–30%), and poikilocrysts of phlogopite in the microlite phlogopite-pyroxene matrix. There are often also carbonate (up to 20%), and sometimes apatite, garnet, and amphibole in the matrix. Along with phenocrysts, the rocks contain megacrysts of olivine, bright green clinopyroxene, and brownish-green Cr-spinel as well as xenoliths of serpentinites, serpentine-talc rocks, fenitized gneisses, and schists. Alkaline varieties of picrites and lamprophyres (Kosyu area) contain phenocrysts of olivine, clinopyroxene, and phlogopite as well as megacrysts of olivine and brownish-green spinel, the matrix is composed of acicular bluish-green amphibole, carbonate, apatite, and tetraferriphlogopite. Olivine phenocrysts are replaced by serpentine and carbonate. These rocks are associated with veins of calcite-dolomite-ankerite carbonatites with REE-mineralization.

REE-carbonatites and accompanying alkaline metasomatites are localized in the same northeastern tectonic zones as dyke ultramafic rocks. Carbonatites compose vein-like bodies, stockworks, and carbonatization zones; they often occur in selvages of ultramafic bodies. The largest carbonatite occurrence is known in the Kosyu, in the area of the swelling of an alkaline ultramafic dyke (Figure 2). Carbonatites form a stock about 100 m in diameter (Kosyu River massif), phlogopite and feldspar metasomatites, and melanocratic fenites are widely represented. Carbonatites are composed of fine- and micro-grained dolomite-ankerite-siderite aggregates (less often calcite, magnesite) and contain micas (phlogopite-tetraferriphlogopite series), sometimes alkaline amphiboles (arfvedsonite-eckermanite series), aegirine, K-feldspar, albite, quartz, and chlorite. Accessory minerals of carbonatites: monazite, bastnäsite, ortite, barite, thorite, ilmenorutile, apatite, titanite, magnetite, ilmenite, and less pyrochlore, columbite, baddeleyite, zircon [26,80–83] as well as apatite, magnetite, pyrite, chalcopyrite, galena, sphalerite, and pyrrhotite. There are also stockwork arcuate zones of goethite-feldspar rocks and quartz-goethite-hematite steeply dipping veins and veinlets, which cross-cut all rocks of the massif, completing the process of carbonatite formation. Additionally, widely developed in these rocks are REE-Th-Nb mineralization: monazite, bastnäsite, xenotime, columbite, ilmenorutile, thorite, and unusual species of thorium phases in REE-carbonates [83–85].

3. Materials and Methods

The electron probe microanalysis (total of 330 EPMA) of ore niobium minerals (pyrochlores and aeschinites, 25 samples, Tables 1 and 2) from deposits of the Ilmeno–Vishnevogorsk and Buldym complexes (Urals) and ore mineralization (rare-metal carbonates and phosphates) from Kosyu carbonatites of the Chetlassky complex (Middle Timan) was carried out on a Cameca SX100 microanalyzer with five wavelength dispersive spectrometers and a Bruker XFlash 6 (Bruker) energy dispersive spectrometer (“Geoanalyst” Center, IGG UD RAS, Ekaterinburg, D.A. Zamyatin, V. Bulatov) and on the “CAMEBAX-micro” at the IGM SD RAS, Novosibirsk (analyst V.V. Sharygin). The following standards were used: apatite (F, P), jadeite (Na), rhodonite (Mn), orthoclase (K), CaSiO₃ (Ca, Si), TiO₂ (Ti), Fe₂O₃ (Fe), ThO₂ (Th), UO₂ (U), PbS (Pb), Nb, Ta, SrSO₄ (Sr), BaSO₄ (Ba), Al₂O₃ (Al), and aluminosilicate glasses doped with REE (La, Ce, Y, Sm, Pr, Nd); the concentrations of Mg, Ca, Si in carbonate-containing minerals were determined using dolomite (Mg), calcite (Ca), and diopside (Si). The parameters of the electron probe microanalysis of carbonates and phosphates were as follows: accelerating voltage 15 kV, probe current 15 nA, beam size 5 μm (apatites and

silicates), and 20 µm (carbonates). The measurement time at the maximum line intensity was 10 s, and for the background it was 5 s. The analysis of the pyrochlores and aeschinites was carried out at an accelerating voltage of 15 kV and an electron probe current of 40 nA using crystal analyzers: TAP, LPC0, LPET, PET, and LIF. The pulse accumulation time at the peak maximum was chosen from 10 to 30 s. The detection limits for F, Fe, Mn, Ti, Pb, La, Y were 0.075–0.1 wt%; Sr, U, Nb, Sm, Ce, Pr, Nd, Ta—0.15–0.2 wt%; and Na, Al, Si, P, Ca, Ba, Th <0.05 wt%.

The sections and grain surface morphology of pyrochlores and aeschinites of the Ural carbonatite complexes as well as rare-metal carbonates and phosphates from Kosyu carbonatites were studied using scanning electron microscopy (SEM). The images of micro-objects were obtained and their composition was analyzed using a Jeol JSM-6390LV (JEOL) scanning electron microscope with INCA Energy 450 X-Max 80 (Oxford Instruments) energy-dispersive spectrometer (“Geoanalyst”, IGG Ud RAS, S.P. Glavatskikh and I.A. Gottman).

Major elements for rocks and ores (19 samples from Ural carbonatite complexes, Table 3, and 13 samples from Chetlassky carbonatite complex of Timan, Table 4) were analyzed by wet chemistry and XRF at the Institute of Geology and Geochemistry UD RAS in Ekaterinburg and at the Institute of Geology Komy Science Center UD RAS in Syktyvkar. The trace and rare element concentrations were determined using acid decomposition of the samples and subsequent mass-spectrometric analysis on a high-resolution tandem-analyzer with ionization in an inductively coupled plasma “HR-ICP-MS Element 2” (IGG UD RAS, Ekaterinburg). The error of multielement analysis is no more than 8–10% if the content of an element is 10–20 times higher than its detection limit.

Sr and Nd isotope compositions and concentrations in carbonates, apatites, amphiboles of carbonatites and whole-rock samples (miarctites, syenites, carbonatites, fenites) of the Ilmeno–Vishnevogorsk and Buldym (olivinites and peridotites) complexes as well as host rocks (calciphyre and plagiogneiss) of the Vishnevogorsk and Ilmenogorsk series (South Urals) were determined at the IGG UD RAS (Ekaterinburg) and GI KSC RAS (Apatity) on a Finnigan MAT-262 (RPQ) seven-channel mass spectrometer in static mode (Table 5). Sm–Nd and Rb–Sr isotope systems of rare-metal minerals (pyrochlore and eschinite groups) of the Urals’ carbonatite complexes were studied by isotope dilution and mass spectrometry using high-resolution mass spectrometers—TRITON, ICP-MS NEPTUNE Plus, Finnigan MAT-262 (Apatity, St. Petersburg, Ekaterinburg) (Table 5). The analytical details of measurements are described in [28].

Measurements of the isotopic composition and concentrations of Sr and Nd in carbonates and apatites from carbonatites of the Chetlassky complex and whole-rock samples (carbonatites and carbonate-bearing lamprophyres) as well as host rocks (dolomite) of the Bystrinskaya Group (Middle Timan) were fulfilled at the IGG UD RAS (Ekaterinburg) by the isotope dilution and mass spectrometric method using a Finnigan MAT-262 (RPQ) seven-channel mass spectrometer in static mode (Table 5). The analytical details of the measurements are described in [28].

4. Results

4.1. Rare Metal (Nb–REE) Ore Mineralization

IVC and Buldym rare-metal mineralization is represented by minerals of the pyrochlore, aeschinite, columbite groups, ilmenite, zircon, titanite, monazite-Ce. Rare-metal accessory minerals such as ilmenorutile, fersmite, thorianite, orthite, davidite-(Ce), britolite-Ce, cerite-(Ce), cerianite-(Ce), bastnäsite-Ce, bastnäsite-(La), synchysite-(Ce), röntgenite-(Ce), ankylite-(Ce), strontianite, barilite, burbankite, chevkinite-(Ce), xenotime-(Y), and catapleite, yttrialite-(Y), huanghoite-(Ce), parisite-(Ce), fergusonite-(Ce) lucasite-(Ce), baddeleyite, and zirconolite are less common [27,86–99]. In the Chetlassky carbonatites, monazite and bastnäsite are widespread, and the rare ilmenorutile, columbite, sphene, ilmenite, pyrochlore, [56], ankylite, strontianite, carbocernaite, thorite/hattonite, anglesite, U-pyrochlore, zircon, baddeleyite, xenotime, and molybdenite were found [80–85].

Since the article is devoted to the ore specialization of carbonatite complexes, we describe precisely only the Nb and REE ore minerals that provide economic interest of ore components. We studied 25 samples of Nb minerals of the pyrochlore and aeschinite groups from the main Nb-deposits and ore occurrences of the Urals' carbonatite complexes (IVC and Buldym) and 10 samples of REE minerals—monazites and REE-carbonates from Kosye REE-occurrence of the Chetlasky complex, Middle Timan. From the IVC, two pyrochlore samples of pegmatoid miaskites, three pyrochlore samples of miaskite-pegmatites (Vishnevogorskoe deposit; Uvildinskoe occurrence), three samples of syenite-pegmatites (Vishnevogorskoe deposit, ore zone 125; Potaninskoe deposit), three samples of sövites I (Potaninskoe deposit, Uvildinskoe occurrence), and eight samples of sövites II (Vishnevogorskoe deposit, ore zone 147, 140, 125) have been studied. In the Buldym complex, pyrochlores from the dolomite-calcite carbonatites (sövites III) and associated phlogopite-richterite metasomatites as well as pyrochlores and aeschinites from beforosite, glimmerite-like rocks, and metasomatites (six samples) were studied. From the Chetlasky complex, monazites, REE-fluorocarbonates and REE-Ca-carbonates (10 samples) were investigated.

Ilmeno–Vishnevogorsk complex (IVC). Ore concentrations of Nb in the IVC carbonatites and miaskites-pegmatites are controlled by the distribution of the pyrochlore group minerals [27]. Accessory Nb-bearing minerals such as aeschinite-(Ce), aeschinite-(Y) columbite, chevkinite-(Ce), and fersmite are found in the fenite halos, in biotite-feldspar, aegirine-feldspar syenite-pegmatites, late quartz-aegirine-amphibole veins, and are rare [87,95]. Representative compositions of IVC pyrochlore varieties of different stages of ore formation are given in Table 1.

In the IVC miaskite-pegmatites, pyrochlore is present in the form of scattered dissemination of black and dark brown (Pcl I, uranpyrochlore). Light brown pyrochlore (Pcl II) occurs as grains and octahedral crystals up to 0.5 cm in size (in miaskite-pegmatites—up to 10 cm (Figure 3a) as well as of 1–10 µm pyrochlore inclusions in nepheline grains, feldspars, and zircon.

In silicocarbonatites (sövites I) and in glimmerite-like carbonate-silicate rocks of the IVC (Potaninskoe deposit, Uvildinskoe ore occurrence, CAB), pyrochlore is also represented by a U-(Ta)-enriched variety (Pcl I, uranpyrochlore) and occurs in the form of small crystals and rounded grains of black and greenish-black color 0.05–1 mm in size. The surface of uranpyrochlore grains often has spherical cavities, which are likely to represent destruction from the alpha particle path as a result of U and Th radioactive decay (Figure 3d). Often, uranpyrochlore grains and crystals from the edges and along the cracks underwent secondary changes of varying degrees with the formation of concentric textures (Figure 3e). Sövites I also contains dark-brown pyrochlore grains (Pcl II) with multiphase inclusions (apatite, calcite, potassium feldspar, chlorite, titanomagnetite) (Figure 3f).

Late carbonatite (sövites II) pyrochlores of the IVC Vishnevogorsk deposit form red-brown, yellow, and orange octahedral and cuboctaeric crystals, 0.05–1.5 cm in size (Pcl III) with inclusions of calcite, apatite, potassium feldspar (Figure 3b,h,i). Bright red and red-brown pyrochlore also occurs in syenite-pegmatite and fenites (Figure 3c). There are crystals of a complex structure with relic cores composed of black U-containing pyrochlore surrounded by rims of newly formed bright red pyrochlore (Pcl IV) (Figure 3g). These features of the internal structure of pyrochlore grains can be associated with its formation as a result of early pyrochlore dissolution and, impossible, new growth of pyrochlore at the later stages of ore formation.

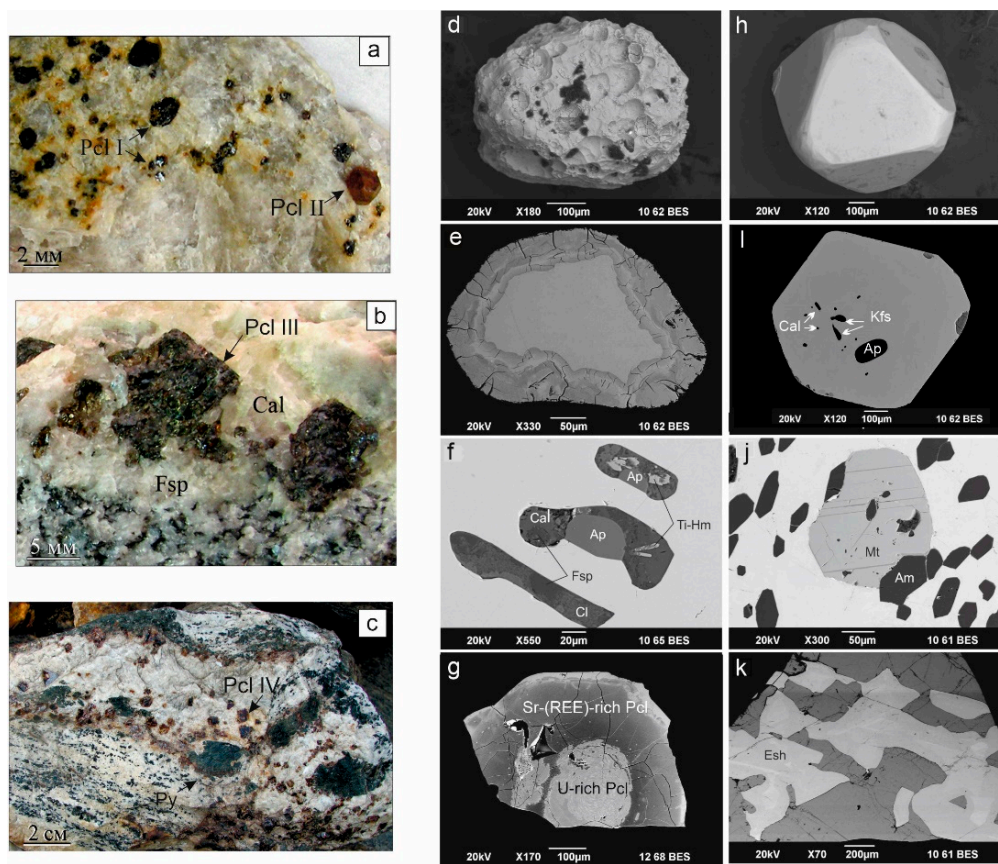


Figure 3. Morphology and inner structure of pyrochlore crystals from carbonatite complexes of the Urals. (a–c) photo: V.A. Popov [94]. Ilmeno–Vishnevogorsk complex: (a) black and light-brown pyrochlore grains and crystals in miaskite-pegmatite, Vishnevogorskoe Nb-deposit; (b) pyrochlore crystals with biotite (Bt) and calcite (Cal) in carbonatite veins (sövite II), ore zone 140, Vishnevogorskoe deposit; (c) pyrochlore crystals in feldspar-pyroxene vein fenite, ore zone 125, Vishnevogorskoe deposit; (d) grain of U-(Ta)-pyrochlore with spherical cavities (sövite I), Potaninskoe deposit; (e) inner structure of hydrated U-(Ta)-pyrochlore (sövite I); (f) multiphase inclusions in the grain of fluorocalciopyrochlore (sövite I); (g) inner structure of a pyrochlore crystal: a relict core composed of U-containing pyrochlore (light-gray in the BSE) bordered by (Sr-REE)-pyrochlore (dark gray) (sövite II, Vishnevogorskoe deposit); (h,i) cuboctahedral crystal of (Sr-REE)-pyrochlore with inclusions of calcite, apatite, feldspar (sövite II, Vishnevogorskoe deposit). Buldym complex: (j) pyrochlore crystals with numerous inclusions of amphibole and magnetite from phlogopite-richterite metasomatites; (k) pyrochlore in intergrowth with aeshinite, Buldym deposit. Py—pyroxene, Am—amphibole, Fsp—feldspar, Kfs—K-feldspar, Mt—magnetite, Ti-Hm—titanium-hematite, Cal—calcite, Ap—apatite, Cl—chlorite, Esh—aeshinite.

The REE-mineralization in the IVC is represented by phosphates (monazite-(Ce), rabdophanite-(Ce)), silicates (orthite-(Ce), chevkinite-(Ce), britolite-Ce, cerite-(Ce)), fluorocarboxides (bastnäsite-(Ce), bastnäsite-(La), synchysite-(Ce), parisite-(Ce), röntgenite-(Ce)), and Sr-REE-carbonates (ankylite-(Ce), burbankite) [86,87,91,93,97,98]. This mineralization is found in the fenite halo (in fenites and fenitized gneisses, in syenite-pegmatites, in late quartz, calcite, and quartz-arfvedsonite veins), outside the miaskite-carbonatite massifs and ore zones. REE-mineralization is manifested very locally in the IVC without any high ore concentrations, and therefore is not described in detail here.

Buldym complex. In the Buldym complex, the Nb ore concentrations are associated with pyrochlore group minerals. Although pyrochlore is the main Nb-bearing ore mineral, aeshinite and columbite are also present in significant quantities [27]. The REE ore concentrations in the Buldym carbonatites and phlogopite-richterite metasomatites are associated with monazite [27]. Accessory REE-minerals such as aeshinite-(Ce), ortite-(Ce), fergusonite-(Ce), chevkinite-(Ce), allanite, and rare polyakovite-(Ce), bastnäsite-(Ce), synchysite-(Ce), parisite-(Ce), and davidite-(Ce) also occur [89,99]. Optical and back-scattered electron

(BSE) images of pyrochlore and aeschynite varieties of the Buldym complex are shown in Figure 3. Representative compositions of pyrochlore and aeschynite group minerals of Buldym complex are given in Table 1.

Table 1. Representative compositions (wt%) of the pyrochlore and aeschynite group minerals of carbonatite complexes of the Urals.

Sample	Pcl I			Pcl II		Pcl III		Pcl IV		Pcl V		Aesh	
	1	2	3	4	5	6	7	8	9	10	11	12	13
	37–95	Soln-1	K2-18	Do-21	43–62	140-1	3296	92	B-331	31-6c	31-6m	31-6r	2–23
Nb ₂ O ₅	38.72	40.58	46.29	64.76	61.56	65.64	66.95	59.97	64.66	60.33	52.08	59.26	44.65
Ta ₂ O ₅	4.02	3.90	0.84	2.21	3.21	0.19	-	-	0.22	0.31	-	-	0.01
SiO ₂	-	-	0.04	-	-	-	0.02	-	-	1.58	-	-	-
TiO ₂	12.50	12.42	8.52	4.32	4.85	4.78	2.96	6.89	4.50	4.45	4.42	3.51	14.58
UO ₂	22.11	23.75	17.57	0.07	1.81	0.07	-	0.42	2.78	3.72	3.72	0.85	0.04
ThO ₂	0.78	0.45	0.69	0.45	1.78	0.27	0.51	1.01	0.41	0.30	0.53	0.59	9.34
Fe ₂ O ₃	0.00	0.19	1.54	0.02	0.11	0.02	0.01	0.07	-	1.52	1.69	1.50	2.20
Y ₂ O ₃	0.12	-	0.11	-	-	-	-	0.10	-	0.10	-	0.03	0.48
La ₂ O ₃	0.31	0.00	0.18	0.32	0.12	0.61	0.05	1.15	0.55	0.37	0.70	1.08	4.29
Ce ₂ O ₃	0.72	0.00	0.40	1.10	0.73	1.27	0.20	2.87	1.45	1.52	2.42	2.98	11.28
Nd ₂ O ₃	0.94	0.19	0.84	0.22	0.24	0.31	0.06	0.96	0.39	n.a.	n.a.	n.a.	3.48
MnO	-	0.09	0.11	-	-	-	0.01	0.02	0.03	0.21	0.42	0.50	0.08
CaO	11.06	12.02	13.91	15.08	15.48	16.06	16.21	13.19	13.74	11.68	6.04	12.24	6.26
BaO	-	-	-	-	-	-	-	-	-	0.77	2.39	0.73	0.20
SrO	0.28	-	0.17	1.00	0.51	0.56	0.67	0.92	1.29	1.97	5.01	3.27	0.06
PbO	0.91	1.00	0.95	-	-	0.25	0.04	0.21	0.29	0.48	0.31	0.05	0.00
Na ₂ O	5.11	5.16	4.88	6.99	6.37	7.23	7.50	7.56	6.94	3.64	0.05	2.09	0.12
F	1.00	1.02	1.76	4.72	4.42	4.59	4.33	5.13	3.75	2.76	0.24	2.13	-
Total	98.56	100.77	98.79	101.24	101.20	101.85	99.51	100.46	101.00	95.71	80.02	90.82	97.07
O = F2	0.42	0.43	0.74	1.99	1.86	1.93	1.82	2.16	1.58	1.16	0.10	0.90	0.00
Total	98.14	100.34	98.05	99.27	99.34	99.92	97.69	98.30	99.42	94.55	79.92	89.92	97.07
Nb, apfu	1.250	1.270	1.455	1.767	1.716	1.780	1.861	1.676	1.789	1.632	1.673	1.753	1.231
Ta	0.078	0.073	0.016	0.036	0.054	0.003	-	-	0.004	0.005	-	-	-
Ti	0.672	0.647	0.445	0.196	0.225	0.216	0.137	0.320	0.207	0.200	0.236	0.173	0.668
Fe ³⁺	-	0.010	0.081	0.001	0.005	0.001	0.001	0.003	0.000	0.068	0.090	0.074	0.101
Si	-	-	0.003	-	-	-	0.001	-	-	0.095	-	-	-
Sum B	2.000	2.000	2.000	2.000	2.000	2.000	2.000	2.000	2.000	2.000	2.000	2.000	2.000
Ca	0.847	0.892	1.036	0.975	1.023	1.032	1.068	0.874	0.901	0.749	0.460	0.858	0.409
Mn	-	0.005	0.007	-	-	-	0.001	0.001	0.002	0.011	0.025	0.028	0.004
Ba	-	-	0.000	-	-	-	-	-	-	0.018	0.067	0.019	0.005
Sr	0.011	-	0.007	0.035	0.018	0.019	0.024	0.033	0.046	0.068	0.206	0.124	0.002
Pb	0.018	0.019	0.018	-	-	0.004	0.001	0.003	0.005	0.008	0.006	0.001	-
Na	0.708	0.693	0.657	0.818	0.761	0.841	0.894	0.906	0.824	0.422	0.007	0.265	0.015
Y	0.004	-	0.004	-	-	-	-	0.003	0.000	0.003	0.000	0.001	0.016
LREE	0.051	0.005	0.036	0.036	0.025	0.048	0.007	0.112	0.053	0.041	0.081	0.097	0.424
U	0.351	0.366	0.272	0.001	0.025	0.001	-	0.006	0.038	0.050	0.059	0.012	0.001
Th	0.013	0.007	0.011	0.006	0.025	0.004	0.007	0.014	0.006	0.004	0.009	0.009	0.130
Sum A	2.003	1.986	2.047	1.871	1.877	1.949	2.001	1.953	1.874	1.374	0.920	1.414	1.004
A- deficit	-0.003	0.014	-0.047	0.129	0.123	0.051	-0.001	0.047	0.126	0.626	1.080	0.586	-
F	0.225	0.223	0.388	0.900	0.861	0.871	0.843	1.004	0.726	0.522	0.054	0.441	-

Note. 1–3—**uranpyrochlore I** (oxy- and hydroxylcalciopyrochlore according to [100]): 1—from sövite I (Potanino deposit), 2—from miaskite-pegmatite (Uvildy); 3—from glimmerite (Buldym); 4, 5—**pyrochlore II** (Ta-containing fluorcalciopyrochlore [100]): 4—from miaskite-pegmatite (Vishnevogorsk deposit), 5—from sövite I (Potanino deposit); 6, 7—**pyrochlore III** (fluorcalciopyrochlore [100]): 6—from sövite II (ore zone 140, Vishnevogorsk deposit), 7—from sövite III (Buldym deposit); 8, 9—**pyrochlore IV** (REE-Sr fluorcalciopyrochlore [100]): 8—from sövite II (Potanino deposit), 9—from sövite II (Vishnevogorsk deposit); 10–12—**pyrochlore V** (Sr-REE-Ba—hydroxyprochlore and hydroxylcalciopyrochlore [100]), altered grain of pyrochlore from sövite II (Vishnevogorsk deposit): 10—U-rich relict core, 11, 12—REE-Sr-rich rims; 13—Ce-nioboaeschnite from beforite IV (Buldym deposit). Formulae calculated to two cations in the B site. A-deficit is the number of vacancies at the A-site. Pcl—pyrochlore, Aesh—aeschnite. (-) is below detection limit. n.a.—not analyzed. Geographic coordinates of the studied samples: Do-21: N55°59.589, E60°38.918; 140-1: 56°00'623, E60°37'777.

In dolomite-calcite carbonatite (sövites III), pyrochlores are represented by red-brown crystals and 0.5–10 cm grains (Pcl III). The associated phlogopite-richterite metasomatites contain a fine dissemination of yellow-brown pyrochlore with numerous inclusions of amphibole (fluorrichterite) (Figure 3j). Beforsite contain unevenly colored black-brown pyrochlore (Pcl IV), which is partially replaced by columbite. Pyrochlore, which has been replaced by aeschinite is described in the beforsites of the Buldym massif [90]. In addition, REE- and Nb-REE-minerals such as monazite and aeschinite are widespread in beforsites and associated phlogopite-richterite, phlogopite metasomatites, while ortite, fergusonite, chevkinite, and polyakovite are less common.

Chetlassky complex. The REE ore concentrations in the Chetlassky carbonatite are associated with bastnäsite and monazite. REE-fluorocarbonates (bastnäsite-(Ce), bastnäsite-(La), parisite-(Ce)), Sr-REE-carbonates (ankylite-(Ce), burbankite), monazite-(Ce), monazite-(La), REE-phosphates (monazite-(Ce), and monazite-(Ce), xenotime) are present in significant amounts in carbonatites and late goethite-feldspar and quartz-goethite-hematite veins [82]. The Nb-mineralization in the Chetlassky carbonatites represented by pyrochlore, columbite, and ilmenorutile group minerals [82,83,85], but in minor quantities. Since Nb-mineralization of the Chetlassky complex does not provide significant ore concentrations, it is not described in detail here. Representative compositions (wt%) of monazites and bastnäsites of the Chetlassky complex are given in Table 2.

Table 2. Representative compositions (wt%) of monazite and bastnäsite.

Sample	Monazites						Bastnäsites				
	1	2	3	4	5	6	7	8	9	10	11
	Pol-8	Pol-9	3-15	2-1	2-2	3-14	3-19	1385(5)	1385(3)	1385(4)	1385(11)
CaO	2.5	1.5	0.15	0.42	-	2.31	2.2	1.29	2.36	1.18	1.29
La ₂ O ₃	21.09	23.4	11.2	12.09	14.53	18.31	20.45	32.51	26.46	32.75	31.44
Ce ₂ O ₃	30.20	32.31	29.72	25.95	33.79	5.89	6.15	34.43	35.93	34.51	33.92
Pr ₂ O ₃	2.37	2.86	3.59	2.59	3.68	6.03	6.46	n.a.	n.a.	n.a.	n.a.
Nd ₂ O ₃	6.24	5.85	14.5	12.3	11.61	29.29	25.53	3.72	5.90	3.93	4.59
Sm ₂ O ₃	1.00	0.26	2.01	3.94	1.54	4.01	3.11	n.a.	n.a.	n.a.	n.a.
Gd ₂ O ₃	0.81	0.26	1	3.3	1.25	1.01	0.5	n.a.	n.a.	n.a.	n.a.
ThO ₂	n.a.	n.a.	3.42	9.27	0.31	0.82	-	n.a.	n.a.	n.a.	n.a.
PbO	n.a.	n.a.	0.49	0.61	0	1.24	2.79	n.a.	n.a.	n.a.	n.a.
P ₂ O ₅	32.20	30.09	33.39	28.36	31.45	29.92	29.54	-	-	-	-
F	-	-	-	-	-	-	-	4.33	4.42	3.34	1.47
CO ₂ *	-	-	-	-	-	-	-	20.00	20.17	20.05	19.8
H ₂ O *	-	-	-	-	-	-	-	2.04	2.03	2.52	3.35
O = F2	-	-	-	-	-	-	-	1.82	1.86	1.41	0.62
Total	96.41	96.53	99.47	98.83	98.16	98.83	96.73	96.50	95.42	96.88	95.25
Ca	0.106	0.063	0.007	0.018	0.000	0.094	0.184	0.051	0.092	0.046	0.05
La	0.308	0.340	0.175	0.181	0.220	0.256	0.294	0.439	0.354	0.441	0.429
Ce	0.437	0.466	0.460	0.385	0.509	0.082	0.088	0.462	0.477	0.461	0.459
Pr	0.034	0.041	0.055	0.038	0.055	0.083	0.092	n.a.	n.a.	n.a.	n.a.
Nd	0.088	0.082	0.219	0.178	0.171	0.397	0.356	0.049	0.076	0.051	0.061
Sm	0.014	0.004	0.029	0.055	0.022	0.052	0.042	n.a.	n.a.	n.a.	n.a.
Gd	0.013	0.004	0.017	0.053	0.020	0.015	0.008	n.a.	n.a.	n.a.	n.a.
Th	n.a.	n.a.	0.033	0.085	0.003	0.007	-	n.a.	n.a.	n.a.	n.a.
Pb	n.a.	n.a.	0.006	0.007	0.000	0.013	0.029	n.a.	n.a.	n.a.	n.a.
Total	1.000	1.000	1.000	1.000	1.000	1.000	1.000	1.000	1.000	1.000	1.000
F	-	-	-	-	-	-	-	0.501	0.507	0.386	0.172
OH	-	-	-	-	-	-	-	0.499	0.493	0.614	0.828

Note. 1, 2—monazites of Buldym carbonatite complex (S. Urals): 1—from richterite metasomatite, 2—from beforsite; 3–7—monazites of the Chetlassky carbonatite complex (M. Timan) [84]: 3–5—early isometric monazite-(Ce) (Mnz 1), 6, 7—late xenomorphic monazite-(La) (Mnz 2); 8–11—bastnäsite-(Ce) of Chetlassky complex (M. Timan): 8–10—from carbonatite, 11—from late quartz-hematite veins (Cosue REE- occurrence). CO₂ * and H₂O * calculated by stoichiometry. (-)—below detection; n.a.—not analyzed. Formula calculated to one cation.

Bastnäsite is the most abundant REE-fluorocarbonate in the Chetlassky carbonatites. It forms relatively large grains up to several hundred microns in size (Figure 4b) and is often confined to late carbonate and quartz-carbonate veinlets. In addition, Sr-REE-carbonates (ankylite-(Ce), burbankite) as well as carbocernaite, strontianite, and barite are present as abundant microinclusions in rock-forming carbonates (Figure 4a,c,d).

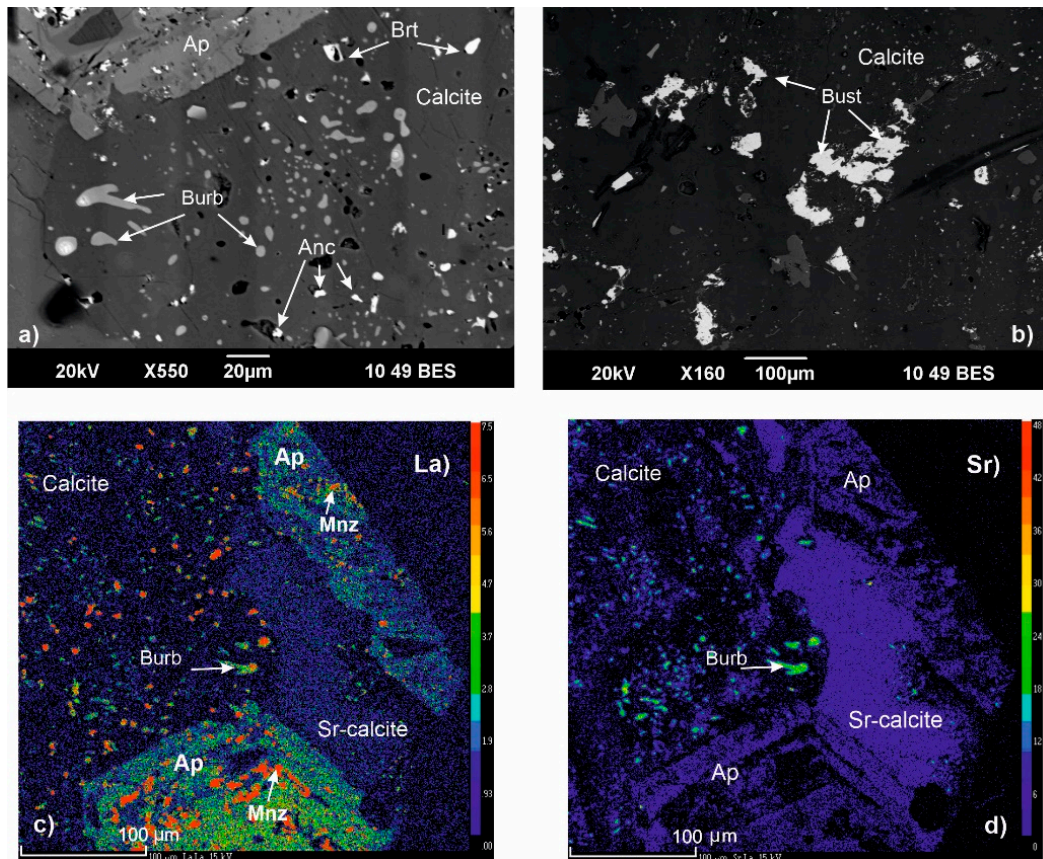


Figure 4. REE-Sr-carbonates and monazites in carbonatites of the Chetlassky complex, Middle Timan. (a,b) Images in back-scattered electrons (BSE): (a) ingrowths of burbankite (gray), ankylite (light gray) and barite (bright white grains) in calcite; (b) segregation of bastnäsite (white) in late carbonate veinlets intersecting grains of early Sr-REE-calcite; (c,d) X-ray images: (c) La, (d) Sr. On the right in both images—high-stromtium calcite (5.44% SrO, 0.44% BaO, 0.23% La₂O₃), on the left—low-stromtium calcite (1.0% SrO, 0.69% BaO, 0.01% La₂O₃) with ankylite and burbankite intergrowths, below—apatite grain with inclusions of monazite. Ap—apatite, Mnz—monazite, Burb—burbankite, Anc—ankylite, Bust—bastnäsite, Brt—barite.

Monazite in the Chetlassky complex occurs in carbonatites and fenites as clusters of micrograins ($n \times \mu\text{m}$) and crystals (Mnz 1), mainly in carbonates (dolomite and calcite) and apatites as well as in quartz and chlorite, in association with fluorocarbonate and Sr-REE-carbonates, barite, albite, potassium feldspar, aegirine, amphibole, and Nb-rutile. Late neogenic monazites (Mnz 2), as a rule, are xenomorphic and often fill hollows or form needle-like aggregates. Accumulations of needle-like aggregates of late monazite in intergrowth with hematite are characteristic [82,84].

4.2. Bulk-Rock Major and Trace Element Composition

Representative chemical compositions and contents of trace elements in the rocks of the Ilmeno–Vishnevogorsk and Buldym complexes of the South Urals as well as the Chetlassky complex of the Middle Timan are given in Tables 3 and 4 and Figures 5–7.

Table 3. Representative chemical composition of rocks from the IVC and Buldym carbonatite complexes, Southern Urals.

	Miaskites				Sövite I				Sövite II			Ultrabasites			Sövite III			Beforsite IV	
	1	2	3	4	5	6	7	8	9	10	11	12	13	14	15	16	17	18	19
Sample	324	337	338	Sav4	Po-4	LPO-1	354	D11-3	LPO2	331	V348	43332	505-27	15-22	T-16	K97-8	3296	1-54	10-21
SiO ₂ , wt%	53.62	57.69	53.62	57.51	53.63	13.02	22.88	36.12	12.86	6.44	0.90	41.39	37.71	40.40	7.4	3.08	3.51	0.72	30.5
TiO ₂	0.58	0.40	0.67	1.24	0.43	2.10	0.38	0.49	0.16	0.51	0.02	0.02	0.02	0.04	0.07	0.03	0.02	0.18	0.11
Al ₂ O ₃	20.98	21.55	18.45	17.55	20.29	4.57	8.71	11.96	3.38	2.00	0.03	0.73	0.76	1.24	1.4	0.56	0.74	0.02	1.29
Fe ₂ O ₃	1.64	1.25	1.43	1.90	1.42	0.01	0.17	1.02	0.70	n.a.	0.2	4.19	2.56	2.50	0.79	0.29	0.33	0.34	1.96
FeO	1.95	1.05	2.10	3.2	1.4	7.00	2.00	3.00	4.50	6.50	1.30	3.70	6.00	5.55	2.10	1.10	1.60	3.00	1.00
MnO	0.16	0.05	0.09	0.21	0.07	0.31	0.25	0.42	0.36	0.32	0.28	0.14	0.19	0.15	1.10	0.27	1.20	1.40	0.21
MgO	0.96	0.55	1.03	1.57	0.72	2.93	1.54	1.3	1.23	0.65	0.55	36.81	42.89	42.20	7.27	6.2	5.12	17.68	25.5
CaO	2.21	1.02	3.95	2.80	3.11	41.26	33.36	21.00	49.00	48.66	54.66	1.41	0.15	1.01	44.00	50.33	48.01	33.22	17.91
Na ₂ O	6.60	6.20	6.00	5.8	9.7	0.90	2.50	5.20	2.20	0.50	0.4	0.20	0.4	0.60	0.60	0.40	0.20	0.15	0.7
K ₂ O	7.97	7.14	7.62	5.66	5.15	3.36	4.32	4.90	1.69	1.48	0.4	0.02	0.12	0.40	1.09	0.54	0.68	0.01	0.01
P ₂ O ₅	0.23	0.02	0.10	0.24	0.04	2.45	0.79	0.42	1.21	2.37	1.22	0.01	0.01	0.02	0.01	0.03	0.01	0.18	1.35
S	n.a.	n.a.	n.a.	n.a.	n.a.	n.a.	n.a.	0.80	1.31	1.24	n.a.	n.a.	n.a.	n.a.	n.a.	n.a.	n.a.	n.a.	n.a.
LOI	2.5	2.0	3.5	1.8	2.7	19.80	19.40	12.70	23.10	28.50	38.30	12.20	7.20	4.60	34.5	38.45	38.4	43.25	17.8
Σ	99.45	98.91	98.61	99.48	98.67	97.71	96.30	100.25	101.70	99.17	98.26	100.82	98.02	98.71	100.33	101.27	99.82	100.15	98.34
Li, ppm	9	2.14	5	32	2.2	10	2.8	13	8	9	12	13	8	14	18	16	50	0.09	3.48
Rb	59	34	42	114	55	120	52	14	64	29	17	2.27	3.8	18	52	42	170	0.4	0.12
Sr	2317	1661	2530	1405	1647	3953	9247	4051	11,527	21,982	16,498	309	26	56	9547	6336	5600	6611	3796
Ba	1816	5667	9857	1589	2406	3405	3054	380	793	282	542	28	24	42	484	198	140	233	302
Sc	1.61	1.25	1.36	2.54	0.96	4.04	3.14	-	5	3	1.2	5.2	6.0	8.2	5.8	0.57	2.0	1.15	1.78
V	179	194	100	78	69	239	61	56	108	134	13	22	19	29	67	1.18	20	8	51
Cr	93	84	70	8	4	53	25	7	14	5	11	1019	1451	911	138	23	50	23	35
Co	0.41	1.6	3.7	9	7	20	4.3	6	13	10	7	83	121	112	7	3.6	12	16	7
Ni	1.07	16	1.8	9	7	16	11	5	22	2.69	33	1519	1570	2363	13	39	190	13	30
Cu	0.33	7	8	34	30	21	15	8	25	8	15	19	26	18	24	32	3.8	20	24
Zn	61	22	64	87	25	174	32	59	36	85	13	39	50	52	88	14	110	47	8
Y	10	2.07	11	20	6	61	98	47	88	73	138	2.80	1.94	8	62	523	50	93	74
Nb	57	45	51	188	54	123	57	660	1598	98	872	0.73	5.6	12	930	8	5800	88	15
Ta	2.4	2.1	3.6	20	4.3	11	16.7	34	7	0.07	3.25	0.07	0.33	0.04	1.24	0.27	7	0.08	0.14
Zr	94	109	144	77	40	21	109	57	32	7	4.7	11	1.69	5.0	42	0.64	4.0	24	37
Hf	1.52	0.78	0.95	1.30	0.71	0.83	1.19	1.20	1.03	0.22	0.26	0.28	0.05	0.12	0.51	0.40	-	0.43	0.46

Table 3. Cont.

	Miaskites				Sövite I				Sövite II			Ultrabasites				Sövite III			Beforsite IV	
	1	2	3	4	5	6	7	8	9	10	11	12	13	14	15	16	17	18	19	
Sample	324	337	338	Sav4	Po-4	LPo-1	354	D11-3	LPo2	331	V348	43332	505-27	15-22	T-16	K97-8	3296	1-54	10-21	
Mo	4	6	1.55	1.47	16	0.11	0.32	54	0.65	1.55	0.5	0.50	0.58	0.07	0.62	0.07	0.90	1.20	0.00	
Pb	2.56	0.94	1.45	12	2.07	4.2	4.89	7	34	12	60	2.34	0.10	2.84	23	38	11	23	59	
Th	1.66	0.32	0.85	13	1.43	1.94	3.07	19	19	14	2.81	0.87	0.08	0.77	22	0.38	21	681	1418	
U	n.a.	n.a.	n.a.	3.2	2.4	0.4	1.01	32	27	n.a.	5	0.12	0.02	0.03	n.a.	0.04	9	n.a.	n.a.	
La	105	15	40	80	23	191	370	373	388	926	849	6.01	1.12	5.78	577	1003	260	2285	18,959	
Ce	162	28	77	142	35	394	641	618	731	1513	1176	9.21	2.82	12.6	1022	1822	400	4092	25,500	
Pr	15	1.30	8.05	17	4.51	56	70	66	71	121	141	0.79	0.37	1.51	58	168	40	180	913	
Nd	41	4.35	27	57	15	211	221	198	239	385	433	2.76	1.58	6.11	180	550	130	543	2273	
Sm	4.76	0.66	3.92	7.62	2.17	31	31	22	41	58	50	0.49	0.37	1.33	38	100	18	70	168	
Eu	1.27	0.26	1.91	2.01	0.87	9.57	8.95	5.84	11.7	16	12	0.11	0.11	0.40	10	26	5.0	34	29	
Gd	3.16	0.55	2.95	6.14	1.75	29	25	14	39	43	43	0.41	0.36	1.21	28	110	16	65	87	
Tb	0.40	0.07	0.40	0.69	0.21	2.70	3.04	1.81	4.03	6.0	4.93	0.07	0.06	0.20	4.3	13	1.60	10	11	
Dy	1.93	0.35	1.99	4.17	1.26	14	15	10.7	23	31	26	0.46	0.35	1.35	23	86	9	60	46	
Ho	0.35	0.07	0.40	0.79	0.25	2.48	3.10	2.13	4.33	5.82	5.85	0.10	0.07	0.29	5.0	20	1.90	11	6.6	
Er	0.96	0.20	1.05	2.25	0.69	5.95	7.97	6.25	11.9	16	16	0.28	0.22	0.81	14	65	6	23	12	
Tm	0.13	0.03	0.14	0.33	0.10	0.72	1.08	0.94	1.67	2.10	2.34	0.05	0.03	0.13	2.20	10	0.90	3.0	1.31	
Yb	0.80	0.18	0.85	2.15	0.69	4.11	6.66	6.21	10.9	14	15	0.33	0.25	0.91	15	71	6.0	16	6.2	
Lu	0.12	0.03	0.13	0.31	0.11	0.56	0.97	0.95	1.63	2.21	2.39	0.05	0.04	0.13	2.37	10	1.10	2.04	0.77	
ΣREE+Y	348	53	178	342	93	1013	1504	1373	1666	3212	2918	23.9	9.69	40.8	2043	4576	946	7487	48,087	

Note: 1–10—Ilmeno–Vishnevogorsk complex: 1–3—miaskites of the Vishnevogorsk massif: 1—miaskite (zone 147, Vishnevogorskoe deposit), 2, 3—leucocratic and melanocratic miaskites of the root part of the massif; 4—miaskite of the Ilmenogorsk massif; 5—antiperthite miaskitis of the CAB; 6–11—carbonatites (sövites I, II): 6, 9—Potaninskoye deposit, 8, 10, 11—Vishnevogorskoe deposit, 7—Central Alkaline Belt (CAB); 12–20—Buldym complex: 12–14—ultramafic rocks: 12—metaperidotite, 13—metadunite, 14—olivinite, with amphibole and phlogopite, 15–19—carbonatites: 15–17—dolomite–calcite carbonatites (sövites III), 18, 19—dolomite carbonatites (beforsite IV), Buldymskoe deposit. (-) is below detection limit. n.a.—not analyzed. Geographic coordinates of the studied samples: 337, 338, 354: N55°56.443', E60°37.525'; Д-11-3: N55°59.589, E60°38.918; K-97-8: N55°01', E60°11'.

Table 4. Representative chemical composition of rocks from the Chetlassky carbonatite complex, Middle Timan.

Sample	Picrites		Lamprophyres			Carbonate-Bearing Lamprophyres				Carbonatites			
	1	2	3	4	5	6	7	8	9	10	11	12	13
	1217	13857a	1290	13205	1284	13422	12701	1328	12242	1374	T-3	13855	1389
SiO ₂ , wt%	37.9	34.02	38.34	37.92	41.58	30.42	32.62	35.64	33.10	13.88	12.17	28.96	28.76
TiO ₂	1.18	0.69	1.67	1.74	1.39	1.45	1.41	1.61	1.13	0.10	0.03	1.10	1.21
Al ₂ O ₃	7.9	5.42	11.45	10.05	9.54	9.11	9.05	9.04	7.14	0.10	0.47	6.66	7.69
Fe ₂ O ₃	6.1	6.57	4.84	6.59	4.43	3.35	5.59	3.2	5.73	1.95	4.28	5.93	8.04
FeO	3.59	3.63	5.46	6.21	4.87	5.75	3.81	11.3	2.97	7.45	8.44	3.77	6.56
MnO	0.15	0.3	0.23	0.27	0.18	0.18	0.19	0.34	0.17	1.87	1.98	0.68	1.08
MgO	21.23	26.32	14.27	16.66	17.01	12.66	13.8	12.72	15.97	9.22	8.65	16.13	15.76
CaO	12.05	6.51	14.69	10.75	12.61	16.23	17.06	7.76	9.72	26.68	24.04	14.58	10.75
Na ₂ O	0.52	0.49	1.23	1.47	0.66	0.9	0.59	0.18	3.68	0.31	0.1	1.48	0.34
K ₂ O	1.4	2.58	2.3	1.76	3.14	5.19	3.72	4.24	3.67	0.05	0.4	4.39	1.38
P ₂ O ₅	0.28	0.51	0.70	0.17	n.a.	0.78	0.75	0.52	0.15	6.10	3.76	2.97	3.28
CO ₂	1.90	3.98	2.06	2.26	1.01	10.78	6.84	10.57	13.34	30.67	32.37	9.46	9.66
LOI	7.19	11.73	4.25	4.96	3.1	12.54	9.99	12.6	16.38	30.69	31.09	11.95	13.78
Total	99.49	98.77	99.43	98.55	98.51	98.56	98.58	99.15	99.81	98.40	96.69	98.60	98.63
Rb, ppm	106	53	77	57	104	191	118	185	99	0.45	4	127	54
Sr	822	1085	993	612	407	1169	1519	165	447	7043	4232	1310	1063
Ba	1994	2725	1186	2428	884	1780	2244	858	613	1596	9607	2994	2518
Sc	15	6.4	30	21	27	22	27	22	15	0.35	4	22	12
V	149	57	209	185	195	222	256	229	135	4	5	122	185
Cr	686	621	514	532	1511	484	504	352	895	22	9	493	187
Co	52	84	52	59	50	51	40	37	45	8	24	39	44
Ni	393	649	222	382	364	235	130	119	466	8	10	145	110
Cu	58	40	78	100	61	80	128	39	46	4	45	27	78
Zn	132	152	69	85	46	53	52	33	50	106	25	69	124
Y	16	10	20	18	14	22	22	17	23	9	12	20	20
Nb	120	100	116	156	71	110	169	96	75	3	22	196	262
Ta	6	5	4	9	3	5	13	8	3.7	0.06	0.08	9	10
Zr	114	37	104	203	100	82	128	90	92	8	5	82	96
Hf	3.1	0.81	2.7	3.8	2.6	1.9	2.6	2.14	2.3	0.94	0.37	1.9	3
Mo	2.3	35	1.9	4.2	1.8	2.6	1.9	1.4	0.34	65	-	37	53
Pb	12	10	9	7	3	11	5	1.10	6	18	9	12	26
Th	24	25	28	14	9	37	14	6.5	45	36	112	22	82
U	2.9	0.99	5	1.6	2	4	4	1.2	0.48	0.21	0.3	0.54	2.7
La	110	476	129	62	54	84	122	74	49	3727	14,573	2610	3397
Ce	166	471	218	132	107	156	222	153	91	4126	17,212	3131	4227
Pr	20	39	22	15	11	17	22	16	10	277	1013	228	305
Nd	72	104	73	57	41	62	73	58	36	768	2286	579	764
Sm	10	9	10	9	6	8	10	9	6	39	100	35	47
Eu	2.8	2.1	2.7	2.7	1.8	2.5	2.9	2.2	2.0	7	19	7.3	9
Gd	7.2	5	7	7	5	7	7	6	6	22	58	23	23
Tb	0.86	0.58	0.79	0.80	0.54	0.93	0.82	0.70	0.91	0.95	1.8	1.08	1.67
Dy	4.5	3	5	5	3	5	5	4	6	3	6	6	7
Ho	0.81	0.52	0.83	0.78	0.58	0.93	0.87	0.70	1.08	0.48	0.7	0.93	1.04
Er	2.02	1.24	2.25	1.90	1.48	2.23	2.25	1.84	3.01	1.13	1.2	2.12	2.38
Tm	0.27	0.16	0.30	0.26	0.19	0.31	0.31	0.23	0.43	0.15	0.11	0.28	0.3
Yb	1.58	0.90	1.81	1.71	1.24	1.85	2.13	1.59	2.84	0.57	1.15	1.50	1.33
Lu	0.22	0.12	0.24	0.26	0.18	0.26	0.32	0.21	0.42	0.09	0.13	0.21	0.18
REE + Y	414	1123	493	313	247	370	493	344	238	8981	35,284	6645	8806

Note. 1–13—Kosyu ore occurrence: 1—subalkaline picrite, 2—alkaline picrite (with apatite–amphibole–tetraferriphlogopite–calcite matrix), 3–9—lamprophyres: 3, 4—spessartites, 5—kersantite, 6–9—carbonate-bearing lamprophyres, 10–11—carbonatites, 12–13—carbonate veins in picrites. (-) is below detection limit. n.a.—not analyzed.

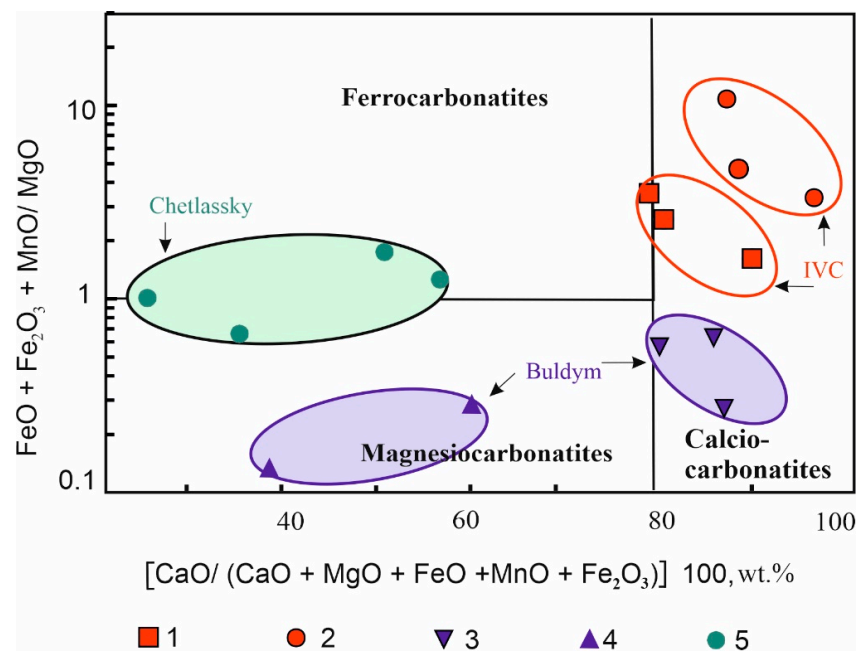


Figure 5. Compositions of the Urals and Timan carbonatites (wt%) on classification diagram [101]. Ilmeny–Vishnevogorsk complex (IVC), Urals: 1—sövite I, 2—sövite II; Buldym complex, Urals: 3—sövite III; 4—beforsite IV; Chetlassky complex, Timan: 5—ferrocarbonatite V.

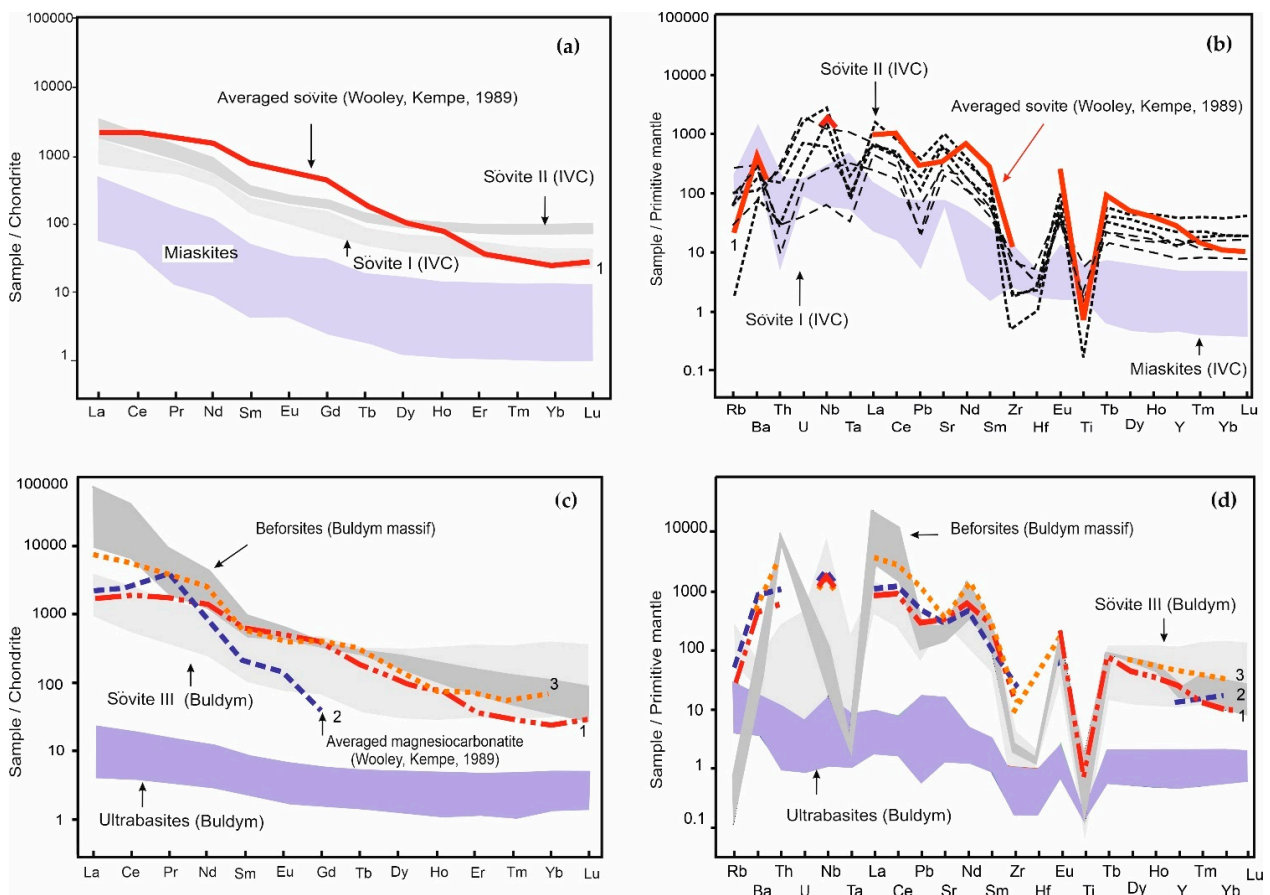


Figure 6. Chondrite-normalized REE patterns and spider-diagrams for the main rock types of the Ilmeny–Vishnevogorsk (a,b) and Buldym (c,d) complexes, South Urals. For comparison, average composition for calcio-carbonatite (1), magnesiocarbonatite (2), and ferrocarbonatite (3), according to [101] are presented.

Ilmeno–Vishnevogorsk complex (IVC). IVC carbonatites have a wide range of CaO (21.0–54.7%), low FeO (2.0–7.0%), and MgO (0.5–2.9%), and thus, correspond in composition to calciocarbonatites (sövites) according to classification [101] (Figure 5). Based on the QAP classification [102], associated nepheline syenites are miaskites (leucocratic varieties of biotite-nepheline monzosyenites with oligoclase and orthoclase-perthite) with high alumina ($\text{Al}_2\text{O}_3 > 20$ wt%), alkalis ($\text{K}_2\text{O} + \text{Na}_2\text{O} > 12.2$ wt%), and a wide range K_2O (5–8%). IVC miaskites are represented by plumazitic $\text{Al}/(\text{Na} + \text{K})$ from 0.98 to 1.23, and have the K-Na type of alkalinity (K/Na , mol., from 0.52 to 0.96), which is their difference from riftogenic carbonatite complexes of intraplate settings, which are characterized by Na type of alkalinity ($\text{K}/\text{Na} < 0.5$) [39].

IVAC carbonatites are enriched in both HFSE (especially Nb, less in Ta, Zr, Hf, V, and Ti) and LILE (Sr, Ba, and total REE with high La/Yb ratio (36–66), similar to the averaged compositions of calciocarbonatites of the world (Table 3, Figure 6) [101]. The Nb/Ta ratio (11–34) in early IVC silicocarbonatites (sövite I) is close to the ratio in magmatic carbonatites [103]; the Eu/Eu* ratio (0.96–0.91) is high and close to associated miaskite ones, which confirms their belonging to the early high-temperature differentiates of miaskite magmas [46]. High enough Nb/Ta ratio (230–1400) and some decrease in Eu/Eu* (down to 0.75) in late IVC carbonatites (sövite II) with a maximum in pyrochlore-bearing varieties are typical for the later high-temperature members of the carbonatite series and fluid-hydrothermal carbonate systems [28].

IVC miaskites show similar mantle-normalized trace element patterns without negative Ti and Zr-Hf anomaly and with similar REE pattern but with low REE contents, compared to the associated carbonatite (Figure 6a,b). IVC miaskites are relatively enriched in LILE: Ba 1600–5700 ppm, Sr 1400–2500 ppm, to a lesser extent, REE 53–350 ppm, Rb 30–110 ppm, and Li 2–30 ppm compared to riftogenic nepheline syenites intraplate setting [104]. At the same time, IVC miaskites have high HFSE: Ti 4000–12,400 ppm, Nb 45–190 ppm, Zr 40–140 ppm, V 70–200 ppm, Ta 2–20 ppm, and low Pb 1–3 ppm, which brings IVC miaskites closer to riftogenic nepheline syenites [104].

Buldym complex. Buldym carbonatites have a wide range of CaO (17.9–50.3%) and MgO (5.1–25.5%), thus belonging to calciocarbonatites (sövites III) and magnesiocarbonatites (beforsites) (Figure 5). Sövites III has similar mantle-normalized trace element patterns and chondrite-normalized REE patterns with high REE-contents (Figure 6c,d) compared to the IVC sövites (Figure 6a,b) and differ by higher contents of Nb (up to 5800 ppm) that are controlled by the distribution of the pyrochlore. Buldym beforsites have extremely high contents of REE (up to 48,000 ppm) and Th (up to 1400 ppm) in the form of single mineral phases—monazite and eshinite, and low Sr, Ba, and Nb. The high ratio La/Yb (to 3050) and Nb/Ta (to 1100) as well as lower Eu/Eu* (0.65) in Buldym beforsites are typical for low-temperature hydrothermal carbonatite facies [28,105].

Chetlassky complex. Chetlassky carbonatites have a high MgO (8.6–16.1%) and FeO + Fe₂O₃ (9.7–14.6%) and CaO (10.7–24%) correspond in composition to magnesiocarbonatites and ferrocarnatites according to classification [101] (Figure 5). Associated ultramafic dyke rocks are subalkaline and alkaline picrites according to [106]. Amphibole-phlogopite varieties of dyke rocks with a clinopyroxene-feldspar matrix were identified according to [106] as calcium-alkaline lamprophyres of the spessartite-kersantite series [60]. A significant part of the rocks of the Chetlassky complex is represented by carbonate-bearing lamprophyres (6.7–13.3 wt% CO₂).

Chetlassky picrites (MgO: 18–27 wt%, mg#: 62–78) correspond to moderately alkaline varieties (SiO₂: 35–40, Na₂O + K₂O: 1.1–2.6 wt%) with variable, in general, increased, CaO (2.6–14 wt%) and Al₂O₃ (6.0–9.8 wt%) [26]. They are a potassium alkaline ($\text{K}/\text{Na} = 1.1–2.5$) and have a miaskitic agpaite coefficient ($\text{K}_{\text{agp}} = 0.12–0.47$), which changes to agpaite in carbonate-bearing lamprophyres ($\text{K}_{\text{agp}} = 0.4–1.4$). Alkaline varieties of picrites have higher $\text{K}_2\text{O}/\text{Na}_2\text{O}$ (mol) 3.5, $\text{K}_2\text{O}/\text{Al}_2\text{O}_3$ (mol) 0.52; and $\text{K}_{\text{agp}} = 0.67$ (Table 4, analysis 2) and associated with carbonatites. Phlogopite and amphibole lamprophyres (kersantites and

spessartites) contain lesser MgO: 14–17 wt%, and higher SiO₂: 38–42, Na₂O + K₂O: 3–4 and Al₂O₃: 9–12 wt%.

Lamprophyres and carbonate-containing lamprophyres are enriched in both incompatible (REE, Sr, Ba, Nb) and compatible (Ni, Co, Cr) elements (Table 4). In terms of trace element content, carbonate-bearing lamprophyres are close (but not identical) to carbonatites from kimberlite associations [107] and aillikites [108] and differ from carbonatites of other formation types (Figure 7c,d). They have rather high contents Ni (120–460 ppm), Co (35–50 ppm), Cr (350–1500 ppm), and lower Ba (< 2200 ppm), Sr (<1500 ppm), Nb (<170 ppm), and REE (<490 ppm) compared to the Chetlassky carbonatites (Table 4, Figure 7).

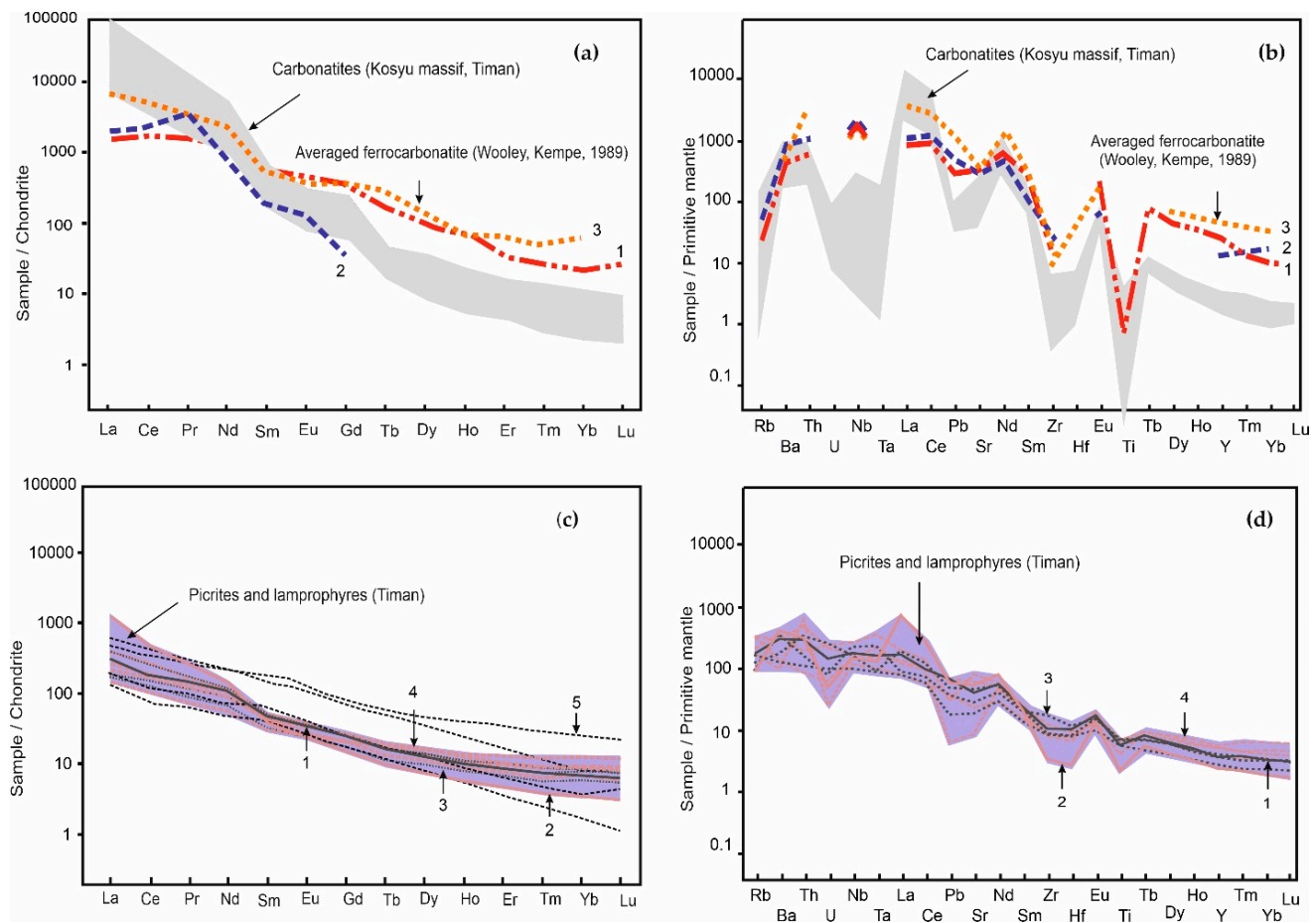


Figure 7. Chondrite-normalized REE patterns and spider-diagrams for carbonatites and ultramafic dyke rocks of the Chetlassky complex, Middle Timan: (a,b) carbonatites (grey field); for comparison, average composition for calciocarbonatite (1), magnesiocarbonatite (2), and ferrocarbonatite (3), according to [101] are presented; (c,d) picrites and lamprophyres (blue field); 1—picrite, 2—alkaline picrite, 3—lamprophyres, 4—carbonate-bearing lamprophyres, 5—aillikites (Aillik Bay, Labrador) according to [108].

Carbonatites are enriched in LREE and depleted in HFSE (Nb, Zr, Ti) relative to the world average compositions of magnesi- and ferrocarbonatites [101] (Figure 7a,b), as well as IVC and Buldym carbonatites (Figure 6a,b). They are distinguished by high fractionation of REE, (i.e., steep slope of the REE spectrum with the highest ratios La/Yb up to 6540 and LREE/HREE up to 240) (see Figure 7a). It should also be noted that was increased Cr, Ni, and Co, which is typical for carbonatites formed from K-ultrabasic picrite-kimberlite magmas [109] as well as low Sr/Ba (0.4–4), which is typical of volcanic and shallow carbonatites [110]. Chetlassky carbonatites have high REE (from 8800 to 35,300 ppm), Ba (up to 9600 ppm), Sr (up to 9700 ppm), Th (20–165 ppm), decreased Nb (3–250, on average

120 ppm), and lower Ni (<145 ppm), Co (<44 ppm), and Cr (<187 ppm) in comparison with the host lamprophyres and are comparable with extrusive carbonatites [45,111].

4.3. Rb-Sr and Sm-Nd Isotope Data

The results obtained on the Rb-Sr and Sm-Nd isotope composition of rocks and minerals of carbonatite complexes of the Urals and Timan fold regions are presented in Table 5 and Figure 8. The initial isotope ratios of neodymium and strontium for the Ilmeno–Vishnevogorsk and Buldym complexes of the Southern Urals were recalculated for a time of 440 m.y. ago [63,69,112], but for the Chetlasky complex at 590 Ma [26,56]. The ϵ_{Sr} and ϵ_{Nd} values were calculated relative to the composition of the model reservoirs UR ($^{87}\text{Rb}/^{86}\text{Sr} = 0.0816$, $^{87}\text{Sr}/^{86}\text{Sr} = 0.7045$) and CHUR ($^{147}\text{Sm}/^{144}\text{Nd} = 0.1967$, $^{143}\text{Nd}/^{144}\text{Nd} = 0.512636$) of the corresponding age.

The rocks of the carbonatite complexes of the Urals have the following isotopic characteristics: (a) for the Ilmeno–Vishnevogorsk miaskite–carbonatite complex, the initial isotope ratios of $^{87}\text{Sr}/^{86}\text{Sr}_I$ vary from 0.70336 to 0.70399, and ϵ_{Nd} from +1.9 to +5.9; only carbonatites of exocontact halos are somewhat enriched in radiogenic strontium and non-radiogenic neodymium $^{87}\text{Sr}/^{86}\text{Sr}_I = 0.70421$; $\epsilon_{\text{Nd}} = -1.4$; (b) for the Buldym ultrabasic-carbonatite complex $^{87}\text{Sr}/^{86}\text{Sr}_I$ has more radiogenic values: 0.70440–0.70513 and less radiogenic for ϵ_{Nd} : from -2.8 up to $+0.7$ (see Table 5, Figure 8A).

Carbonatites of the Chetlasky complex have initial isotopic compositions ($^{87}\text{Sr}/^{86}\text{Sr}_I = 0.70348$ – 0.70369 , $\epsilon_{\text{Nd}} = +5.1$ – $+5.7$) similar to the composition of unaltered lamprophyres ($^{87}\text{Sr}/^{86}\text{Sr}_I = 0.70364$ – 0.70376 , $\epsilon_{\text{Nd}} = +5.4$ – $+6.2$). However, some lamprophyres of the Chetlasky complex have a more radiogenic strontium and a less radiogenic neodymium isotopic composition ($^{87}\text{Sr}/^{86}\text{Sr}_I = 0.70489$ – 0.70589 , $\epsilon_{\text{Nd}} = 1.8$ – 2.1) [60,113] (see Table 5, Figure 8B).

Table 5. Sm-Nd and Rb-Sr-isotope data for the rocks and minerals of carbonatite complexes of the Urals and Timan.

N ^o	Sample	Rock	Mineral	Rb, ppm	Sr, ppm	(⁸⁷ Sr/ ⁸⁶ Sr) _t	ε Sr (T)	Sm, ppm	Nd, ppm	¹⁴⁷ Sm/ ¹⁴⁴ Nd	¹⁴³ Nd/ ¹⁴⁴ Nd	(¹⁴³ Nd/ ¹⁴⁴ Nd) _t	ε Nd (T)
<i>Ilmeno–Vishnevogorsk miaskite–carbonatite complex, Southern Urals</i>													
1	338W	Miaskite		79	2095	0.70341	−8.2	3.9	27	0.08635	0.512569	0.512320	4.9
2	324W	Miaskite		122	1994	0.70342	−7.9	4.8	42	0.06878	0.512549	0.512351	5.5
3	Dol-2W	Miaskite		181	4525	0.70336	−8.8	8.3	75	0.09310	0.512550	0.512282	4.1
4	Po-1W	Miaskite		157	2791	0.70380	−8.5	13.8	94	0.08839	0.512511	0.512256	3.6
5	330-1	Syenite		105	383	0.70338	−8.6	18.0	133	0.08211	0.512609	0.512372	5.9
6	LPo-1_Ca	Sövite I	Calcite	0.06	12,231	0.70371	−8.5	50.1	328	0.09232	0.512584	0.512318	4.8
7	37-95_Pcl	Sövite I	U-Pyroxhlore	9.4	8140	0.70343	−7.8	37	280	0.08067	0.512501	0.512268	3.8
8	354W	Sövite I		65	8576	0.70350	−6.8	27.4	1984	0.08359	0.512491	0.512250	3.5
9	354_Ca	Sövite I	Calcite	-	9247	0.70356	−6.0	50.9	368	0.08510	0.512460	0.512219	2.9
10	329_Ca	Sövite I	Calcite	45	12,340	0.70361	−5.3	8.0	47	0.09972	0.512533	0.512235	3.2
11	D11-3W	Sövite I		124	4971	0.70350	−6.9	19.2	170	0.06811	0.512447	0.512251	3.5
12	331_Ca	Sövite II	Calcite	29	21,982	0.70359	−5.6	58.3	385	0.09160	0.512507	0.512243	3.4
13	B331W	Sövite II		n.a.	n.a.	n.a.	n.a.	52	429	0.07368	0.512486	0.512274	3.9
14	B331_Ca	Sövite II	Calcite	n.a.	n.a.	n.a.	n.a.	47.5	358	0.08022	0.512506	0.512275	4.0
15	B331_Pcl	Sövite II	Pyroxhlore	7.1	3731	0.70341	−8.1	381	3876	0.05954	0.512447	0.512275	4.0
16	LPo-2W	Sövite II		n.a.	n.a.	n.a.	n.a.	33.6	255	0.07973	0.512398	0.512168	1.9
17	Dol-2I	Ne-pegmatite	Pyroxhlore	n.a.	n.a.	0.70399	−2.8	458	5324	0.05200	0.512380	0.512233	3.1
18	140-1_Ca	Sövite II *	Calcite	0.55	16,718	0.70421	3.2	51.9	392	0.08001	0.512230	0.511999	−1.4
19	140-1_Pcl	Sövite II *	Pyroxhlore	1.48	8332	0.70438	5.7	104	930	0.0677	0.512187	0.511992	−1.5
20	330-2W	Fenite *		n.a.	n.a.	n.a.	n.a.	14.8	109	0.08243	0.511564	0.511326	−14.5
<i>Host metamorphic rocks, Vishnevogorsk, and Ilmenogorsk suites (PR1), South Urals</i>													
21	Mo-1_Ca	Calciphyre	Calcite	0.99	1202	0.70817	59.4	4.36	32	0.08291	0.511992	0.511753	−6.2
22	Vish-2W	Plagiogneiss		90	328	0.72550	305	20.1	127	0.09521	0.511069	0.510795	−24.9
<i>Buldym ultrabasite-carbonatite complex, Southern Urals</i>													
23	43332W	Metaperidotite		2.27	309	0.70497	12.1	0.35	2.1	0.100140	0.512310	0.512021	−0.97
24	505-27W	Metadunite		3.52	21.2	0.70513	16.3	0.37	1.4	0.162076	0.512495	0.512028	−0.16
25	503-27W	Olivinite		n.a.	n.a.	n.a.	n.a.	5.2	58	0.054602	0.512213	0.512055	−0.30
26	15-22W	Olivinite		n.a.	n.a.	n.a.	n.a.	1.6	8.8	0.112044	0.512293	0.511970	−2.0
27	3311W	Sövite III		n.a.	n.a.	n.a.	n.a.	42.0	314	0.08091	0.512168	0.511935	−2.7
28	3311_Ca	Sövite III	Calcite	-	8373	0.70455	8.0	52.1	391	0.08048	0.512172	0.511940	−2.6
29	3311_Rch	Sövite III	Richterite	n.a.	n.a.	n.a.	n.a.	0.46	3	0.09476	0.512187	0.511914	−3.1
30	3311_Do	Sövite III	Dolomite	n.a.	n.a.	0.70455	8.0	8.10	64	0.07611	0.512166	0.511947	−2.4
31	915_Ca	Sövite III	Calcite	-	10,279	0.70440	5.9	39.3	292	0.08138	0.512164	0.511929	−2.8
32	3296_Pcl	Sövite III	Pyroxhlore	8.7	7058	0.70425	3.9	127	117	0.068640	0.512160	0.511962	−2.1
33	154_Do	Beforsite IV	Dolomite	-	9097	0.70447	6.9	24.5	181	0.08150	0.512292	0.512057	−0.3
34	1021_Do	Beforsite IV	Dolomite	-	5334	0.70450	7.3	12.6	93	0.08190	0.512341	0.512105	0.7
35	K18_Pcl	Phlog-Do	U-Pyroxhlore	41	3772	0.70766	52	391	2603	0.090700	0.512315	0.512054	−0.3
36	K21_Pcl **	Phlog-Do	Pyroxhlore	1.26	2990	0.70715	45	2928	11,154	0.15865	0.512232	0.511775	−5.8
37	K23_Ash	Phlog-Do	Aeschynite	1.02	1156	0.70617	31	4762	37,700	0.076342	0.512254	0.512034	−0.7

Table 5. Cont.

№	Sample	Rock	Mineral	Rb, ppm	Sr, ppm	$(^{87}\text{Sr}/^{86}\text{Sr})_t$	ϵ Sr (T)	Sm, ppm	Nd, ppm	$^{147}\text{Sm}/^{144}\text{Nd}$	$^{143}\text{Nd}/^{144}\text{Nd}$	$(^{143}\text{Nd}/^{144}\text{Nd})_t$	ϵ Nd (T)
<i>Chetlassky complex of dike ultramafic-mafic rocks and carbonatites, Middle Timan</i>													
38	1374K	Carbonatite	Dolomite	n.a.	n.a.	0.70348	−4.6	1.2	50	0.01468	0.512194	0.512137	5.1
39	1387/2	Carbonatite	Apatite	n.a.	n.a.	0.70300	−11.3	5.2	80	0.0392	0.512326	0.512174	5.8
40	1385-5	Carbonatite	REE-carbonate	90	1272	0.70369	−1.6	1.3	52	0.01524	0.512227	0.512168	5.7
41	1385-5	Carbonatite		129	1262	0.70367	−1.8	n.a.	n.a.	n.a.	n.a.	n.a.	n.a.
42	T-450	Lamprophyre	Dolomite	n.a.	n.a.	0.70364	−6.2	0.04	5.5	0.00462	0.512183	0.512165	5.6
43	1270-1	Lamprophyre		116	1535	0.70365	−2.2	0.11	6.1	0.01048	0.512235	0.512194	6.2
44	1284	Lamprophyre		104	432	0.70376	−0.6	5.2	75	0.04190	0.512317	0.512155	5.4
45	55/46.3	Lamprophyre		121	901	0.70554	24.6	8.1	56	0.0875	0.512310	0.511972	1.8
46	55/38.7	Lamprophyre		100	575	0.70589	29.7	7.3	45	0.0982	0.512365	0.511985	2.1
47	55/172	Lamprophyre		87	1127	0.70489	15.5	13	93	0.0853	0.512314	0.511984	2.1
<i>Host carbonate-sedimentary strata of the Bystrinskaya Group (Rf3), Middle Timan</i>													
48	1445	Dolomite		0.5	77	0.71380	142	0.19	0.89	0.12621	0.512084	0.511596	−5.5

Note.: The errors in the values (2σ) for $^{87}\text{Sr}/^{86}\text{Sr}$ do not exceed 0.01%, for $^{143}\text{Nd}/^{144}\text{Nd}$ —0.002%. The initial ratio of isotopes of neodymium and strontium for the Ilmeno–Vishnevogorsk and Buldym complexes of the Southern Urals was calculated for an age of 440 Ma [63–66,69,70]; for the Chetlassky complex of the Timan—by an age of 590 Ma [26,56]. The ϵSr and ϵNd values were calculated relative to the model reservoirs UR ($^{87}\text{Rb}/^{86}\text{Sr} = 0.0816$, $^{87}\text{Sr}/^{86}\text{Sr} = 0.7045$) and CHUR ($^{147}\text{Sm}/^{144}\text{Nd} = 0.1967$, $^{143}\text{Nd}/^{144}\text{Nd} = 0.512636$). (−) is below the detection limit. n.a.—not analyzed. 1–20—Ilmeno–Vishnevogorsk miaskite–carbonatite complex, Southern Urals: 1–4—miaskites: 1–3—Vishnevogorsk massif, 4—antiperthite miaskite, CAB; 5—syenite, ore zone 125; 6–16—early and late calcite carbonatites (Sövites I, II): 6–7, 16—CAB, Potaninskoye deposit; 8–15—Vishnevogorsk massif: 8, 9—root part, 10–15—apical part, ore zone 147; 17—miaskite-pegmatite, ore zone 147; 18–20—rocks of exocontact halos of Vishnevogorsk massif; 18, 19—calcite carbonatite of ore zone 140; 20—fenite, zone 125; 21, 22—host metamorphic rocks of Vishnevogorsk and Ilmenogorsk suites (PR₁); 21—calciphyre, Ilmenogorsk suite, mine 15, 22—plagiogneiss of the Vishnevogorsk suite, quarry veins 35. 23–37—Buldym complex, South Urals: 23–26—ultrabasites of the Buldym massif: 23—metaperidotite, 24—metadunite, 25, 26—richterite olivinite; 27–34—carbonatites of the Buldym massif: 27–32—dolomite-calcite (Sövity III), 33, 34—dolomite (beforsite IV); 35–37—dolomite-phlogopite metasomatites; 38–47—Chetlassky complex (Middle Timan): 41–43—Kosyu REE-occurrences: 38, 39—minerals of carbonatites, 40, 43—acid extracts from bulk samples of carbonate-containing rocks (carbonatite and lamprophyre, respectively), 41—carbonatite, 42, 43—carbonate-bearing lamprophyres, 45–47—lamprophyres of spessartite-kersantite series of Chetlassky complex, data from [60,113]; 48—dolomite of the Bystrinskaya Series of the Chetlassky Formation (Rf₃). *—rocks of exocontact halos; **—aeshinitized pyrochlore.

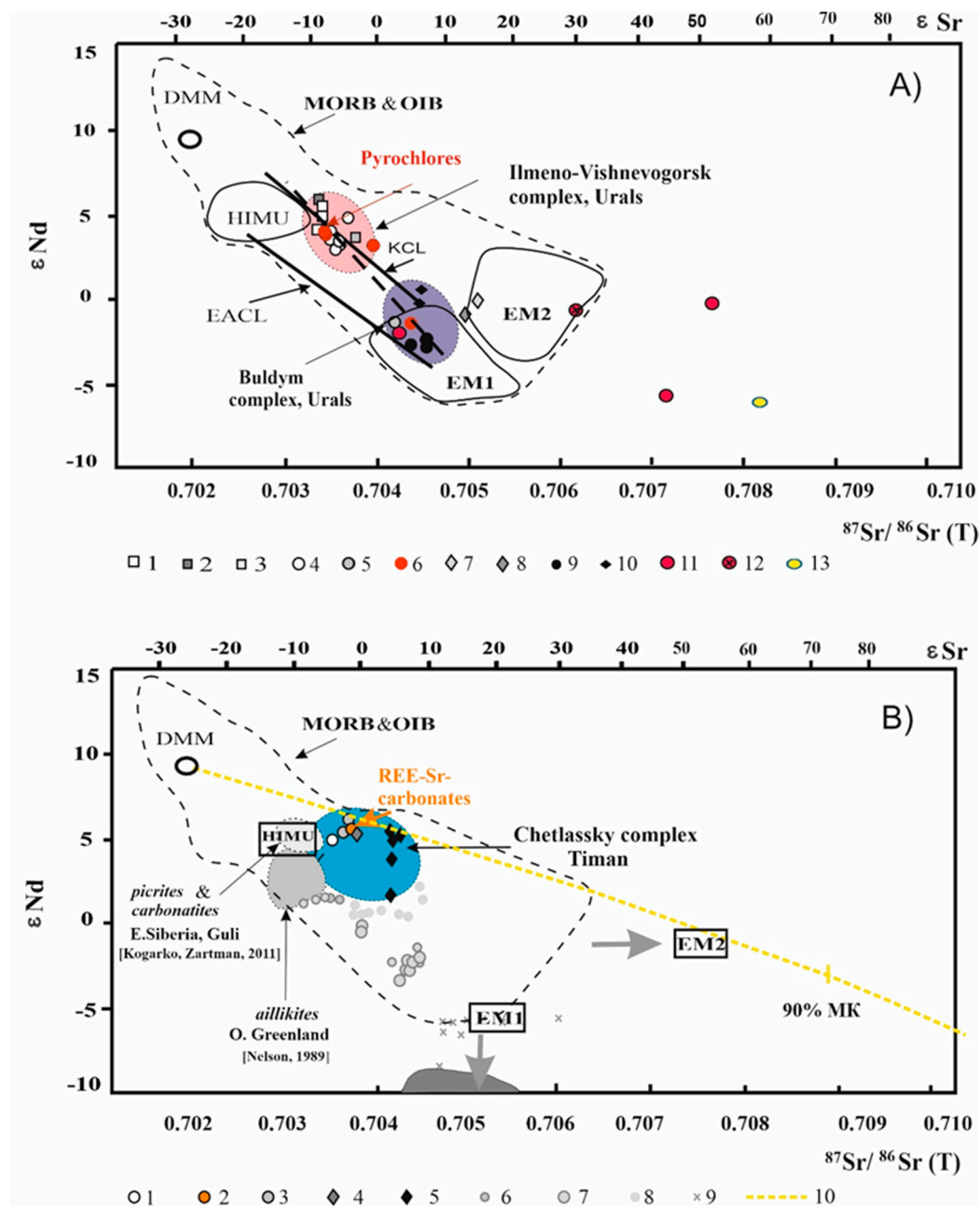


Figure 8. Nd–Sr isotope diagram for carbonatites and alkaline rocks of the Ilmeno–Vishnevogorsk (IVC) and Buldym carbonatite complexes, South Urals (A) and Chetlassky complex, Middle Timan (B). (A) 1–6: Ilmeno–Vishnevogorsk miaskite-carbonatite complex: 1—miaskites of the Vishnevogorsk massif and CAB, 2—syenites, Vishnevogorsk massif, 3—antiperthite miaskite, CAB, 4—carbonatites in miaskites of the Vishnevogorsk massif and CAB, 5—carbonatites from the exocontact halos of Vishnevogorsk massif, 6—pyrochlores; 7–11: Buldym ultramafic-carbonatite complex: 7—peridotite, 8—olivinite, 9—sövites III, 10—beforsites IV, 11—pyrochlores; 12—aeshinite; 13—calciphyres of the host Vishnevogorsk Series (PR₁). The initial isotopic compositions of rocks and minerals of the IVC and the Buldym complex were recalculated for an age of 440 Ma [64,69,70]. The mantle array, MORB, OIB, and the end-member components: DMM, HIMU, EM1, EM2, are pictured from [41,114]. For comparison are shown the Kola carbonatite line (KCL) [21] and the East African carbonatite line (EACL) [33]. (B) 1–5: Chetlassky dike ultramafic-carbonatite complex: 1—carbonates from carbonatites, 2—REE–Sr fluorocarbonates from carbonatites, 3—carbonate-bearing lamprophyres, 4, 5 picrites and lamprophyres: 5—after [113]. The initial isotopic compositions of the Chetlassky complex were recalculated for an age of 590 Ma [26,56]. MORB and OIB compositions are from [41,114]. Mantle reservoirs: DMM, HIMU, EM1, and EM2 are present in accordance with their modern isotopic parameters [115–118]. For comparison, the compositions of the rocks of aillikite-carbonatite complexes are given: 6, 7: Torngat, E. Canada (V) [119]: 6—aillikite-carbonatites, 7—melaillikites; 8–9: Aillik-Bay, Labrador (V) [120]:

8—aillikite-carbonatites, 9—lamproites. Light-gray field—compositions of alkaline picrites and carbonatites, Guli, E. Siberia (Pz) [121]; gray and dark-gray field—compositions of aillikites and lamproites, E. Greenland (V) [122]; 10—(yellow dotted line) line of mixing DM with the host terrigenous-carbonate strata of the Bystrinskaya Group of the Chetlasskaya Series (Rf₃); MK is the mantle component. To calculate the mixing line, we used the DM values of the source $^{143}\text{Nd}/^{144}\text{Nd}_{590} = 0.512325$ ($\epsilon_{\text{Nd}} = +8.75$), $^{87}\text{Sr}/^{86}\text{Sr}_{590} = 0.70182$ [123], Sr—6 ppm, Nd—0.33 ppm, and host carbonate strata of the Chetlasskaya Series, Middle Timan— $^{87}\text{Sr}/^{86}\text{Sr}_{590} = 0.71380$, $^{143}\text{Nd}/^{144}\text{Nd}_{590} = 0.511596$ ($\epsilon_{\text{Nd}} = -5.5$), Sr—77 ppm, Nd—0.89 ppm.

5. Discussion

5.1. Composition, Evolution, and Genesis of Ore Rare-Metal Mineralization

Pyrochlore group mineral species of the IVC and Buldym carbonatite complexes are determined according to the latest nomenclature of the pyrochlore group (pyrochlore supergroup) based on the predominant cation or anion in the positions B = Nb, Ti, Ta; A = Ca, Na, REE, Y, Sr, Ba, Mn, Mg, U, Th, and Y = O, OH, F [100]. According to [100], pyrochlores of the Urals and carbonatite complexes are represented by U-(Ta)-rich hydroxyl- and oxycalciopyrochlores (or uranopyrochlores, according to the classification [124]) and fluorocalciopyrochlores (including Ta-, REE_{Ce}-, and Sr-containing varieties). Hydrothermally altered and supergene pyrochlores are represented by hydroxylcalciopyrochlores and hydroxyrochlores. The pyrochlore population compositions are given in Table 1 and are illustrated in ternary diagrams characterizing the cation filling of the A and B positions (Figure 9).

The IVC and Buldym pyrochlore varieties (Pyrochlore I–V, see Table 1, Figure 9) are associated with certain types of rocks and a certain stage of the alkaline-magmatic system evolution. Thus, *U-(Ta)-rich oxycalciopyrochlores* (uranopyrochlore I according to [124]) are found in the pegmatoid varieties of miaskites, in miaskite-pegmatites, and sövites I of the IVC (Potaninskoe deposit, Uvildinskoe ore occurrence), and glimmerite-like rocks (Buldym deposit) (Figure 3a,d,e). This type of pyrochlore is enriched in UO₂ (17–24 wt%) and Ta₂O₅ (1–4 wt%), and has low Nb/Ta ratios (17–91) (Table 1), which is typical for primary magmatic pyrochlore [125,126] (see Figure 9b). This type of pyrochlore is formed earlier than other pyrochlores at the late magmatic crystallization stage, as evidenced by relics of U-containing pyrochlore in later generations of pyrochlore from late carbonatites (sövites II) (Figure 3g) [27].

Fluorocalciopyrochlore (Pcl II) of IVC containing less UO₂ (0–1.8 wt%) but enriched Ta₂O₅ (2–3 wt%), with a low Nb/Ta ratio (28–67), and rich in Nb₂O₅ (60–65 wt%) and F (3.4–5 wt%) (see Table 1), occurs in more evolved miaskite-pegmatites of IVC (Vishnevogorsk deposit, ore zones 147 and 140) as well as in early silicocarbonatites at the Potanino deposit. The Pcl II composition is typical for primary magmatic pyrochlore of carbonatite complexes (see Figure 9b) [125,126]. In the IVC, this pyrochlore is formed at the pegmatite and early carbonatite stages of the alkaline melt crystallization.

Fluorocalciopyrochlore (Pcl III), which does not contain Ta and U, with low trace element contents, with the highest Nb₂O₅ (65–67 wt%), F (>4%) is widespread in early carbonatites of the IVC and Buldym complex (Figure 3b). The main ore zones of the Buldym and Vishnevogorsk (ore zone 140) deposits are composed of these pyrochlore varieties; they are also found at the Potanino deposit. It is in Pcl III that oscillatory zoning is sometimes noted, although usually zoning in the IVC pyrochlore is poorly developed as well as in other a plutonic carbonatite complex (for example, Tchivira carbonatite, Angola [127]). As known, oscillatory zoning in pyrochlore is a typical magmatic feature, originating from higher crystal growth rates [128]. In general, fluorocalciopyrochlore III, with fully filled A-sites and low trace element content is similar to the main pyrochlore varieties in magmatic carbonatites (Figure 9) [129–132]. High F content in these pyrochlore is consistent with experimental data on the crystallization of pyrochlores from evolved F-saturated carbonatite magmas [132].

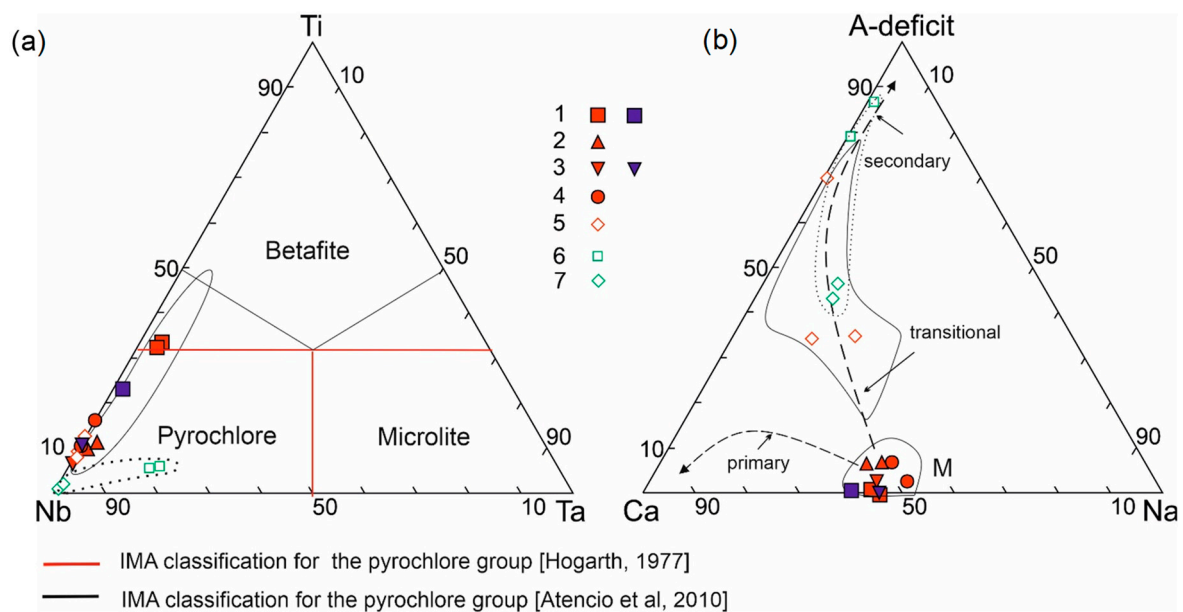


Figure 9. Pyrochlore compositions of the Urals and Timan carbonatite complexes: triangular diagrams reflecting the filling of B- and A-positions (p.f.u.) in the structure of pyrochlore in accordance with the IMA classifications [100,124]. 1–5—Ilmeno–Vishnevogorsk (red signs) and Buldym complexes (blue signs), S. Urals: 1—**uranpyrochlore I** (U–(Ta)-rich oxy- and hydroxylcalciopyrochlore), 2—**pyrochlore II** (Ta-containing fluorocalciopyrochlore), 3—**pyrochlore III** (fluorocalciopyrochlore), 4—**pyrochlore IV** (REE–Sr-containing fluorocalciopyrochlore); 5—**pyrochlore V** (Sr-REE-Ba hydroxylcalciopyrochlore and hydroxyrochlore); 6, 7—Chetlasky complex (green sign), M. Timan [82]: 6—uranhydroxyrochlore, 7—Sr-Ba hydroxyrochlore. Solid line shows the composition fields for pyrochlore of Urals carbonatite complexes, dotted line—for pyrochlore of Timan carbonatites. (a) diagram Nb–Ti–Ta, after [100,124]; (b) diagram Ca–A-deficit–Na, after [133,134]. Dashed lines show the primary trend of magmatic (M) pyrochlore and an increase in the number of vacancies (A-deficit, see Table 1) during transitional (hydrothermal) and secondary (supergene) alteration of pyrochlore.

Fluorocalciopyrochlore (Pcl IV), enriched in comparison with the early generations of SrO (1–1.5 wt%) and LREE₂O₃ (3–5 wt%), with a high F (4–5 wt%) and Nb/Ta (> 300), is formed in late calciocarbonatites (sövites II) of IVC as well as in fenite surroundings (Figure 3c). It occurs in the form of single crystals, sometimes forming borders around U-containing relict pyrochlore cores (Figure 3g). In the Buldym complex, REE-containing fluorocalciopyrochlores occur in intergrowth with aeshinite in late dolomite carbonatites and associated metasomatites (Figure 3k). The fully filled A-sites (0.05–0.13 apfu), high F (4–5 wt%) in the Pcl 4 are common for primary pyrochlore (Figure 9b), but their Nb/Ta ratio (>300) higher than in magmatic carbonatite (Nb/Ta < 70) [125]. It is likely that the formation of these pyrochlore varieties occurs at the final late carbonatite stage with the participation F-rich fluid. Fluid nature of pyrochlores of similar composition Petyayan-Vara carbonatites (Kola, Russia) was also assumed [135].

Hydroxylcalciopyrochlore and *hydroxyrochlore (Pcl V)* are quite rare in the IVC and Buldym complex compared to primary pyrochlores (I–IV). These varieties of pyrochlore are enriched by SrO (2–5 wt%), LREE₂O₃ (2–4 wt%), BaO (0.7–2.4 wt%), Fe₂O₃ (1.5–1.7 wt%), SiO₂ (1.6 wt%), and in some cases Ta₂O₅ (to 13 wt%) [136,137]. They are naturally substituted by varieties, whereas in the A-site, Na contents decrease and as a result, vacancies in the A-site are formed (from 35 to 70%, to 1 a.p.f.u.), and Sr, LREE, and Ba become the significant cations. In the B-site, a decrease in Nb content isomorphically substituted by Si and Fe occurs. In the Y-site, F decreases until it disappears and replaced by OH-groups. This feature of pyrochlores is usually associated with subsolidus [138], hydrothermal [139–143], or supergene [144] processes. Pcl V occurs in pegmatites and early siliciocarbonatites and is most developed in late carbonatites. We assumed that these pyrochlores are formed as a result of subsolidus hydrothermal alteration of early pyrochlore generations (hydrothermal trend, see Figure 9b) at the final stages of the IVC complex evolution.

It is known that variations in the composition of HFSE pyrochlores are usually associated with the crystallization stage of alkaline rocks and carbonatites. For example, the highest concentrations U and Ta were measured at the pyrochlore crystal cores in early carbonatites [145]. Early population of U-Ta-enriched pyrochlore, which is commonly resorbed and surrounded by late pyrochlore have been described as a multi-stage magmatic evolution in several carbonatites worldwide [124,128,145–148]. At the Kaiserstuhl, resorbed U- and Ta-rich cores in pyrochlore have been interpreted as originally crystallized from a silicate alkaline magma and subsequently entrained in the carbonatite magma during emplacement [126]. In addition, early-crystallizing uranpyrochlore is a common accessory in nepheline syenites at the Lovozero alkaline complex, Russia [149].

In the IVC complex (Urals), U-(Ta)-rich pyrochlores (uranpyrochlore I) also crystallize at the early magmatic stage of the evolution of the alkaline-carbonatite magmatic system in pegmatoid miaskites, miaskite-pegmatites, and glimmerite-like rocks as well as early carbonatites (sövites I). Fluorocalciopyrochlores (Pcl II, Pcl III) with a low Nb/Ta ratio (<70), characteristic of primary magmatic pyrochlore [125,126], also forms at the pegmatite and early carbonatite stages in the IVC. Crystallization of early pyrochlore generations in paragenesis with nepheline, potassium spar, albite, biotite, zircon, ilmenite, and calcite occurred at $T = 750\text{--}590\text{ }^{\circ}\text{C}$ and $P = 3.5\text{--}2.5\text{ kbar}$ (according to the thermobarometry of miaskite-pegmatites [150]). Fluorocalciopyrochlores of a later generation (Pcl IV) are formed in late calciocarbonatites (sövites II) in paragenesis with apatite, calcite, biotite, ilmenite, pyrrhotite, and pyrite at $T = 590\text{--}490\text{ }^{\circ}\text{C}$ according to [46]. Highest F content (4–5 wt%) and Nb/Ta ratio (>300) subsolidus temperatures suggest the participation of F-containing fluid in the formation of these pyrochlore generations [135]. Finds of pyrochlore of a similar composition in associating fenites a priori confirm its fluid nature.

Late generations of Sr-REE-Ba-enrich hydroxylcalciopyrochlore in IVC replace early generations of pyrochlore (Pcl I, Pcl II), both in pegmatites and carbonatites, but are most developed in late carbonatites. Their formation is probably associated with subsolidus and hydrothermal processes at the final stage of the evolution of miaskite and carbonatite magmas, as in other carbonatite complexes. The insignificant scale of development and lower contents of Sr, REE, and Ba in these pyrochlores distinguishes them from the Sr-Ba pyrochlores of late low-temperature magnesio- and ferrocarnatites, which complete the carbonatite series in alkaline-ultramafic complexes of intraplate settings [141].

Thus, IVC pyrochlore, as in other alkaline rock and carbonatite complexes, is a product of residual crystallization of carbonated alkaline magma and crystallizes at the pegmatite and carbonatite stages of magma evolution. Evolution of IVC pyrochlore composition from early generations, with high U and Ta and low (<70) Nb/Ta ratio (in miaskite-pegmatites and silicocarbonatites) to later generations, with low U and Ta and high Sr, REE and F and Nb/Ta ratio >300 (in late carbonatites) is a well-known feature of the pyrochlore evolution in carbonatite complexes throughout the world [124,128,145–147]. At the same time, hydrothermal varieties represented by Sr-REE-Ba-enrich hydroxylcalciopyrochlore associated with subsolidus processes of primary pyrochlore transformation are weakly manifested in the IVC.

Monazites of the Chetlassky complex are represented by Ce-rich and Nd-rich varieties—monazite-(Ce) and monazite-(Nd). It exists as early crystals and late xenomorphic (or needle-like) generations with different La/Ce and La/Nd ratios: 0.38–0.47 or 3.12–3.34 and 0.8–1.29 or 0.64–0.83, respectively. The early generations are characterized by a high ThO₂ content (to 9.27 wt%), which is typical for high-temperature monazites [50]. In later generations, a higher PbO content is noted (up to 2.79 wt%). La contents as well as La/Ce and La/Nd ratio in the early monazites of the Chetlassky complex are lower than those in monazites of the Buldym complex (Table 2, Figure 10). It is known that La-depleted monazites are found in ferrocarnatites of the Fen Massif (Norway) transformed into hematite-rich rock (rodbergite) [151]. The La-depleted trend with an increase in the Ce content relative to La and Nd is also characteristic for compositions of monazite from the Tomtor rare-metal deposit of a highly differentiated alkaline-ultramafic carbonatite complex

in Siberia (Figure 10b). This trend is likely to mean precipitation from hydrothermal fluids altering previous phase [50]. Monazite compositions (Mz I) of Chetlassky carbonatites are at the beginning of this trend, and are close to the compositions of monazite in carbonatite of the Qinling and Mianning–Dechang orogenic belt (giant Bayan Obo REE deposit, Miaoya, Maoniuping, and other largest REE-deposits) (Figure 10b).

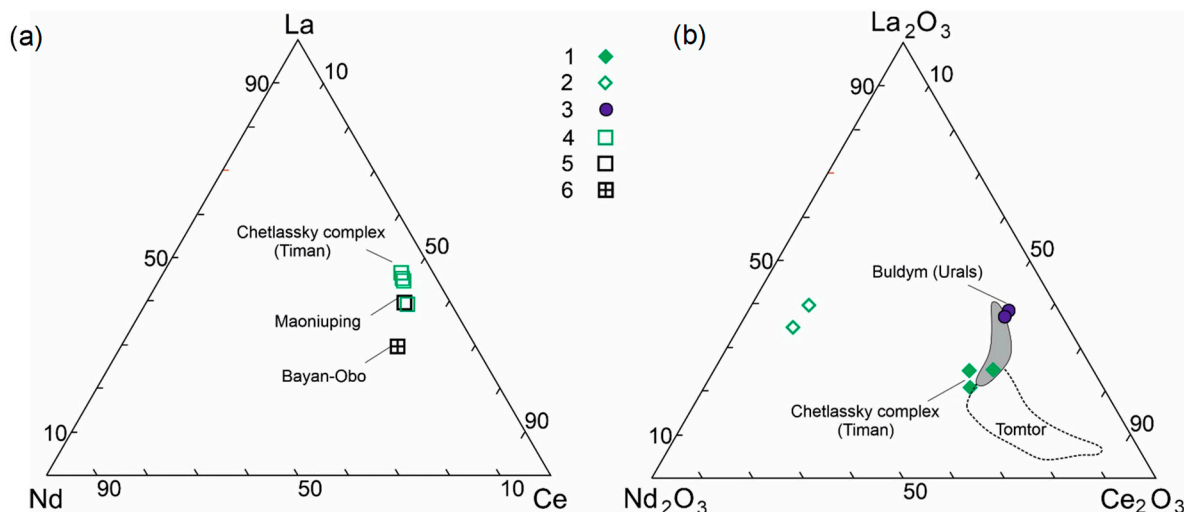


Figure 10. Chemistry of bastnäsite and monazite: (a) ternary diagram with major REE cation vertices showing bastnäsite compositions; (b) ternary diagram showing relative La₂O₃, Ce₂O₃, and Nd₂O₃ (wt%) contents in monazite: 1, 2—monazites of Chetlassky complex (M. Timan) [84]: 1—early Mnz I, 2—late Mnz II; 3—monazites of Buldym complex (S. Urals); 4–6—bastnäsites from: 4—Chetlassky complex (M. Timan); 5—Maoniuping, China, 6—Bayan Obo, China. Monazite compositions in carbonatites of other localities worldwide are plotted for reference: Siberian craton (Tomtor rare-metal deposit), China craton with Qinling and Mianning–Dechang orogenic belts (Bayan Obo, Dashigou, Yuantao, Miaoya, Daluxiang and Maoniuping REE-deposits) (grey field) [152–156].

Bastnäsites from the Chetlassky complex can be classified as bastnäsite-(Ce), with a formula (Ce,La,Nd)(CO₃)(F,OH) and hydroxylbastnäsite-(Ce) (Ce,Nd,La)(CO₃)(OH,F) (Figure 10a; Table 2). They are characterized by relatively uniform compositions with molar La/Ce ratios of 0.74–0.96, and La/Nd ratios of 4.66–8.96. All bastnäsites contain much higher contents of LREEs compared with CaO. Although the CaO content (1.18–2.36 wt%) is not high, it is a substitute for La and Ce in all studied bastnäsite varieties. The Ce and Nd concentrations in the bastnäsites of the Chetlassky complex are lower than those in the Bayan Obo REE-deposit (Figure 10a) and are close to the bastnäsite of the Mianning–Dechang REE belt with the largest REE carbonatite deposits such as Maoniuping (Figure 10a) [15,52,157].

Although carbonatite complex REE-minerals can form under magmatic environments (for example, Mountain Pass, California [157,158]), they occur mainly within carbonatite emplacement at the later sequences of carbonatite complexes, forming at the final stages of the evolution of the alkaline–carbonatite magmatic system. Various mechanisms of REE accumulation in the late facies of carbonatites of alkaline–ultramafic complexes have been proposed: (1) magmatic REE concentrations in the orthomagmatic fluid created by fractional crystallization [159], (2) remobilization of REEs leached from primary minerals, such as carbonate or apatite [14,51,160,161], and (3) remobilization of REEs from the early magmatic REE minerals.

Our studies of carbonates from the Kosyu carbonatites of the Chetlassky complex evidenced that early calcites of Chetlssky carbonatites are enriched in Ba, TR, and Sr (SrO 5.44 wt%, BaO 0.44 wt%, La₂O₃ 0.23 wt%) (Figure 4a,b,d,e), and later calcites have low contents of isomorphic addition of these elements (SrO 1.0 wt%, BaO 0.69 wt%, La₂O₃ 0.01 wt%), but at the same time contain ultrafine (µm) ingrowths of REE–Sr–

carbonate phases: ankylite ($\text{Sr}_{0.59-0.68}\text{Ca}_{0.23-0.28}\text{O}_{0.97-0.91}(\text{La}_{0.54-0.55}\text{Ce}_{0.48-0.51})_{1.01-1.06}(\text{OH}) \times \text{H}_2\text{O}(\text{CO}_3)$) and burbankite ($\text{Na}_{2.05-2.26}\text{Ca}_{0.95-0.74}\text{O}_{3.0}(\text{Sr}_{1.82-1.71}\text{Ca}_{0.65-0.83}\text{La}_{0.13-0.17}\text{Ce}_{0.1-0.16}\text{Ba}_{0.09-0.11})_{2.87-2.97}(\text{CO}_3)_5$). Carbonates also contain inclusions of carbocernaite, strontianite, and barite, while small inclusions of monazite are associated with grains of phosphates (apatite) (see Figure 4). Late carbonate veinlets contain larger segregations (up to $n \times 100 \mu\text{m}$) of rare earth fluor-carbonates—bastnäsite ($\text{Ce}_{0.46-0.48}\text{La}_{0.44-0.35}\text{Nd}_{0.05-0.08}\text{Ca}_{0.05-0.09}\text{O}_{0.99-1.02}(\text{CO}_3)$) ($\text{F}_{0.51-0.17}\text{OH}_{0.49-0.83}$) (Figure 4b), less often parisite as well as apatite, barite, hematite, ilmenorutile, quartz, and fluorite. These data support the model of formation of REE-deposits of the Chetlasky complex from primary REE-enriched carbonatite melt, from which REE-rich rock-forming minerals crystallize on liquidus with subsequent remobilization of REEs from primary minerals (calcite and apatite) at the final (hydrothermal) stages of the carbonatite genesis.

5.2. Evolution of Alkaline–Carbonatite Magmas as a Factor of Ore Specialization

Carbonatite complexes are enriched in HFSE (Nb, Ta, Zr, Hf, V, Ti) and LILE (Sr, Ba, LREE, Th) and often form economically significant deposits of these elements. Nb deposits are associated with carbonatites, accounting for 99% of the world's niobium (Nb) [2,162]. In most carbonatite deposits, the main niobium concentrators are minerals of the pyrochlore group and less frequently, the perovskite, columbite, and euxenite group minerals [2]. Nb carbonatite deposits with pyrochlore-type ores are the main manufacturing type of niobium deposits. REE deposits, related with carbonatites, account for more than 50% of global rare-earth element (REE) resources [163]. The main concentrators of REE are the fluorocarbonates (bastnäsite, parisite) and monazite group minerals [16]. Bastnäsite carbonatites are the main manufacturing type of REE deposits.

It is well known that carbonatite complexes have different ore specialization (a set of ore-forming and associated components and the mineral type of ores, which determines the manufacturing type of deposits). Multicomponent Nb-(Ta)-REE deposits with pyrochlore, pyrochlore–gattchetolite, and pyrochlore–columbite–monazite ores are associated with alkaline–ultrabasic carbonatite complexes of intraplate settings (for example, Nb-REE Tomtor and Nb-REE Chuktukonskoe deposits (Siberian platform, Russia), Nb-Ta-P Neske-Vaara deposit (Kola carbonatite province) and some others). REE specialization is typical for alkaline–mafic carbonatite complexes of folded areas. LREE-deposits of bastnäsite carbonatites with bastnäsite–parisite–monazite ores are associated with these complexes (REE Mountain Pass deposit, USA).

One of the important issues of ore formation associated with carbonatite complexes is the reason for their enrichment with various ore components. In alkaline–ultrabasic carbonatite complexes, which are usually highly differentiated, this is associated with the temperature evolution of carbonatite melts, when early calciocarbonatites were replaced by magnesiocarbonatites, and later ferrocarnatites [164]. It is well known that carbonatites of different stages of formation are enriched in HFSE (Nb, Ta, Zr, Hf, Ti) to varying degrees as well as Sr, Ba, LREE and P, F. HFSE accumulation with crystallization of ore minerals in early carbonatites is confined to the magmatic stage of the carbonatite genesis [110]. Decrease in HFSE content occurs from early to late carbonatites [165]. Unlike HFSE, REE, Sr, and Ba enrichment is related to the latest low temperature facies of carbonatites [16,166]. Along with this, abnormally the REE-enriched metasomatic mantle source (SCLM with subducted component) and liquid immiscibility in the carbonatite–syenite magma is discussed as the reason for the formation of large REE-deposits related to bastnäsite carbonatites (Mianning–Dechang, China) [17,44,167]. In both cases, models involving fluids derived from carbonatite or alkaline magmatism, and ore-forming hydrothermal fluids released from carbonatite magmas are key.

The **Ilmeno–Vishnevogorsk complex** of the Southern Urals is a type-locality for carbonatite complexes of the “linear type”—an independent formation type of carbonatites associated with linear zones of alkaline metasomatites, nepheline–syenite, and alkaline–syenite rocks, also called “the carbonatites of linear-fractured zones” [46]. To date, similar

“linear type” carbonatite complexes associated with nepheline syenites and fenites are known in Siberia (Penchenga, Yenisei ridge), Ukraine (Chernigov, Dubrava), Norway (Stjernoy, Sorrow), Finland (Siilinjärve), Canada (Lonny, Perry River, Cravier, Nisikatch), India (Corati, Newania), Brazil (Anjiko Dos Diaz), Australia (Mud Tank), Pakistan (Loe Shilman and Sillai Patti), and China (Qinling) (database “Rare metal carbonatites and diamondiferous kimberlites of the world”).

IVC has a Nb specialization and is a representative of Nb-deposits with a pyrochlore type ore (Vishnevogorskoe, Potaninskoe deposits). The average Nb₂O₅ content in carbonatite ores of one of the IVC deposits is 0.168 wt%; the contents of associated components are as follows: SrO—1 wt%, ZrO₂—0.078 wt%, TR₂O₃—0.15 wt%, P₂O₅—1.1 wt%, U—0.0065 wt%, Th—0.0026 wt%, Ta₂O₅—0.0008 wt% [27,76]. The ores of the Vishnevogorsky and Potanino deposits are represented by Nb (pyrochlore) carbonatite manufacturing type of ores (with by-product components P, REE, Zr, U, Th, Sr) [76], similar to those in the deposits of intraplate carbonatite complexes of the alkaline–ultramafic formation. At the same time, the content of ore components, in particular Nb₂O₅, in them is somewhat lower than in ores of carbonatite deposits of the alkaline–ultramafic complexes (e.g., 0.5% Nb₂O₅—Beloziminskoe, 1.02% Nb₂O₅—Bol’shetagninskoye (Siberia, Russia), 0.42% Nb₂O₅—Niobec, Saint-Honoré complex, Canada) [168].

The **Buldym complex** of the Southern Urals is associated with the Nb–REE type of deposits with the pyrochlore–monazite type of ores (Buldym and Spirikhinskoe deposits). The average contents of the main ore components in the Buldym ores are Nb₂O₅—0.164 wt% (Buldym deposit), Nb₂O₅—0.22 wt%, and TR₂O₃—0.71 wt% (Spirikhinskoe deposit) [27]. The ores of the Buldym deposit are represented by the REE–Nb (pyrochlore–monazite) type of ore, and the Spirikhinskoe deposit by the REE–Nb (monazite–aeshinite) type of ore [27]. These indicate the Nb–REE specialization of the deposits of the Buldym complex.

The main ore minerals of the rare-metal Nb-deposits of the IVC are the pyrochlore group minerals, while the late REE–Sr–Ba mineralization (fersmite, orthite, chevkinite, fergusonite, bastnäsite, synchysite, parisite, ankylite, strontianite, barilite, burbankite, xenotime, lucasite) is very rare and has no mining potential. However, in the Buldym complex, along with pyrochlore, the REE-mineralization (monazite) has an economic potential [27]. Furthermore, aeschynite and columbite group minerals are also present in significant quantities.

The IVC pyrochlores, as in other complexes of alkaline rocks and carbonatites, are a product of the residual crystallization of carbonated alkaline magma and crystallizes at the pegmatite and carbonatites (see Section 5.1). At the same time, IVC carbonatites are represented by high-temperature mono-facies varieties of calciocarbonatites (see Figure 5), enriched in HFSE and LILE (Figure 6a,b). The HFSE and REE contents in the IVC carbonatites are comparable to the averaged compositions of calciocarbonatites of the world (Table 3, Figure 6) [101]. However, IVC carbonatites are significantly enriched in Sr (to 22,000 ppm) in comparison with the early facies of carbonatites from the intraplate alkaline–ultrabasic complexes (on average, 5800 ppm). Low Nb/Ta (<35) and La/Yb (<60) ratios as well as high Sr content and Eu/Eu* ratio (near 1) in early IVC silicocarbonatites indicate an insignificant degree of differentiation of IVC carbonatite magmas. High Nb/Ta ratio (230–1400) and decreasing Zr/Hf (to 18), Y/Ho (to 13), and Eu/Eu* (to 0.75) [28] as well as a high F content in IVC calciocarbonatites II are typical for the fluid-hydrothermal carbonate systems [169].

Estimates of the formation temperatures of the IVC early silicocarbonatites (sövite I) with uranopyrochlore mineralization are 650–600 °C (according to biotite–pyroxene and amphibole–pyroxene thermometers [46]) and are close to the crystallization temperatures of miaskite–pegmatites (750–590 °C and 3.5–2.5 kbar according to the thermobarometry data [150]). The most evolved varieties of calciocarbonatites (sövite II) with fluorocalciopyrochlore of late generations (Pcl IV) were formed at 590–490 °C [46]. IVC sövite formation temperatures are also estimated by high temperatures (640–670 °C) using a titanium thermometer in zircons [71].

Thus, in contrast to the intraplate alkaline–ultramafic carbonatite complexes, late low-temperature ferrocarnatites with Sr–Ba–REE-mineralization are absent in the IVC. IVC carbonatites contain only HFSE accessory mineralization (pyrochlore, zircon, ilmenite, titanite, ilmenorutile), while the proper minerals of LILE (Sr, REE, Ba) are absent in these carbonatites. REE–Sr–Ba mineralization in IVC is very poorly developed and occurs only in fenite halos in late feldspar, calcite, and quartz–arfvedsonite veinlets.

In the Buldym complex (Urals), high-temperature varieties of calciocarnatites (see Figure 5) with pyrochlore mineralization are also widespread. U–(Ta)-rich pyrochlores (uranpyrochlore I) are formed in early glimmerite-like rocks, probably at the early stages of ore formation. Fluorocalciopyrochlores (Pcl III) (see Figure 9), with low trace element contents, are formed in early calcite–dolomite carbonatites (calciocarnatites according to [101]) enriched in HFSE and LILE and isofacial with IVC sövites II (see Figure 6c,d). Fluorocalciopyrochlores in calcite–dolomite carbonatites crystallize in paragenesis with tetraferriphlogopite, fluorrichterite, apatite, ilmenite, magnetite, pyrrhotite, and pyrite at high temperatures of 575–410 °C and $P = 1.6\text{--}1.2$ kbar (according to the calcite–dolomite thermobarometer [46,170]).

In contrast to the IVC, in the Buldym complex, along with high-temperature calciocarnatites, lower-temperature varieties are widespread—beforsites (magnesiocarnatites according to [101] (see Figure 5)) are enriched in LREE and Th relative to the early facies of Buldym and IVC carbonatites (Figure 6c,d). REE enrichment of beforsites is associated with REE and REE–Nb mineralization, represented by REE–phosphates (monazite, rarely rhabdophanite) and REE–tantalonibates (aeshinite, less often chevkinite, polyakovite, ortite, fergusonite, fersmite), which are formed at lower temperatures 315–230 °C and $P = 0.9\text{--}0.36$ kbar [46] in paragenesis with amphibole, apatite, columbite, ilmenite, zircon, and phlogopite (replacing chlorite). Buldym beforsites are depleted in Ba and Sr with respect to the average compositions of magnesiocarnatites (Figure 6c,d). Accordingly, Ba–Sr-mineralization is very poorly developed in them (strontianite, ankyllite, barite are found, but very rare). It should be noted that, in contrast to the intraplate alkaline–ultramafic carbonatite complexes in the Buldym complex as well as in the IVC, the latest ferrocarnatites with Sr–Ba–REE-mineralization are absent.

Chetlassky complex of ultramafic–mafic dykes and carbonatites of the Middle Timan has a REE specialization and is a representative of cerium–earth carbonatite deposits with the bastnäsite–monazite ore type. The average TR_2O_5 content in carbonatite ores of the Kosyu occurrence is 1.84% in concentration, according to the estimated prognoses resource [82], with variations from 1 to 4%, which corresponds to the ore grade of rare-earth deposits. At the same time, the average Nb_2O_5 content is 0.04%, which is lower than the cut-off grade for niobium deposits, with a high Ta_2O_5 content of 0.007%. The ores of the Kosyu deposit are represented by the rare-earth (bastnäsite–monazite) carbonatite manufacturing type (with associated Fe, Th, Ba, and F components as coproducts), similar to those in the bastnäsite carbonatite deposits of the alkaline–mafic complexes. The ore component content (TR_2O_5 1–4 wt%) in them is slightly lower than in rich ores (5–10 wt%) of the largest deposits of this type (e.g., 7.98% TR_2O_5 —Mountain Pass, USA and 6.8% Bayan-Obo).

Unlike IVC and Buldym, hypabyssal medium- and low-temperature facies ($T = 500\text{--}150$ °C) [26] of carbonatites are widely developed in the Chetlassky complex, represented by magnesio- and ferrocarnatites (Figure 5). Carbonatites of the Chetlassky complex are enriched in LREE and depleted in HFSE (Nb, Zr, Ti) relative to the world average compositions of magnesio- and ferrocarnatites [101] (see Figure 7b) as well as to IVC calciocarnatites (see Figure 6a,b). Having similar compositions of HFSEs with beforsites of the Buldym massif, Chetlassky carbonatites are distinguished by high fractionation of REE (with maximum La/Yb ratio and pronounced “tetrahedral effect” [169]) (Figure 7a), which is typical for fluid-hydrothermal carbonate systems.

LREE enrichment in the Chetlassky ferrocarnatites is associated with phosphates (monazite, apatite), REE–fluorocarbonates (bastnäsite group of minerals), REE–Sr–Ba–

carbonates (burbankite, ankylite-(Ce), carbocernaite, strontianite), which are formed in paragenesis with ankerite, siderite, calcite, amphibole, phlogopite (replaced by chlorite), barite, hydroxylpyrochlore, columbite, and ilmenorutile. Pyrochlore is represented by hydroxyl- and hydroxy-pyrochlore, tracing the hydrothermal trend in the composition diagram (Figure 9b). In the later low-temperature associations of quartz–goethite–feldspar and quartz–goethite–hematite veins ($T = 150\text{--}200\text{ }^{\circ}\text{C}$ [26]), late monazites (with relics of early Th-rich generations), bastnäsite, columbite, Nb–rutile, xenotime, zircon, Mn–Ce, and Fe–Ce oxides are formed [84,85].

Summarizing the above-mentioned, the different ore specialization of the Urals and Timan carbonatite complexes can be related, first of all, with the intracrustal processes of alkaline and carbonatite magma evolution as well as with the prevailing specific facies of carbonatites in each of the complexes. Thus, the Nb specialization and formation of the IVC Nb-deposit in the Southern Urals is associated with the late magmatic (pegmatite and high-temperature calciocarbonatite) facies of rocks with pyrochlore mineralization. According to thermobarometric data, crystallization of alkaline rocks and IVC carbonatites occurred at high pressures (5–2.5 kbar) and temperatures (850–490 °C) [27,46,170,171]. Uranpyrochlores and fluorocalciopyrochlores (with a low Nb/Ta, less than 70) crystallized at the late magmatic stage in pegmatites and siliciocarbonatites. Fluorocalciopyrochlores of late generations (with a high Nb/Ta value, > 300, and high F 4–5 wt%) were formed in evolved calciocarbonatites and in fenites from high-temperature fluid carbonate systems with high F.

The Nb–REE specialization of the deposits of the Buldym complex is due to the simultaneous development of high- and medium-temperature facies of calcio- and magnesiocarbonatites with pyrochlore and monazite–eshinite–columbite mineralization, respectively. According to the thermobarometric data, their formation took place in a wider temperature range (575–230 °C) and at lower pressures (1.6–0.56 kbar) [105]. Fluorocalciopyrochlores (with a low content of impurities and high F ~4.5 wt%) crystallize in early high-temperature facies of calciocarbonatites at subsolidus temperatures from fluid-saturated carbonate systems. Aeshinite, columbite (replacing pyrochlore), and monazite (Ce) are formed in the mid-temperature facies of carbonatites (beforsites).

The REE specialization of the Chetlassky dike complex is associated with hypabyssal medium-low-temperature facies (500–200 °C [26]) of magnesio- and ferrocarnatites and low-temperature (200–150 °C) quartz–goethite–hematite formations (of the redbergite type). REE ore mineralization, represented by minerals of the bastnäsite and monazite groups as well as REE–Sr–Ba-carbonates (burbankite, ankylite-(Ce), carbocernaite), formed in carbonatites as a result of subsolidus remobilization of REEs leached from primary carbonatite minerals such as carbonate or apatite. Hydrothermal fluids derived from carbonatite have been the source for monazite, bastnäsite, xenotime, columbite, ilmenorutile, Mn–Ce, and Fe–Ce oxides in late quartz–goethite–hematite veins and in fenites.

5.3. Mantle Source Characteristics: Rb–Sr and Sm–Nd Isotope Signatures

Nd and Sr isotopic composition is widely used to interpret the origin of carbonatite complexes and mantle sources of alkaline and carbonatite magmatism [31,38]. The magma source, depleted to varying degrees, suggests that the origin of intraplate ultramafic–alkaline carbonatite complexes, which are widespread on the shields and along the edges of platforms, is associated with a deep mantle source, possibly with a mantle plume (HIMU, FOZO), but does not exclude a mixing of plume substances with an enriched component of the EMI type [31,33,34,37]. At the same time, mixed mantle–crustal sources, usually enriched in radiogenic strontium isotopes and non-radiogenic neodymium, have been identified for many carbonatite complexes of folded areas [9,20–22]. The enrichment of carbonatite complexes in radiogenic Sr isotopes can be caused by recycling and enrichment of mantle reservoirs with components of the oceanic and continental crust [17,44,45,48,167].

The ϵNd — ϵSr diagram (Figures 8A and 11) shows the isotopic compositions of the IVC and the Buldym complex (Southern Urals) rocks in comparison to the carbonatite complexes

of cratons and platforms—the Kola province (KCL) [33–35,38], East African province (EACL) [32], Siberia [121,172,173], Aldan [40,173], and collisional carbonatite complexes of fold regions—Altai, Tien Shan, Himalayan [8,9,17,20–22]. The isotopic signatures of mantle reservoirs (MORB and OIB [41,114], DM, HIMU, FOZO, EM1, EM2 [115,116,118]) as well as the compositions and the lines of isotope system evolutions are also shown.

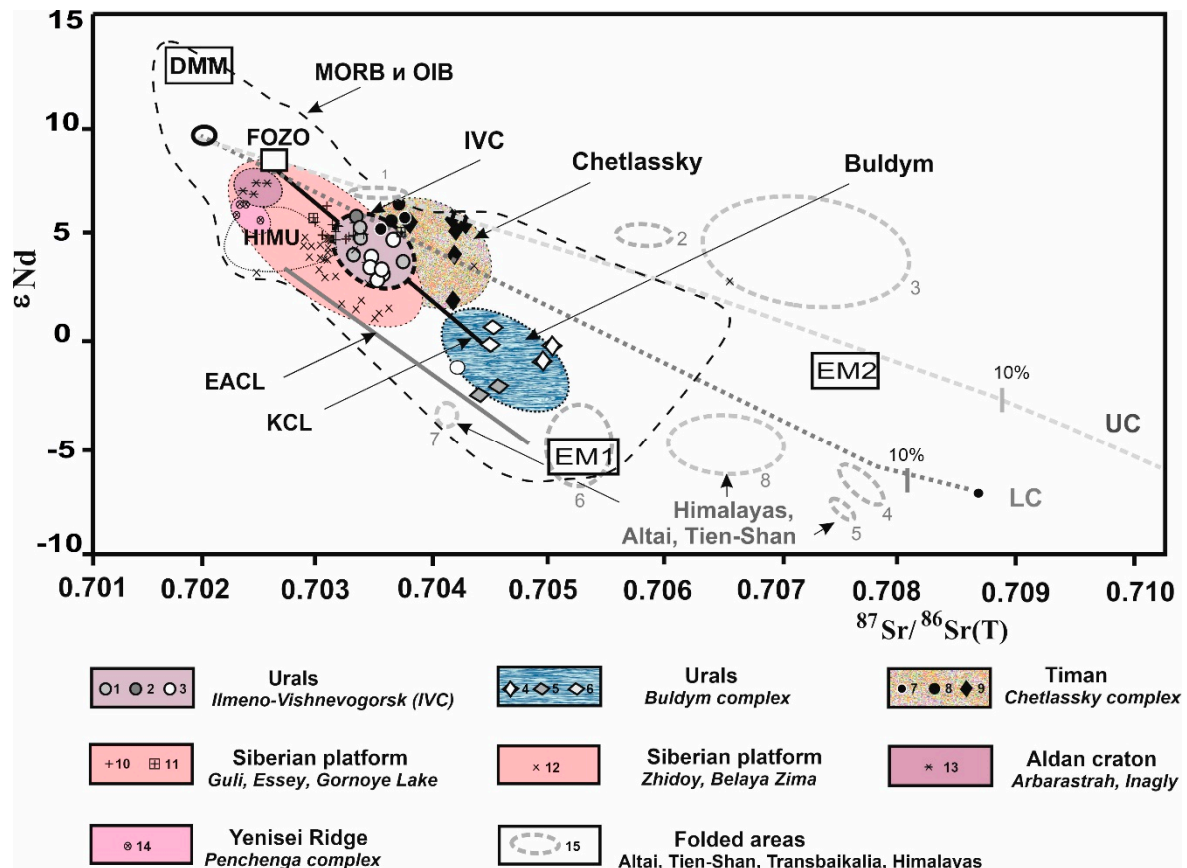


Figure 11. $\epsilon_{\text{Nd}}-^{87}\text{Sr}/^{86}\text{Sr}(\text{T})$ diagram for carbonatite complexes of the Urals and Timan in comparison with carbonatite complexes of shields and platforms: Kola province (KCL) [33,38], East African Province (EACL) [32], East Siberian platform and its framing [121,172–176], the Aldan Shield [173], and with collision carbonatite complexes of folded regions: Altai, Tien Shan, Transbaikalia, Himalayan [8,9,12,17,20–22,42,43]. The elongated dotted line limits the field of mantle isotopic compositions [41]. The Kola carbonatite line (KCL) [33] and the East African carbonatite line (EACL) [32]. The mantle end-members: DMM, EM1, EM2 are given in accordance with their modern isotopic signatures [115,116,118]. FOZO—mantle reservoir according to [116,118]. To calculate the DM–LC mixing line, values of the DM source: $^{143}\text{Nd}/^{144}\text{Nd}_{440} = 0.512534$ ($\epsilon_{\text{Nd}} = +9.05$), $^{87}\text{Sr}/^{86}\text{Sr}_{440} = 0.70187$, Sr = 6 ppm, Nd = 0.33 ppm according to [123] and the lower crust (LC): $^{143}\text{Nd}/^{144}\text{Nd}_{440} = 0.511694$ ($\epsilon_{\text{Nd}} = -7.4$), $^{87}\text{Sr}/^{86}\text{Sr}_{440} = 0.7087$, Sr = 370 ppm, Nd = 30 ppm according to [177] were used. 1, 2: Ilmenite–Vishnevogorsk complex (IVC), South Urals (Pz): 1—miaskites, 2—syenites, 3—carbonatites (sövites I, II); 4–5: Buldym complex, South Urals: 4—ultramafic rocks, 5—carbonatites (sövites III), 6—beforsites; 7–9: Chetlassky complex, Middle Timan (V): 7—carbonatites, 8—carbonate-bearing lamprophyres, 9—picrites and lamprophyres; 10–12: carbonatite complexes of the East Siberian platform and its framing: 10—Guli, Essey, Maymecha-Kotui province (Pz); 11—Gornoye Lake, Sette-Daban province (Pz); 12—White Winter, Middle Winter, Zhidoy, East Sayan province (V); 13—Arbarastrakh, Inagly, Aldan Shield (V), 14—Penchenginsky, Yenisei ridge (RF₃-V); 15—collision carbonatite complexes of fold regions—Altai, Tien Shan, Transbaikalia, Himalayas (1—Edelweiss, 2—Upper Petropavlovsk, Altai-Sayan fold region (Pz); 3—Kharly, Bayankol, Dakhunur, Chik, Sangilen (C); 4—Matchaisky, 5—Darai-Pioz, S. Tien Shan (Mz); 6—carbonatite complexes of Transbaikalia (Mz); 7—Loe-Shilman, Pakistan (Kz); 8—Maoniuping, Lizhuang, Himalayas (Kz).

The IVC carbonatites and miaskites (Vishnevogorsk and Potanino Nb deposits) have low values of $^{87}\text{Sr}/^{86}\text{Sr}_i$ from 0.70336 to 0.70380 (ϵ_{Sr} from -8.8 to -2.6) and a maximum of

$^{143}\text{Nd}/^{144}\text{Nd}_i$ (ϵ_{Nd} from +2.9 to +4.9), which corresponds to the signatures of a moderately depleted mantle. The Sr–Nd isotopic composition of pyrochlores is in the range of the miaskite–carbonatite complex compositions (see Table 5), which suggests a common source of ore matter and IVC rocks (miaskites and carbonatites). Only carbonatites of exocontact halos (ore zone 140) are rather enriched in radiogenic strontium and non-radiogenic neodymium: $^{87}\text{Sr}/^{86}\text{Sr}_i$ at 0.70421 and ϵ_{Nd} from -1.4 to -1.5 .

The IVC rock composition data-points are shown on the $^{87}\text{Sr}/^{86}\text{Sr}_i$ — ϵ_{Nd} diagram within the mantle trend, on the line connecting the depleted (DM) and enriched (EM1) mantle (Figures 8A and 11). A similar line of the isotope system evolution is characteristic of carbonatite complexes of the Kola province located within Baltic craton. According to Kramm [33] and Kogarko [38], the Kola carbonatite line reflects the mixing of the mantle reservoirs DM (or plume-like component FOZO) and EM1 during magma generation. A similar isotopic composition was also found in carbonatite complexes framing the Siberian platform (Maymecha-Kotui and East Aldan provinces) [39,121,173].

The carbonatites of the Buldym complex (Buldym Nb-REE deposit) form a field in the diagram with higher $^{87}\text{Sr}/^{86}\text{Sr}_i$ values from 0.70421 to 0.70470 ($\epsilon_{\text{Sr}}(t)$ from +3.2 to +10.2) and low $^{143}\text{Nd}/^{144}\text{Nd}_i$ values with negative $\epsilon_{\text{Nd}}(t)$ from -1.4 to -3.4 , corresponding to a more enriched source EM1 type. The calciocarbonatite pyrochlore has the same isotopic composition (see Table 5), which indicates a single source of carbonatites and ore. The REE–Nb ore mineralization has a more radiogenic Sr isotopic composition ($^{87}\text{Sr}/^{86}\text{Sr}_i$ from 0.70617 to 0.70715) and negative $\epsilon_{\text{Nd}}(t)$ from -0.7 to -5.8 , which may be associated with the participation of crustal fluids in the alkaline metasomatism and ore formation within the Buldym complex. The Sr–Nd isotopic compositions of the Buldym carbonatites are also on the DM–EM1 mixing line, but closer to the enriched mantle compositions of the EM1 type compared to the IVC. It should be noted that similar isotopic compositions of the EM1 type are also found in carbonatite complexes of rift zones of shields with the deepest mantle sources (e.g., the East African Rift, Aldan Shield, Eastern Siberia), in the formation of which the possible participation of the plume HIMU component is assumed [32,173].

The carbonatites of the Chetlassky complex of Middle Timan (Kosyu REE ore-occurrence) show a narrow variation: $^{87}\text{Sr}/^{86}\text{Sr}_i$ from 0.70336 to 0.70369 and $\epsilon_{\text{Nd}}(t)$ from +5.1 to +5.7, which are close to the signatures of the moderately depleted mantle array, but show a slight deviation toward high ϵ_{Nd} (Figure 11). This isotopic composition is close to those associated with Kosyu lamprophyres ($^{87}\text{Sr}/^{86}\text{Sr}_i$ from 0.7037 to 0.7043, ϵ_{Nd} from +5.4 to +6.2) (see Table 5). These isotopic data indicate a rather common mantle source for the Kosyu carbonatite and lamprophyre substances. However, the lamprophyres of the Chetlassky complex are characterized by more significant variations in the initial isotope ratios and a more enriched isotopic composition ($^{87}\text{Sr}/^{86}\text{Sr}_i$ from 0.70365 to 0.70589 and ϵ_{Nd} from +1.8 to +6.2) (see Table 5), which are close to those for the Proterozoic (V) diamondiferous aillikite–carbonatite dike complexes (e.g., Aillik-Bay, Labrador) [120] (see Figure 8B). It should be mentioned that the most radiogenic Sr isotopic composition ($^{87}\text{Sr}/^{86}\text{Sr}_i$ up to 0.711) in Chetlassky lamprophyres [60,113] is the same as previously noted for Italian lamprophyres and its origin was associated with recycling and enrichment of mantle reservoirs with oceanic and continental crust components [45].

Previous studies indicate that most of the intraplate carbonatites share significant isotopic similarities with young oceanic island basalts (OIB) [47]. In contrast, off-craton carbonatites often have a higher initial $^{87}\text{Sr}/^{86}\text{Sr}$ and/or lower ϵ_{Nd} values (Figure 11) that are outside the Sr–Nd mantle array [41]. For example, carbonatite complexes of the Tien Shan, Altai-Sayan fold area, Transbaikalia, and the Himalayas [8,9,17,20–22,42–44] are usually contaminated with crustal or recycled components and, as a consequence, are enriched in radiogenic Sr and non-radiogenic Nd (see Figure 11). Highest $^{87}\text{Sr}/^{86}\text{Sr}_i$ (0.7045–0.7095) and lowest ϵ_{Nd} were found in the giant carbonatite-associated REE deposits (CARDs) (the world's largest Bayan-Obo [48,178]), Maoniuping (the giant LREE deposit [17]) as well as Laiwu, Shandong, China [179].

Crustal assimilation [8,9,20–22], sedimentary carbonate contamination [180] and heterogeneous mantle sources [17,174,179] are discussed as the cause of Sr and REE enrichment and deviation from the typical Sr–Nd carbonatite isotopic composition similar to OIBs. Ying [179] and How [17] substantiated that carbonatite-associated REE deposits (CARDS), highly enriched in radiogenic Sr and non-radiogenic Nd, were derived by the recycling of marine sediments. This two-stage model assumes that REE carbonatites are formed “by melting of the sub-continental lithospheric mantle (SCLM), which have been previously metasomatized by high-flux REE- and CO₂-rich fluids derived from subducted marine sediments” [17].

To assess the possibility of contamination of mantle magmas of the Urals carbonatite complexes with crustal substances, we calculated the Nd–Sr isotope mixing lines of a DM-type mantle source with lower crustal [177] and upper crustal components (i.e., IVC and Buldym complex host rocks are gneisses of the Vishnevogorskaya Formation) (see Table 5). The calculation was carried out according to the equation of mixing the Sr and Nd isotopic ratios taking into account the concentrations of elements in the mantle and crustal components [181]. Calculations have shown the possibility of the presence of an insignificant amount of lower crustal material (<3%) in the isotopic composition of IVC alkaline feldspar syenites, while the possibility of the mixing of IVC and Buldym carbonatite magmas with upper crustal material is extremely unlikely (see Figure 11).

Calculation of the Nd–Sr isotope mixing-lines of the DM-type mantle source with the marine sedimentary-carbonate rocks showed that the mantle component reached more than 95% in lamprophyres of the Chetlassky complex and the marine sedimentary component did not exceed 5% (see Figure 8B). Contamination by marine sediments with a high ⁸⁷Sr/⁸⁶Sr (>0.712) can lead to a synchronous increase in ⁸⁷Sr/⁸⁶Sr, δ¹⁸O, and δ¹³C values in carbonatites [17]. However, such contamination cannot explain why the REE–carbonatites of the Chetlassky complex had low ⁸⁷Sr/⁸⁶Sr (Figure 8A), the lowest δ¹³C values (−3.4‰), and the highest δ¹⁸O (15.2‰) among the Chetlassky rocks [112]. Therefore, we can assume that these Sr–Nd isotopic signatures in the REE–carbonatites of the Chetlassky complex reflect the heterogeneity of the mantle source, probably associated with different degrees of enrichment of the depleted mantle in components of subducted marine sediments. The Buldym REE–Nb carbonatites also support this hypothesis, showing binary mixing between the DM and EM1 mantle reservoirs (since “enriched mantle EMI is caused by the recycling of continental crust or lithosphere” [182]).

Thus, heterogeneous mantle sources slightly enriched in subducted oceanic crust (EMI type [182]) and marine sediments are likely to have been the melting substrate for the magmas of Ural and Timan carbonatite complexes. The IVC carbonatites with Nb specialization had the least contaminated Sr–Nd isotopic compositions, while REE–Nb and REE carbonatites of the Buldym and Chetlassky complexes showed different degrees of contamination. Based on the Sr–Nd isotope data, major composition of rocks and minerals and trace element pattern, we suggest that the ore specialization of carbonatite complexes in the Urals and Timan may be related (associated) not only with the evolution of carbonatite magmas, but also with the heterogeneity of mantle sources, which were probably produced by the mixture of a mantle component with subducted oceanic crust and marine sediments.

6. Conclusions

(1) The Ilmeno–Vishnevogorsk (IVC), Buldym, and Chetlassky carbonatite complexes are representatives of the off-cratonic carbonatite complexes with different ore specialization (Nb, Nb–REE, and REE, respectively). Nb specialization of the IVC deposits is associated with magmatic abyssal facies of miaskite–pegmatite and calciocarbonatites with pyrochlore ore mineralization. The Nb–REE specialization of the Buldym deposits is due to the presence of both facies of calcio- and magnesiocarbonatites, with pyrochlore and monazite–aeshinite–columbite mineralization, respectively. The REE specialization of the Chetlassky dyke complex (M. Timan) is associated with hypabyssal facies of magnesio- and

ferrocarbonatites and late hydrothermal quartz–goethite–hematite veins with monazite–bastnäsite ore mineralization.

(2) The IVC is characterized by low $^{87}\text{Sr}/^{86}\text{Sr}_I$ (0.70336 to 0.70399), coupled with positive $\epsilon\text{Nd}(t)$ (+2 to +6), suggesting a single moderately depleted mantle source (DM-type) for carbonatites and associated miaskites, and pyrochlore ore mineralization. The Buldym complex had a higher $^{87}\text{Sr}/^{86}\text{Sr}_I$ (from 0.70440 to 0.70513) with negative $\epsilon\text{Nd}(t)$ (−0.2–−3), which corresponds to a more enriched mantle source (EMI-type). The Chetlassky REE–carbonatite and associated lamprophyres are characterized by low $^{87}\text{Sr}/^{86}\text{Sr}_I$ (0.70336 to 0.70369) and a high $\epsilon\text{Nd}(t)$ (+5–+6), which is close to a moderately depleted mantle source with ~5% marine sedimentary component.

(3) Sr–Nd composition of Urals and Timan carbonatites is close to those of intraplate carbonatite complexes located in the Baltic craton (Kola Province) and at the edges of the Siberian platform (Maymecha-Kotuiszkaya, East-Sayan, Udzhinskaya, Sette-Dabanskaya, East-Aldan Alkaline provinces). Urals and Timan carbonatites differ by less contaminated mantle Sr–Nd isotopic signatures from collisional carbonatite complexes of Altai-Sayan, Transbaikalia, Tien Shan, and Himalayan fold regions, which are often highly contaminated by crustal recycled components and, as a consequence, enriched in radiogenic Sr and non-radiogenic Nd.

(4) The Sr–Nd isotopic compositions of Urals and Timan carbonatite complexes suggest that their different ore specialization can be caused not only by crustal evolution of alkaline and carbonatite magmas, but also by the heterogeneity of mantle sources associated with varying degrees of enrichment in subducted components of oceanic crust and marine sediments. To address these issues, further research with the use of various isotopic systems is expected.

Author Contributions: Conceptualization, investigation, writing—original draft preparation, visualization, I.N.; Conceptualization, investigation, supervision, N.V.; Resources, funding acquisition O.U.; Writing—review, editing and translation, B.B. All authors have read and agreed to the published version of the manuscript.

Funding: The work was performed within the framework of topic No. AAAA-A18-118052590028-9 of the IGG UB RAS state assignment and was funded by RFBR and Komi Republic, project number 20-45-110010.

Acknowledgments: We are grateful to T.B. Bayanova, V.I. Popova, V.A. Popov, Ya.L. Ronkin, V.V. Sharygin, S.V. Pribavkin, D.A. Zamyatin, I.G. Gottman, and V. Bulatov for their assistance in the research.

Conflicts of Interest: The authors declare no conflict of interest. The funders had no role in the design of the study; in the collection, analyses, or interpretation of data; in the writing of the manuscript, or in the decision to publish the results.

References

- Smith, M.; Moore, K.; Kavecsánszki, D.; Finch, A.A.; Kynicky, J.; Wall, F. From mantle to critical zone: A review of large and giant sized deposits of the rare earth elements. *Geosci. Front.* **2016**, *7*, 315–334. [[CrossRef](#)]
- Mitchell, R.H. Primary and secondary niobium mineral deposits associated with carbonatites. *Ore Geol. Rev.* **2015**, *64*, 626–641. [[CrossRef](#)]
- Bell, K. *Carbonatites: Genesis and Evolution*; Unwin Hyman: London, UK, 1989; p. 618. [[CrossRef](#)]
- Kogarko, L.N.; Kononova, V.A.; Orlova, M.P.; Wooley, A.R. *Alkaline Rocks and Carbonatites of the World. P. 2. Former USSR*; Chapman and Hall: London, UK, 1995; p. 226. [[CrossRef](#)]
- Woolley, A.R.; Kjarsgaard, B.A. Carbonatite Occurrences of the World: Map and Database. Geological Survey of Canada, Open File Report 5796. *Miner. Mag.* **2008**, *71*, 718. [[CrossRef](#)]
- Frolov, A.A.; Tolstov, A.R.; Belov, S.V. *Carbonatite Deposits in Russia*; NIA-Priroda: Moscow, Russia, 2003; p. 494. (In Russian)
- Tilton, G.R.; Bryce, J.G.; Mateen, A. Pb-Sr-Nd isotope data from 30 and 300 Ma collision zone carbonatites in Northwest Pakistan. *J. Petrol.* **1998**, *39*, 1865–1874. [[CrossRef](#)]
- Vrublevsky, V.V. *Petrology of Carbonatite Complexes of Consolidated Folded Areas: The Case of Southern Siberia and the Tien Shan*. Doctoral Thesis, Tomsk University, Tomsk, Russia, 2003; p. 303. (In Russian).

9. Hou, Z.Q.; Tian, S.H.; Yuan, Z.X.; Xie, Y.L.; Yin, S.P.; Yi, L.S.; Fei, H.C.; Yang, Z.M. The Himalayan collision zone carbonatites in western Sichuan, SW China: Petrogenesis, mantle source and tectonic implication. *Earth Planet. Sci. Lett.* **2006**, *244*, 234–250. [[CrossRef](#)]
10. Hou, Z.; Cook, N.J. Metallogeneses of the Tibetan collisional orogen: A review and introduction to the special issue. *Ore Geol. Rev.* **2009**, *36*, 2–24. [[CrossRef](#)]
11. Xu, C.; Wang, L.; Song, W.; Wu, M. Carbonatites in China: A review for genesis and mineralization. *Geosci. Front.* **2010**, *1*, 105–114. [[CrossRef](#)]
12. Doroshkevich, A.G.; Ripp, G.S.; Izbrodin, I.A.; Savatenkov, V.M. Alkaline magmatism of the Vitim province, West Transbaikalia, Russia: Age, mineralogical, geochemical and isotope (O, C, D, Sr and Nd) data. *Lithos* **2012**, *152*, 157–172. [[CrossRef](#)]
13. Woodard, J.; Hetherington, C.J. Carbonatite in a post-collisional tectonic setting: Geochronology and emplacement conditions at Naantali, SW Finland. *Precambrian Res.* **2014**, *240*, 94–107. [[CrossRef](#)]
14. Moore, M.; Chakhmouradian, A.R.; Mariano, A.N.; Sidhu, R. Evolution of rare-earth mineralization in the Bear Lodge carbonatite, Wyoming: Mineralogical and isotopic evidence. *Ore Geol. Rev.* **2015**, *64*, 499–521. [[CrossRef](#)]
15. Xue, S.; Ling, M.-X.; Liuc, Y.L.-L.; Kangd, Q.-Q.; Huange, R.-F.; Zhanga, Z.-K.; Sunf, W. The formation of the giant Huayangchuan U-Nb deposit associated with carbonatite in the Qingling Orogenic Belt. *Ore Geol. Rev.* **2020**, *122*, 103498. [[CrossRef](#)]
16. Lapin, A.V.; Tolstov, A.V. *Minerageny of Carbonatite Weathering Crusts*; Geokart: Geos, Moscow, 2011; p. 308. (In Russian)
17. Hou, Z.; Liu, Y.; Tian, S.; Yang, Z.; Xie, Y. Formation of carbonatite-related giant rare-earth-element deposits by the recycling of marine sediments. *Sci. Rep.* **2015**, *5*, 1–10. [[CrossRef](#)]
18. Xu, C.; Huang, Z.; Liu, C.; Qi, L.; Li, W.; Guan, T. Geochemistry of carbonatites in Maoniuping REE deposit, Sichuan Province, China. *Sci. China* **2004**, *46*, 246–256. [[CrossRef](#)]
19. Yuhenga, J.; Yan, L. Factors controlling the generation and diversity of giant carbonatite-related rare earth element deposits: Insights from the Mianning–Dechang belt. *Ore Geol. Rev.* **2020**, *121*, 103472. [[CrossRef](#)]
20. Vrublevsky, V.V.; Gertner, I.F. Nature of Carbonatite Containing Complexes of Folded Areas: Isotope Evidence of Mantle–Crust Interaction. In *Problems of Deep Magmatism and Plume Sources*; Innset of Geography of SB RAS: Irkutsk, Russia, 2005; pp. 30–49.
21. Vrublevskii, V.V. Sources and geodynamic setting of petrogenesis of the Middle Cambrian Upper Petropavlovka alkaline basic pluton (Kuznetsk Alatau, Siberia). *Russ. Geol. Geophys.* **2015**, *56*, 379–401. [[CrossRef](#)]
22. Vrublevskii, V.V.; Krupchatnikov, V.I.; Izokh, A.E.; Gertner, I.F. The alkaline and carbonatitic rocks of Gorny Altai (Edel’veis complex) as indicators of Early Paleozoic plume magmatism in the Central Asian Fold Belt. *Russ. Geol. Geophys.* **2012**, *53*, 721–735. [[CrossRef](#)]
23. Nikiforov, A.V.; Bolonin, A.V.; Sugorakova, A.M.; Popov, V.A.; Lykhin, D.A. Carbonatites of Central Tuva: Geological structure, mineral and chemical composition. *Geol. Ore Depos.* **2005**, *47*, 360–382.
24. Doroshkevich, A.G.; Ripp, G.S. The Arshan REE carbonatites, Southwestern Transbaikalia, Russia: Mineralogy, paragenesis and evolution. *Can. Mineral.* **2008**, *46*, 807–823. [[CrossRef](#)]
25. Ivensen, Y.P. *Timan’s Magmatism and the Kanin Peninsula*; Nauka: Leningrad, Russia, 1964; p. 124. (In Russian)
26. Kostyukhin, M.N.; Stepanenko, V.I. *Baikal Magmatism of Kanino-Timan Region*; Shurkin, K.A., Makhlaev, L.V., Eds.; Nauka: Leningrad, Russia, 1987; p. 232. (In Russian)
27. Levin, V.Y.; Ronenson, B.M.; Samkov, V.S.; Levina, I.A.; Sergeev, N.S.; Kiselev, A.P. *Alkaline and Carbonatite Complexes of the Urals*; Uralgeolkom: Ekaterinburg, Russia, 1997; p. 270. (In Russian)
28. Nedosekova, I.L.; Belousova, E.A.; Sharygin, V.V.; Belyatsky, B.V.; Baynova, T.B. Origin and evolution of the Il’meny–Vishnevogorsky carbonatites (Urals, Russia): Insights from trace–elements compositions, Rb–Sr, Sm–Nd, U–Pb and Lu–Hf isotope data. *Mineral. Petrol.* **2013**, *107*, 101–123. [[CrossRef](#)]
29. Vrublevskii, V.V.; Pokrovskii, B.G.; Zhuravlev, D.Z.; Anoshin, G.N. Composition and age of the Penchenga linear carbonatite complex, Yenisei Range. *Petrology* **2003**, *11*, 130–146.
30. Bell, K.; Rukhlov, A.S. Carbonatites from the Kola Alkaline Province: Origin, evolution and source characteristics. In *Phoscorites and Carbonatites from Mantle to Mine: The Key Example of the Kola Alkaline Province*; Zaitsev, A., Wall, F., Eds.; The Mineralogical Society of Great Britain and Ireland: London, UK, 2004; pp. 421–455.
31. Bell, K.; Blenkinsop, J. Neodymium and strontium isotope geochemistry of carbonatites. In *Carbonatites: Genesis and Evolution*; Bell, K., Ed.; Unwin Hyman: London, UK, 1989; pp. 278–300.
32. Bell, K.; Petersen, T. Nd and Sr Isotope Systematics of Shombole Volcano, East Africa, and the Links between Nephelinite, Phonolites and Carbonatites. *Geology* **1991**, *19*, 582–585. [[CrossRef](#)]
33. Kramm, U. Mantle components of carbonatite from the Kola Alkaline Province, Russia and Finland: A Nd–Sr study. *Eur. J. Mineral.* **1993**, *5*, 985–989. [[CrossRef](#)]
34. Kramm, U.; Kogarko, L.N. Nd and Sr isotope signatures of the Khibina and Lovozero agpaitic centers, Kola alkaline province, Russia. *Lithos* **1994**, *32*, 225–242. [[CrossRef](#)]
35. Zaitsev, A.N.; Bell, K. Sr and Nd isotope data of apatite, calcite and dolomite as indicators of source, and the relationships of phoscorites and carbonatites from Kovdor massif, Kola peninsula, Russia. *Contrib. Mineral. Petrol.* **1995**, *121*, 324–335. [[CrossRef](#)]
36. Dunworth, E.; Bell, K. The Turuy massif, Kola Peninsula, Russia: Isotopic and geochemical evidence for multi-source evolution. *J. Petrol.* **2001**, *42*, 377–405. [[CrossRef](#)]

37. Bell, K. Carbonatites: Relationships to mantle plume activity. In *Mantle Plumes: Their Identification Through Time*; Ernst, R., Buchan, K.L., Eds.; Geological Society of America: Boulder, CO, USA, 2001; Volume 352, pp. 267–290.
38. Kogarko, L.N.; Lahaye, Y.; Brey, G.P. Plume-related mantle source of super-large rare metal deposits from the Lovozero and Khibina massifs on the Kola Peninsula, Eastern part of Baltic shield: Sr, Nd and Hf isotope systematics. *Mineral. Petrol.* **2010**, *98*, 197–208. [[CrossRef](#)]
39. Vladykin, N.V.; Pirajno, F. Types of carbonatites: Geochemistry, genesis and mantle sources. *Lithos* **2021**, *386–387*, 105982. [[CrossRef](#)]
40. Vladykin, N.V. Model of nucleation and crystallization of ultrabasic-alkaline carbonatite magmas of Siberian region, problems of their ore content, mantle sources and connection with plume process. *Russ. Geol. Geophys.* **2016**, *57*, 889–905. [[CrossRef](#)]
41. Hofmann, A.W. Mantle Geochemistry: The Message from Oceanic Volcanism. *Nature* **1997**, *385*, 219–229. [[CrossRef](#)]
42. Vrublevskii, V.V.; Nikiforov, A.V.; Sugorakova, A.M.; Kozulina, T.V. Petrogenesis and tectonic setting of the Cambrian Kharly alkaline–carbonatite complex (Sangilen Plateau, Southern Siberia): Implications for the Early Paleozoic evolution of magmatism in the western Central Asian Orogenic Belt. *J. Asian Earth Sci.* **2020**, *188*, 104163. [[CrossRef](#)]
43. Vrublevskii, V.V.; Morova, A.A.; Bukharova, O.V.; Konovalenko, S.I. Mineralogy and geochemistry of Triassic carbonatites in the Matcha alkaline intrusive complex (Turkistan–Alai Ridge, Kyrgyz Southern Tien Shan), SW Central Asian orogenic belt. *J. Asian Earth Sci.* **2018**, *153*, 252–281. [[CrossRef](#)]
44. Xu, C.; Chakhmouradian, A.R.; Taylor, R.N.; Kynicky, J.; Li, W.; Song, W.; Fletcher, I.R. Origin of carbonatites in the South Qinling orogen: Implications for crustal recycling and timing of collision between the South and North China Blocks. *Geochim. Cosmochim. Acta* **2014**, *143*, 189–206. [[CrossRef](#)]
45. Stoppa, F.; Rukhlov, A.C.; Bell, K.; Schiazza, M.; Vichi, G. Lamprophyres of Italy: Early Cretaceous alkaline lamprophyres of Southern Tuscany, Italy. *Lithos* **2014**, *188*, 97–112. [[CrossRef](#)]
46. Nedosekova, I.L.; Vladykin, N.V.; Pribavkin, S.V.; Bayanova, T.B. Ilmeno-Vishnevogorskiy myaskit-carbonatite complex: Origin, ore content, sources of substance (Ural, Russia). *Geol. Ore Depos.* **2009**, *51*, 157–181. [[CrossRef](#)]
47. Bell, K.; Tilton, G.R. Nd, Pb and Sr Isotopic Compositions of East African Carbonatites: Evidence for Mantle Mixing and Plume Inhomogeneity. *J. Petrol.* **2001**, *42*, 1927–1945. [[CrossRef](#)]
48. Yang, X.-Y.; Sun, W.-D.; Zhang, Y.-X.; Zheng, Y.-F. Geochemical constraints on the genesis of the Bayan Obo Fe-Nb-REE deposit in Inner Mongolia, China. *Geochim. Cosmochim. Acta* **2009**, *73*, 1417–1435. [[CrossRef](#)]
49. Castor, S.B. The Mountain Pass rare-earth carbonatite and associated ultrapotassic rocks, California. *Can. Mineral.* **2008**, *46*, 779–806. [[CrossRef](#)]
50. Wall, F.; Zaitsev, A.N. Rare earth minerals in Kola carbonatites. In *Phoscorites and Carbonatites from Mantle to Mine: The key Example of the Kola Alkaline Province*; Zaitsev, A., Wall, F., Eds.; The Mineralogical Society of Great Britain and Ireland: London, UK, 2004; pp. 43–72.
51. Chakhmouradian, A.; Zaitsev, A.N. Rare Earth Mineralization in Igneous Rocks: Sources and Processes. *Elements* **2012**, *8*, 347–353. [[CrossRef](#)]
52. Guo, D.; Liu, Y. Occurrence and geochemistry of bastnasite in carbonatite-related REE deposits, Mianning–Dechang REE belt, Sichuan Province, SW China. *Ore Geol. Rev.* **2019**, *107*, 266–282. [[CrossRef](#)]
53. Puchkov, V.N. Uralides and Timanides: Their structural relationship and position in the geologic history of the Ural-Mongolian Fold Belt. *Rus. Geol. Geophys.* **2003**, *44*, 28–39. (In Russian)
54. Kuznetsov, N.B.; Soboleva, A.A.; Udoratina, O.V.; Hertseva, M.V.; Andreichev, V.L.; Dorokhov, N.S. Pre-Uralian Tectonic Evolution of the North-East and East Frame of the East European Craton. Part 1. Pre-Uralides, Timanides and Pre-Ordovician granitoid volcano-plutonic associations of the North Urals and Timan-Pechora Region. *Lithosphere* **2006**, *4*, 3–22. (In Russian)
55. Puchkov, V.N. *Geology of the Urals and the Trans.-Urals (Topical Issues of Stratigraphy, Tectonics, Geodynamics and Metallogeny)*; DesignPoligrafService: Ufa, Russia, 2010; p. 280. (In Russian)
56. Udoratina, O.V.; Travin, A.V. Alkaline picrites of the Chetlas complex of Middle Timan: Ar–Ar data. In Proceedings of the Ore Potential of Alkaline, Kimberlite and Carbonative Magmatism: Materials XXX Internl Conference, Moscow, Russia, 29 September–2 October 2014; pp. 82–84. (In Russian)
57. Bogdanova, S.V.; Pisarevsky, S.A.; Li, Z.X. Assembly and Breakup of Rodinia (Some Results of IGCP Project 440). *Stratigr. Geol. Correl.* **2009**, *17*, 259–274. [[CrossRef](#)]
58. Andreichev, V.L.; Soboleva, A.A.; Udoratina, O.V.; Ronkin, Y.L.; Coble, M.A.; Miller, E.L. Granites of the Northern Timan—probable indicators of Neoproterozoic stages of Rodinia breakup. *Geodyn. Tectonophys.* **2020**, *11*, 201–218. [[CrossRef](#)]
59. Kuznetsov, N.B.; Soboleva, A.A.; Udoratina, O.V.; Andreichev, V.L.; Hertseva, M.V. Pre-Ordovician tectonic evolution and volcano-plutonic associations of the Timanides and Northern Pre-Uralides, Northeast part of the East European Craton. *Gondwana Res.* **2007**, *12*, 305–323. [[CrossRef](#)]
60. Makeev, A.B.; Lebedev, V.A.; Bryanchaninova, N.I. *Magmatites of the Middle Timan*; Yushkin, N.P., Ed.; UB RAS: Ekaterinburg, Russia, 2008; p. 348. (In Russian)
61. Shilov, L.P.; Plyakin, A.M.; Alekseev, V.I. (Eds.) *Timan Ridge. T.2. Lithology and Stratigraphy, Geophysical Characteristics of the Earth's Crust, Tectonics, Mineral Resources*; USTU: Ukhta, Russia, 2009; p. 460. (In Russian)
62. Udoratina, O.V.; Travin, A.V.; Kulikova, K.V.; Varlamov, D.A. Evidence for an Early Permian pulse of ultrapotassic magmatism in the Middle Timan. *MOIP* **2016**, *91*, 29–35. (In Russian)

63. Kononova, V.A.; Dontsova, E.I.; Kuznetsova, L.D. Isotopic composition of oxygen and strontium of the Ilmeno-Vishnevogorsk alkaline complex and questions of the genesis of miaskites. *Geochemistry* **1979**, *12*, 1784–1795.
64. Kramm, U.; Blaxland, A.B.; Kononova, V.A.; Grauert, B. Origin of the Ilmenogorsk–Vishnevogorsk nepheline syenites, Urals, USSR, and their time of emplacement during the history of the Ural fold belt: A Rb–Sr study. *J. Geol.* **1983**, *91*, 427–435. [[CrossRef](#)]
65. Kramm, U.; Chernyshev, I.V.; Grauert, B.; Kononova, V.A.; Bröcker, B. Zircon typology and U–Pb systematics: A case study of zircons from nepheline syenite of the Il'meny Mountains, Urals. *Petrology* **1993**, *1*, 474–485.
66. Krasnobaev, A.A.; Rusin, A.I.; Busharina, S.V.; Lepekhina, E.N.; Medvedeva, E.V. Character of zircon distribution on amphibole miaskite of the Ilmenogorsk Massif (Southern Urals). *Dokl. Earth Sci.* **2010**, *430*, 76–79. [[CrossRef](#)]
67. Krasnobaev, A.A.; Rusin, A.I.; Valizer, P.M.; Busharina, S.V. Zirconology of calcite carbonatite of the Vishnevogorsk Massif, Southern Urals. *Dokl. Earth Sci.* **2010**, *431*, 390–393. [[CrossRef](#)]
68. Krasnobaev, A.A.; Busharina, S.; Valizer, P.M.; Medvedeva, E.V. Zirconology of miaskites of the Ilmeny Mountains (South Urals). *Geochem. Intern.* **2016**, *54*, 765–780. [[CrossRef](#)]
69. Nedosekova, I.L.; Belyatsky, B.V. Age and substance sources of the Ilmeno–Vishnevogorsky Alkaline Complex (South Urals): Rb–Sr, Sm–Nd, U–Pb, and Lu–Hf isotope data. *Dokl. Earth Sci.* **2012**, *446*, 1071–1076. [[CrossRef](#)]
70. Krasnobaev, A.A.; Valizer, P.M.; Rusin, A.I.; Busharina, S.V.; Medvedeva, E.V. Zirconology of ultrabasic rocks of the Buldym Massif (Il'meno–Vishnevogorskii Complex, Southern Urals). *Dokl. Earth Sci.* **2015**, *461*, 235–241. [[CrossRef](#)]
71. Nedosekova, I.L.; Belyatsky, B.V.; Belousova, E.A. Trace elements and Hf isotope composition as indicators of zircon genesis in the evolution of the alkaline-carbonatite magmatic system (Ilmeno-Vishnevogorsky complex, Urals, Russia). *Rus. Geol. Geophys.* **2016**, *57*, 891–906. [[CrossRef](#)]
72. Baluev, A.S. Continental Riftingogenesis of the North of the Eastern European Platform in Neogee: Geology, History of Development, Comparative Analysis. Doctoral Thesis, Geological Institute RAS, Moscow, Russia, 2013; p. 303. (In Russian).
73. Nedosekova, I.L.; Koroteev, V.A.; Bayanova, T.B.; Serov, P.A.; Popova, V.I.; Chervyakovskaya, M.V. On the age of pyrochlore carbonatites of the Ilmeno-Vishnevogorsk alkaline complex, South Ural (according to Sm-Nd and Rb-Sr isotope methods). *Lithosphere* **2020**, *20*, 486–498. (In Russian) [[CrossRef](#)]
74. Nedosekova, I.L.; Belousova, E.A.; Sharygin, V.V. Sources of matter for the Il'meno-Vishnevogorsky Alkaline Complex: Evidence from Lu-Hf Isotopic data for zircons. *Dokl. Earth Sci.* **2010**, *435*, 1487–1491. [[CrossRef](#)]
75. Ivanov, K.S.; Kontorovich, V.A.; Puchkov, V.N.; Fyodorov, Y.N.; Erokhin, Y.V. Tectonics of the Urals and the basement of West Siberia: The main features of the geological structure and development. *Reg. Geol.* **2014**, *2*, 22–35. (In Russian)
76. Zoloev, K.K.; Levin, V.Y.; Moril, S.I.; Shardakova, G.Y. *Mineralogy and Deposits of Rare Metals, Molybdenum, Tungsten from the Urals*; Ministry of Natural Resources RF, Sverdlovsk Region State Department for Natural Resources, IGG UD RAS, JSC UGSE: Yekaterinburg, Russia, 2004; p. 336. (In Russian)
77. Golubeva, I.I.; Remizov, D.N.; Burtsev, I.N.; Filippov, V.N.; Shuyskiy, A.S. Fluid-explosion ultramafic rocks of the Middle Timan dyke complex and their paragenetic association with carbonatite. *Reg. Geol. Metallog.* **2019**, *80*, 1–15. (In Russian)
78. Nedosekova, I.L.; Udoratina, O.V.; Vladykin, N.V.; Pribavkin, S.V.; Gulyaeva, T.Y. *Petrochemistry and Geochemistry of Dyke Ultrabasites and Carbonatites of the Chetlassky Complex (Middle Timan)*; Yearbook-2010; IGG UD RAS: Ekaterinburg, Russia, 2011; pp. 122–130. (In Russian)
79. Makeev, A.B.; Bryanchaninova, N.I. Lamprophyres of Chetlassky Stone, Middle Timan. *Reg. Geol. Metallog.* **2009**, *37*, 51–73. (In Russian)
80. Kovalchuk, N.S.; Shumilova, T.G.; Kozyreva, I.G. Mineralogy of rare-earth phases of Kosyui carbonatites. In *Mineralogical Intervention in Micro—and Nanoworld: Mater. International. Mineralogical Seminar*; IG KNS UB RAS: Syktyvkar, Russia, 2009; pp. 296–297. (In Russian)
81. Kovalchuk, N.S. Evolution of the Chemical Composition of Pyrochlore from Carbonatites in the Kosyu Massif. In *Structure, Substance, History of Lithosphere of Ural–Timan Segment*; Geoprint: Syktyvkar, Russia, 2011; pp. 74–76. (In Russian)
82. Kovalchuk, N.; Shumilova, T.G.; Stepanenko, V.I. Rare earth mineralization in carbonatite of Kosyu massif (Middle Timan). *Zap. RMO* **2013**, *142*, 109–132. (In Russian)
83. Udoratina, O.V.; Kozyreva, I.V.; Shvetsova, I.V.; Kapitanova, V.A.; Filippov, V.N. Features of rare-metal accessory mineralization of the vein series of carbonatites (Kosyu ore field, Middle Timan). In *Crystalline and Solid Non-Crystalline State of Mineral Substance*; Geoprint: Syktyvkar, Russia, 2012; pp. 331–333.
84. Varlamov, D.A.; Udoratina, O.V.; Burakov, N.N. Unusual monazites and Ce Segregation process during alkaline metasomatism of acid substrates (Kosyu ore field, Middle Timan). In *Proceedings of the XXXIV International Confence: Magmatism of the Earth and Related Strategic Metal Deposits, Miass, Russia, 4–9 August 2017*; pp. 292–295.
85. Varlamov, D.A.; Udoratina, O.V. Minerals of rare-metal-rare-earth ore fields of the Chetlassky Kamen of the Middle Timan, Geology and Mineral Resources of the European North-East of Russia. In *Proceedings of the XVII Geological Congress of the Komi Republic, Syktyvkar, Russia*; IG Komi SC UB RAS: Syktyvkar, Russia, 2019; pp. 160–162.
86. Khalezova, E.B.; Nazarenko, I.I. About bastnesite the Cherry Mountains. *Proc. IMGRE AS USSR* **1959**, *2*, 99–101. (In Russian)
87. Eskova, E.M.; Zhabin, A.; Muhitdinov, G. *Mineralogy and Geochemistry of Rare Elements of the Cherry Mountains*; Nauka: Moscow, Russia, 1964; p. 319. (In Russian)
88. Efimov, A.F.; Eskova, E.M.; Lebedeva, S.I.; Levin, V.Y. Typochimism of accessory pyrochlore in rocks of the Ural alkaline complex. *Geochemistry* **1985**, *2*, 202–208. (In Russian)

89. Polyakov, V.O.; Nedosekova, I.L. Mineralogy of apohyperbasite phenites and carbonatites of the southern part of the Ilmensky mountains. In *Minerals of Deposits and Zones of Technogenesis of Ore Regions of the Urals*; UB RAS: Sverdlovsk, Russia, 1990; pp. 24–35. (In Russian)
90. Lebedeva, I.O.; Nedosekova, I.L. About process of eshinitization of pyrochlore from carbonatites of Buldym massif (Cherry Mountains, Ural). *Zap. WMO* **1993**, *2*, 69–75. (In Russian)
91. Kobylashev, Y.S.; Magakonov, E.P.; Nikandrov, S.N. *Minerals Vishnyevye Potanino Mountains*; Ilmensky State Nature Reserve of the UB RAS: Miass, Russia, 1998; p. 77. (In Russian)
92. Popov, V.A.; Popova, V.I. *Mineralogy of Pegmatites in the Ilmensky Mountains. Mineralogical Almanac*; Ecost: Moscow, Russia, 2006; Volume 9, p. 151. (In Russian)
93. Popova, V.I.; Popov, V.A.; Blinov, I.A.; Kotlyarov, V.A.; Kasatkin, A.V.; Škoda, R.; Lebedeva, S.M. New findings of rare minerals in pegmatites of Vishnevye Mountains in the Southern Urals. *Mineralogy* **2019**, *1*, 1–14. (In Russian)
94. Popova, V.I.; Popov, V.A.; Blinov, I.A.; Kotlyarov, V.A. New data on pyrochlore of alkali pegmatites and ore zones of the Vishnevye Mountains (Southern Urals). *Mineralogy* **2018**, *4*, 46–60. (In Russian)
95. Popova, V.I.; Popov, V.A.; Kasatkin, A.V.; Kuznetsov, A.M. Aeschynite group minerals from Vishnevye Mountains (South Urals). *Mineralogy* **2019**, *5*, 16–25. (In Russian) [[CrossRef](#)]
96. Popov, V.A. Titanite of the Vishnevogorsky Alkaline Complex (South Ural). *Mineralogy* **2019**, *1*, 29–35. (In Russian)
97. Cherednichenko, S.V.; Kotlyarov, V.A. Mineralogy of zirconium and niobium in calcite-nepheline-feldspar pegmatite of the Ilmeno-Vishnevogorsk complex (South Urals). *Zap. RMO* **2019**, *2*, 87–99. (In Russian) [[CrossRef](#)]
98. Kasatkin, A.V.; Škoda, R.; Nestola, F.; Kuznetsov, A.M.; Belogub, E.V.; Agakhanov, A.A. Röntgenite-(Ce) and other rare fluorocarbonates from vein No. 35, Vishnevye Mountains, Southern Urals. *Mineralogy* **2019**, *5*, 10–22. (In Russian) [[CrossRef](#)]
99. Popov, V.A.; Rassomakhin, M.A.; Kolisnichenko, S.V. A unique ore locality of polyakovite-(Ce) in the Ilmeny Mountains, South Urals—new finds. *Mineralogy* **2020**, *6*, 17–32. (In Russian) [[CrossRef](#)]
100. Atencio, D.; Andrade, M.B.; Christy, A.G.; Giere, R.; Kartashov, P.M. The pyrochlore supergroup of minerals: Nomenclature. *Can. Mineral.* **2010**, *48*, 673–698. [[CrossRef](#)]
101. Woolley, A.R.; Kempe, D.R.C. Carbonatites: Nomenclature, average compositions, and element distribution. In *Carbonatites: Genesis and Evolution*; Bell, K., Ed.; Unwin Hyman: London, UK, 1989; pp. 1–14.
102. Le Maitre, R.W. *Igneous Rocks: A Classification and Glossary of Terms*; Cambridge University Press: Cambridge, UK, 2002; p. 236.
103. Bagdasarov, Y.A. Rare-metal ore potential of igneous and hydrothermal metasomatic carbonatites. *Geol. Ore Depos.* **1994**, *36*, 326–335.
104. Arzamastsev, A.A.; Bea, F.; Glaznev, V.N.; Arzamastseva, L.V.; Montero, P. Kola alkaline province in the Palaeozoic: Evaluation of primary mantle magma composition and magma generation conditions. *Rus. J. Earth Sci.* **2001**, *3*, 1–32. [[CrossRef](#)]
105. Nedosekova, I.L. New data on carbonatites of the Il'mensky–Vishnevogorsky alkaline complex, the Southern Urals, Russia. *Geol. Ore Depos.* **2007**, *49*, 129–146. [[CrossRef](#)]
106. Petrov, O.V.; Sharpenok, L.N. (Eds.) *Petrographic Code of Russia: Magmatic, Metamorphic, Metasomatic, Impact Formations*; VSEGEI: Saint Petersburg, Russia, 2008; p. 198. (In Russian)
107. Frolov, A.A.; Lapin, A.V.; Tolstov, A.V.; Zinchuk, N.N.; Belov, S.V.; Burmistrov, A.A. *Carbonatites and Kimberlites*; NIA–Nature: Moscow, Russia, 2005; p. 540. (In Russian)
108. Rock, N.M.S. The nature and origin of Ultramafic Lamprophyres: Alnoites and Allied Rocks. *J. Petrol.* **1986**, *27*, 155–196. [[CrossRef](#)]
109. Vladykin, N.V. Formation types of carbonatites, their geochemistry and genesis. In *Depth Magmatism, its Sources and Plumes. Proceed of VIII Intern Workshop*; IG SD RAS: Irkutsk, Russia, 2008; pp. 45–58. (In Russian)
110. Mitchell, R.H. Carbonatites and carbonatites and carbonatites. *Can. Mineral.* **2005**, *43*, 2049–2068. [[CrossRef](#)]
111. Stoppa, F.; Pirajno, F.; Schiazza, M.; Vladykin, N.V. State of the art: Italian carbonatites and their potential for critical-metal deposits. *Gondwana Res.* **2016**, *37*, 152–171. [[CrossRef](#)]
112. Nedosekova, I.L.; Vladykin, N.V.; Udoratina, O.V. Carbonatites of the Chetlassky Complex (Middle Timan): Geochemical and Isotope Data. In *Yearbook-2012*; IGG UD RAS: Ekaterinburg, Russia, 2013; Volume 160, pp. 150–158. (In Russian)
113. Bryanchaninova, N.I.; Makeev, A.B.; Larionova, Y.O. Sm–Nd isotope systematics of Timan's lamprophyre. In *Proceedings of the Vseros Confence, IGEM RAS, Moscow, Russia, 8–11 November 2010*; pp. 414–415.
114. Hanyu, T.; Nakamura, E. Constraints on HIMU and EM by Sr and Nd isotopes re-examined. *Earth Planets Space* **2000**, *52*, 61–70. [[CrossRef](#)]
115. Zindler, A.; Hart, S.R. Chemical geodynamics. *Ann. Rev. Earth Planet. Sci.* **1986**, *14*, 493–571. [[CrossRef](#)]
116. Hart, S.R.; Hauri, E.; Oschmann, L.A.; Whitehead, J.A. Mantle plumes and entrainment: Isotopic evidence. *Science* **1992**, *256*, 517–520. [[CrossRef](#)]
117. Salters, V.J.M.; Stracke, A. Composition of the depleted mantle. *J. Earth Sci.* **2004**, *5*. [[CrossRef](#)]
118. Stracke, A.; Hofmann, A.W.; Stan, R.; Hart, S.R. FOZO, HIMU, and the rest of the mantle zoo. *J. Earth Sci.* **2005**, *6*. [[CrossRef](#)]
119. Tappe, S.; Foley, S.F.; Kjarsgaard, B.A.; Romer, R.L.; Heaman, L.M.; Stracke, A.; Jenner, G.A. Between carbonatite and lamproite–Diamondiferous Torngat ultramafic lamprophyres formed by carbonate-fluxed melting of cratonic MARID-type metasomes. *Geochim. Cosmochim. Acta* **2008**, *72*, 3258–3286. [[CrossRef](#)]

120. Tappe, S.; Foley, S.F.; Stracke, A.; Romer, R.L.; Kjarsgaard, B.A.; Heaman, L.M.; Joyce, N. Craton reactivation on the Labrador Sea margins: $^{40}\text{Ar}/^{39}\text{Ar}$ age and Sr–Nd–Hf–Pb isotope constraints from alkaline and carbonatite intrusives. *Earth Planet. Sci. Lett.* **2007**, *256*, 433–454. [[CrossRef](#)]
121. Kogarko, L.; Zartman, R.E. New Data on the age of the Guli Intrusion and Implications for the relationships between Alkaline Magmatism in the Maymecha–Kotuy Province and the Siberian Superplume: U–Th–Pb Isotopic Systematics. *Geochem. Intern.* **2011**, *49*, 439–448. [[CrossRef](#)]
122. Nelson, D.R. Isotopic characteristics and petrogenesis of the lamproites and kimberlites of central West Greenland. *Lithos* **1989**, *22*, 265–274. [[CrossRef](#)]
123. Goldstein, S.J.; Jacobsen, S.B. Nd and Sr isotopic systematics of river water suspended material implications for crystal evolution. *Earth Plan. Sci. Lett.* **1988**, *87*, 249–265. [[CrossRef](#)]
124. Hogarth, D.D. Classification and nomenclature of the pyrochlore group. *Am. Mineral.* **1977**, *62*, 403–410.
125. Möller, P. REE (Y), Nb, and Ta enrichment in pegmatites and carbonatite–alkalic rock complexes. In *Lanthanides, Tantalum and Niobium*; Möller, P., Ed.; Springer: Berlin/Heidelberg, Germany, 1989; pp. 38–67. [[CrossRef](#)]
126. Walter, B.F.; Parsapoor, A.; Braunger, S.; Marks, M.A.W.; Wenzel, T.; Martin, M.; Markl, G. Pyrochlore as a monitor for magmatic and hydrothermal processes in carbonatites from the Kaiserstuhl volcanic complex (SW Germany). *Chem. Geol.* **2018**, *498*, 1–16. [[CrossRef](#)]
127. Bambi, A.C.J.M.; Costanzo, A.; Gonc Alves, A.O.; Melgarejo, J.C. Tracing the chemical evolution of primary pyrochlore from plutonic to volcanic carbonatites: The role of fluorine. *Mineral. Mag.* **2012**, *76*, 377–392. [[CrossRef](#)]
128. Hogarth, D.D.; Williams, C.T.; Jones, P. Primary Zoning in Pyrochlore Group Minerals from Carbonatites. *Mineral. Mag.* **2000**, *64*, 683–697. [[CrossRef](#)]
129. Torro, L.; Villanova, C.; Castillo, M.; Campeny, M.; Gonalves, A.O.; Melgarejo, J.C. Niobium and rare earth minerals from the Virulundo carbonatite, Namibe, Angola. *Mineral. Mag.* **2012**, *76*, 393–409. [[CrossRef](#)]
130. Boniface, N. Crystal chemistry of pyrochlore from the Mesozoic Panda Hill carbonatite deposit, western Tanzania. *J. Afr. Earth Sci.* **2017**, *126*, 33–44. [[CrossRef](#)]
131. Sharygin, V.V.; Doroshkevich, A.G. Mineralogy of secondary olivine-hosted inclusions in calcite carbonatites of the Belaya Zima alkaline complex, Eastern Sayan, Russia: Evidence for late-magmatic Na–Ca-rich carbonate composition. *J. Geol. Soc. India* **2017**, *90*, 524–530. [[CrossRef](#)]
132. Jago, B.C.; Gittins, J. Pyrochlore crystallization in carbonatites: The role of fluorine. *S. Afr. J. Geol.* **1993**, *96*, 149–159.
133. Nasraoui, M.; Bilal, E. Pyrochlores from the Lueshe carbonatite complex (Democratic Republic of Congo): A geochemical record of different alteration stages. *J. Asian Earth Sci.* **2000**, *18*, 237–251. [[CrossRef](#)]
134. Deditius, A.P.; Smith, F.N.; Utsunomiya, S.; Ewing, R.C. Role of vein phases in nanoscale sequestration of U, Nb, Ti, and Pb during the alteration of pyrochlore. *Geochim. Cosmochim. Acta* **2015**, *150*, 226–252. [[CrossRef](#)]
135. Kozlov, E.; Fomina, E.; Sidorov, M.; Shilovskikh, V. Ti–Nb Mineralization of Late Carbonatites and Role of Fluids in Its Formation: Petyayan–Vara Rare-Earth Carbonatites (Vuoriyarvi Massif, Russia). *Geosciences* **2018**, *8*, 281. [[CrossRef](#)]
136. Nedosekova, I.L.; Pribavkin, S.V. *Ore niobium Mineralization of Rare Metal Deposits and Ore Occurrences of the Ilmeno–Vishnevogorsk Alkaline–Carbonatite Complex (South Urals)*; Yearbook-2014; IGG UD RAS: Ekaterinburg, Russia, 2015; pp. 175–183. (In Russian)
137. Nedosekova, I.L.; Pribavkin, S.V. Ore niobium minerals of the pyrochlore group of carbonatite complexes of the Urals: Compositional features and geochemical evolution. *Izv. USGU* **2019**, *3*, 46–57. (In Russian) [[CrossRef](#)]
138. Melgarejo, J.C.; Costanzo, A.; Bambi, A.C.J.M.; Gonalves, A.O.; Neto, A.B. Subsolidus processes as a key factor on the distribution of Nb species in plutonic carbonatites: The Tchivira case, Angola. *Lithos* **2012**, *152*, 187–201. [[CrossRef](#)]
139. Chakhmouradian, A.R.; Mitchell, R.H. Lueshite, pyrochlore and monazite-(Ce) from apatite-dolomite carbonatite, Lesnaya Varaka complex, Kola Peninsula, Russia. *Mineral. Mag.* **1998**, *62*, 769–782. [[CrossRef](#)]
140. Zheng, L.; Gu, X.; Zhang, Y. Pyrochlore Chemistry from the Bonga Carbonatite-type Nb Deposit, Huila Province, Angola: Implications for Magmatic-Hydrothermal Processes of Carbonatite. *Acta Geol. Sin. Engl.* **2014**, *88*, 487–488. [[CrossRef](#)]
141. Khromova, E.A.; Doroshkevich, A.G.; Sharygin, V.V.; Izbrodin, L.A. Compositional Evolution of Pyrochlore-Group Minerals in Carbonatites of the Belaya Zima Pluton, Eastern Sayan. *Geol. Ore. Depos.* **2017**, *59*, 752–764. [[CrossRef](#)]
142. Tremblay, J.; Bdard, L.P.; Matton, G. Columbitization of fluorcalciopyrochlore by hydrothermalism at the Saint-Honor alkaline complex, Qubec (Canada): New insights on halite in carbonatites. *Ore Geol. Rev.* **2017**, *91*, 695–707. [[CrossRef](#)]
143. Chebotarev, D.A.; Doroshkevich, A.G.; Klemm, R.; Karmanov, N.S. Evolution of Nb-mineralization in the Chuktukon carbonatite massif, Chadobets upland (Krasnoyarsk Territory, Russia). *Period. Mineral.* **2017**, *86*, 99–118. [[CrossRef](#)]
144. Wall, F.; Williams, C.T.; Woolley, A.R.; Nasraoui, M. Pyrochlore from Weathered Carbonatite at Lueshe, Zaire. *Mineral. Mag.* **1996**, *60*, 731–750. [[CrossRef](#)]
145. Lee, M.J.; Lee, J.I.; Garcia, D.; Moutte, J.; Williams, C.T.; Wall, F.; Kim, Y. Pyrochlore chemistry from the Sokli phoscorite-carbonatite complex, Finland: Implications for the genesis of phoscorite and carbonatite association. *Geochem. J.* **2006**, *40*, 1–13. [[CrossRef](#)]
146. Chakhmouradian, A.R.; Zaitsev, A.N. Calcite-amphibole-clinopyroxene rock from the Afrikanda Complex, Kola Peninsula, Russia; mineralogy and a possible link to carbonatites; I, Oxide minerals. *Canad. Mineral.* **1999**, *37*, 177–198.
147. Chakhmouradian, A.R.; Williams, C.T. Mineralogy of high-field-strength elements (Ti, Nb, Zr, Ta, Hf) in phoscoritic and carbonatitic rocks of the Kola Peninsula, Russia. In *Phoscorites and Carbonatites from Mantle to Mine: The Key Example of the Kola Alkaline Province*; The Mineralogical Society of Great Britain and Ireland: London, UK, 2004; Volume 10, pp. 293–340.

148. Chakhmouradian, A.R. High-field-strength elements in carbonatitic rocks: Geochemistry, crystal chemistry and significance for constraining the sources of carbonatites. *Chem. Geol.* **2006**, *235*, 138–160. [[CrossRef](#)]
149. Chakhmouradian, A.R.; Mitchell, R.H. The mineralogy of Ba- and Zr-rich alkaline pegmatites from Gordon Butte, Crazy Mountains (Montana, USA): Comparisons between potassic and sodic agpaite pegmatites. *Contrib. Mineral. Petrol.* **2002**, *143*, 93–114. [[CrossRef](#)]
150. Simonov, V.A. *Mineral. Formation Conditions in Nongranite Pegmatites*; Science: Novosibirsk, Russia, 1981; p. 169. (In Russian)
151. Andrsen, T. Composition variation of some rare metal minerals from the Fen complex (Telemark, SE, Norway): Implications for the mobility of rare earth in a carbonatite system. *Miner. Mag.* **1986**, *50*, 503–509. [[CrossRef](#)]
152. Smith, M.P.; Henderson, P.; Campbell, L.S. Fractionation of the REE during hydrothermal processes: Constraints from the Bayan Obo Fe-REE-Nb deposit, Inner Mongolia, China. *Geochim. Cosmochim. Acta* **2000**, *64*, 3141–3160. [[CrossRef](#)]
153. Xu, C.; Campbell, I.H.; Kynicky, J.; Allen, C.M.; Chen, Y.; Huang, Z.; Qi, L. Comparison of the Daluxiang and Maoniuping carbonatitic REE deposits with Bayan Obo REE deposit, China. *Lithos* **2008**, *106*, 12–24. [[CrossRef](#)]
154. Xu, C.; Kynicky, J.; Chakhmouradian, A.R.; Campbell, I.H.; Allen, C.M. Trace element modeling of the magmatic evolution of rare-earth-rich carbonatite from the Miaoya deposit, Central China. *Lithos* **2010**, *118*, 145–155. [[CrossRef](#)]
155. Lapin, A.V.; Tolstov, A.V.; Kulikova, I.M. Distribution of REE, Y, Sc, and Th in the unique complex rare-metal ores of the Tomtor deposit. *Geochem. Int.* **2016**, *54*, 1061–1078. [[CrossRef](#)]
156. Yang, X.M.; Le Bas, M.J. Chemical compositions of carbonate minerals from Bayan Obo, Inner Mongolia, China: Implications for petrogenesis. *Lithos* **2004**, *72*, 97–116. [[CrossRef](#)]
157. Wall, F.; Mariano, A.N. Rare earth minerals in carbonatites: A discussion centred on the Kangankunde carbonatite, Malawi. In *Rare Earths Minerals: Chemistry, Origin and Ore Deposits*; Jones, A.P., Wall, F., Williams, C.T., Eds.; Chapman & Hall: London, UK, 1996; Volume 7, pp. 193–225.
158. Wang, Z.-Y.; Fan, H.-R.; Zhou, L.; Yang, K.-F.; She, H.-D. Carbonatite-related REE deposits: An overview. *Minerals* **2020**, *10*, 965. [[CrossRef](#)]
159. Fournier, A. *Magmatic and Hydrothermal Controls of LREE Mineralization of the St.—Honoré Carbonatite*; McGill: Québec, QC, Canada, 1993; pp. 1–95.
160. Andrade, F.R.D.; Möller, P.; Lüders, V.; Dulski, P.; Gilg, H.A. Hydrothermal rare earth elements mineralization in the Barra do Itapirapuã carbonatite, southern Brazil: Behaviour of selected trace elements and stable isotopes (C, O). *Chem. Geol.* **1999**, *155*, 91–113. [[CrossRef](#)]
161. Szucs, A.M.; Stavropoulou, A.; O'Donnell, C.; Davis, S.; Rodriguez-Blanco, J.D. Reaction Pathways toward the Formation of Bastnäsite: Replacement of Calcite by Rare Earth Carbonates. *Cryst. Growth Des.* **2021**, *21*, 512–527. [[CrossRef](#)]
162. Boyarko, G.Y. Dynamics of global production and commodity flows of niobium raw materials. *Bull. Tomsk. Polytech. Univ. Geo. Assets Eng.* **2019**, *330*, 216–229. [[CrossRef](#)]
163. Weng, Z.; Jowitt, S.M.; Mudd, G.M.; Haque, N. A Detailed Assessment of Global Rare Earth Element Resources: Opportunities and Challenges. *Econ. Geol.* **2015**, *110*, 1925–1952. [[CrossRef](#)]
164. Jones, A.P.; Genge, M.; Carmody, L. Carbonate Melts and Carbonatites. *Rev. Mineral. Geochem.* **2013**, *75*, 289–322. [[CrossRef](#)]
165. Samoilov, V.S. *Geochemistry of Carbonatites*; Nedra: Moscow, Russia, 1984; p. 190. (In Russian)
166. Goodenough, K.M.; Wall, F.; Merriman, D. The Rare Earth Elements: Demand, Global Resources, and Challenges for Resourcing Future Generations. *Nat. Resour. Res.* **2018**, *27*, 201–216. [[CrossRef](#)]
167. Xu, C.; Chakhmouradian, A.R.; Kynicky, J.; Li, Y.; Song, W.; Chen, W.A. Paleoproterozoic mantle source modified by subducted sediments under the North China craton. *Geochim. Cosmochim. Acta* **2019**, *245*, 222–239. [[CrossRef](#)]
168. Chakhmouradian, A.R.; Reguir, E.P.; Kressall, R.D.; Crozier, J.; Pisiak, L.K.; Sidhu, R.; Yang, P. Carbonatite-Hosted Niobium Deposit at Aley, Northern British Columbia (Canada): Mineralogy, Geochemistry and Petrogenesis. *Ore Geol. Rev.* **2015**, *64*, 642–666. [[CrossRef](#)]
169. Bau, M. Controls on the fractionation of isovalent trace elements in magmatic and aqueous systems: Evidence from Y/Ho, Zr/Hf, and lanthanide tetrad effect. *Contrib. Mineral. Petrol.* **1996**, *123*, 323–333. [[CrossRef](#)]
170. Talantsev, A.S.; Petrova, G.A. *Conditions and Mechanism of Formation of Carbonatites of the Ilmenogorsk-Vishnevogorsk Alkaline Complex*; IGG UD RAS: Sverdlovsk, Russia, 1991; p. 70. (In Russian)
171. Levin, V.Y. *Alkaline Province of the Il'Meny-Vishnevye Mountains (Nepheline Syenites of the Urals)*; Nauka: Moscow, Russia, 1974; p. 221. (In Russian)
172. Kogarko, L.N.; Henderson, M.; Foland, K. Evolution and isotopic sources of Guli ultrabasic alkaline massif. *Dokl. Earth Sci.* **1999**, *364*, 235–247.
173. Vladykin, N.V. Geochemistry of Sr and Nd isotopes of alkaline and carbonatite complexes of Siberia and Mongolia and some geodynamic consequences. In *Problems of Sources of Deep Magmatism and Plumes*; IG SD RAS: Irkutsk, Russia, 2005; pp. 13–29.
174. Sazonov, A.M.; Vrublevsky, V.V.; Gertner, I.F.; Fedorova, A.V.; Gavrilenko, V.V.; Zvyagina, E.A.; Leont'ev, S.I. The Transangara Alkaline Pluton, Yenisei Range: Rb–Sr and Sm–Nd isotope ages and sources of feldspathoid magmas in Late Precambrian. *Dokl. Earth Sci.* **2007**, *413*, 469–473. [[CrossRef](#)]
175. Vrublevskii, V.V.; Bukharova, O.V.; Nebera, T.S.; Sveshnikova, V.L. Composition and origin of rare-metal (Nb–Ta, REE) and sulfide mineralization in magnesio-carbonatites from the Yenisei Ridge, Central Siberia. *Ore Geol. Rev.* **2019**, *111*, 1–26. [[CrossRef](#)]

176. Khromova, E.A.; Doroshkevich, A.G.; Izbrodin, I.A. Geochemical and Sr-Nd-Pb isotope characteristics of alkaline rocks and carbonates of the Beloziminsky Massif (East Sayan). *Geospheric. Res.* **2020**, *1*, 33–55. (In Russian) [[CrossRef](#)] [[PubMed](#)]
177. Kempton, P.D.; Harmon, R.S.; Hawkesworth, C.J. Petrology and geochemistry of lower crustal granulites from the Geronimo volcanic field, Southeastern Arizona. *Geochim. Cosmochim. Acta* **1990**, *54*, 3401–3426. [[CrossRef](#)]
178. Yang, K.-F.; Fan, H.-R.; Santosh, M.; Hu, F.-F.; Wang, K.-Y. Mesoproterozoic carbonatitic magmatism in the Bayan Obo deposit, Inner Mongolia, North China: Constraints for the mechanism of super accumulation of rare earth elements. *Ore Geol. Rev.* **2011**, *40*, 122–131. [[CrossRef](#)]
179. Ying, J.-F.; Zhou, X.-H.; Zhang, H.-F. Geochemical and isotopic investigation of the Laiwu–Zibo carbonatites from western Shandong Province, China, and implications for their petrogenesis and enriched mantle source. *Lithos* **2004**, *75*, 413–426. [[CrossRef](#)]
180. Demeny, A.; Ahijado, R.; Casillas, T.W.; Vennemann, M. Crustal contamination and fluid rock interaction in the carbonatites of Fuerteventura-Canary Islands, Spain: A C, O, H isotope study. *Lithos* **1998**, *44*, 101–115. [[CrossRef](#)]
181. Faure, G. *Principles of Isotope Geology*; Wiley: Hoboken, NJ, USA, 1989; p. 590.
182. Kalt, A.; Hegner, E.; Satir, M. Nd, Sr, and Pb isotopic evidence for diverse lithospheric mantle sources of East African Rift carbonatites. *Tectonophysics* **1997**, *278*, 31–45. [[CrossRef](#)]